

Master thesis : Sensitivity and robustness analysis of thalamic neurons models at the cellular and network level

Auteur : Coutisse, Kathleen

Promoteur(s) : Drion, Guillaume

Faculté : Faculté des Sciences appliquées

Diplôme : Master en ingénieur civil électricien, à finalité spécialisée en "electrical engineering"

Année académique : 2017-2018

URI/URL : <http://hdl.handle.net/2268.2/5187>

Avertissement à l'attention des usagers :

Tous les documents placés en accès ouvert sur le site le site MatheO sont protégés par le droit d'auteur. Conformément aux principes énoncés par la "Budapest Open Access Initiative"(BOAI, 2002), l'utilisateur du site peut lire, télécharger, copier, transmettre, imprimer, chercher ou faire un lien vers le texte intégral de ces documents, les disséquer pour les indexer, s'en servir de données pour un logiciel, ou s'en servir à toute autre fin légale (ou prévue par la réglementation relative au droit d'auteur). Toute utilisation du document à des fins commerciales est strictement interdite.

Par ailleurs, l'utilisateur s'engage à respecter les droits moraux de l'auteur, principalement le droit à l'intégrité de l'oeuvre et le droit de paternité et ce dans toute utilisation que l'utilisateur entreprend. Ainsi, à titre d'exemple, lorsqu'il reproduira un document par extrait ou dans son intégralité, l'utilisateur citera de manière complète les sources telles que mentionnées ci-dessus. Toute utilisation non explicitement autorisée ci-avant (telle que par exemple, la modification du document ou son résumé) nécessite l'autorisation préalable et expresse des auteurs ou de leurs ayants droit.



Sensitivity and robustness analysis of thalamic neuron models at the cellular and network levels

*Master thesis realized with the aim of obtaining the degree of Master in
Electrical Engineering*

Kathleen Coutisse

Supervisors:

G. Drion

Jury members:

P. Geurts

R. Sepulchre

V. Seutin

M. Van droogenbroeck

UNIVERSITY OF LIÈGE
FACULTY OF APPLIED SCIENCES
ACADEMIC YEAR 2017 - 2018

“ *Do what you like, but like what you do.*

”

Winston Churchill

Sensitivity and robustness analysis of thalamic neuron models at the cellular and network levels

Kathleen Coutisse

Supervisor: G. Drion

Master in Electrical Engineering, University of Liège
Academic year 2017-2018

Abstract

In the early fifties, Hodgkin and Huxley developed a model of the electrical activity of the neuron. Based on a simple RC circuit with non-linear conductances, they reproduced very well the electrical behavior of a squid neuron. Over the last fifty years, thanks to the increase of experimental data and knowledge in neuroscience, scientists have extended the Hodgkin and Huxley's model to more complex neurons. But they have often increased the complexity which makes their models less robust.

This thesis focuses on thalamic neurons. The thalamus is the relay-station for the sensory inputs travelling to the cortex. Depending on the state, the thalamic neurons exhibit two different firing patterns. During sleep, the neurons are bursting, which stops the information processing. During wakefulness, the neurons are spiking and the thalamus processes the inputs. In order to study diseases such as absence seizures in children, or to describe more precisely the thalamic behavior, a robust model of neuron activity switch is necessary. This robustness has to be maintained when the study is performed at the network level.

Recent evidences have highlighted the critical role of the slow dynamics of neuronal calcium currents in the switch from spiking to bursting. Inspired by this line of work, this thesis gathers conductance-based models of thalamic neuron in the literature. The major difference between them is the presence of the slow kinetics of the calcium current. The first contribution is their robustness comparison at the cellular level. Models which lack this slow dynamic are fragile when they are subjected to perturbation.

The second contribution is to show that this slow dynamic is necessary to reproduce the correct rhythmicity of the thalamus at the network level.

The conductance-based models are powerful tools to simulate a neuron with a great biophysical realism. However, they consist in high-dimensional non-linear differential equations that lead to time-consuming simulations. Therefore, the second part of this thesis investigates simple, qualitative modeling of neuron and network activity. This type of model, called hybrid model, is more mathematical; it captures the subthreshold dynamics of the neuron through differential equations and adds a reset rule to mimic the all-or-none nature of the spike. A hybrid model of a thalamic neuron has to be able to switch from spiking to bursting. Its robustness at the cellular level relies on its ability to mimic the slow dynamics of the calcium current without mathematical manipulation.

The third contribution of the thesis is to confirm this discussion with a network level analysis. It shows that previously available simple models of thalamocortical neurons such as the well-known Izhikevich models lack the slow dynamics, hence they generate pathological behaviors while connected within a circuit.

The key message is the comparison between two classes of thalamic neuron models. The first class integrates the slow dynamics of the calcium current while the second class assumes that this dynamics is fast. This work shows that the first class provides better results in terms of robustness. This demonstration is led at the cellular and network levels, for conductance-based models or reduced models. Therefore, the models belonging to this class are suitable for studies concerning the neuromodulation or the synaptic plasticity.

Sensitivity and robustness analysis of thalamic neuron models at the cellular and network levels

Kathleen Coutisse

Promoteur: G. Drion

Master en ingénieur civil en électricité, à finalité approfondie, Université de Liège
Année académique 2017-2018

Résumé

Au début des années cinquante, Hodgkin et Huxley ont développé un modèle de l'activité électrique neuronale. Basé sur un simple circuit RC caractérisé par des conductances non-linéaires, ils ont réussi à reproduire de manière précise le comportement électrique d'un neurone de calamar. Durant ces dernières années, l'augmentation du nombre de données expérimentales disponibles, ainsi qu'une amélioration des connaissances dans le domaine de la neuroscience, ont permis aux scientifiques d'étendre le modèle de Hodgkin et Huxley au cas de neurones plus complexes. Cependant, ces modèles augmentent également en complexité mathématique, ce qui les rend moins robustes.

Cette thèse se concentre uniquement sur les neurones du thalamus. Cette partie du cerveau est le centre-relais des informations sensorielles voyageant vers le cortex. En fonction de leur état, les neurones du thalamus sont caractérisés par deux motifs de décharge. Durant le sommeil, les neurones "burstent", ce qui bloque le traitement de l'information. Durant la phase d'éveil, les neurones présentent un enchaînement régulier de pics qui permettent au thalamus de traiter l'information et de l'envoyer au cortex. Un modèle robuste décrivant ce changement d'activité est primordial afin de mieux comprendre certaines maladies telles que l'absence d'épilepsie ou de décrire plus précisément le comportement du thalamus.

De récentes études ont mis en évidence le rôle critique de la dynamique lente des courants calciques présents dans les neurones dans la transition entre les deux modes de décharge. Inspirée par ces recherches, cette thèse rassemble des modèles à conductances des neurones du thalamus présents dans la littérature. La différence majeure entre ces modèles réside dans l'intégration ou non de la cinétique lente des courants calciques. La première contribution de ce travail est la comparaison de leur robustesse à l'échelle cellulaire. Les modèles qui omettent cette dynamique lente sont fragiles lorsqu'ils sont soumis à des perturbations. La deuxième contribution consiste à montrer que cette caractéristique des courants calciques est nécessaire pour reproduire le rythme d'une population de neurones du thalamus.

Les modèles à conductances sont des outils puissants pour simuler un neurone avec une bonne interprétation biophysique. Cependant, ils sont formés d'un grand nombre d'équations différentielles non-linéaires menant à des simulations coûteuses en temps. Par conséquent, la deuxième partie de cette thèse s'oriente vers une modélisation plus simple et plus qualitative des neurones et de leur activité en réseau. Ce type de modèle, appelé modèle hybride, est plus mathématique ; il capture la dynamique du signal neuronal au travers une équation différentielle. Ensuite, une équation de remise à zéro, appelée la règle du « reset », tient compte de la nature « tout ou rien » des pics présents dans le signal électrique. Un modèle hybride d'un neurone du thalamus doit être capable de reproduire la transition entre les deux modes de décharges. Sa robustesse à l'échelle cellulaire repose sur son aptitude à imiter la dynamique lente des courants calciques sans manipulation mathématique.

La troisième contribution de cette thèse est de confirmer cette hypothèse avec une analyse à l'échelle d'un réseau de neurones. Cette étude prouve que les modèles plus simples des neurones du thalamus présents dans la littérature, tels que les modèles d'Izhikevich, n'intègrent pas cette cinétique lente. Par conséquent, ils ne sont pas capables de reproduire l'activité rythmique du thalamus.

Pour résumer, cette thèse a pour but de comparer deux classes de modèles de neurones du thalamus. Une classe intègre la dynamique lente des courants calciques en opposition à l'autre classe qui assume que cette dynamique est rapide. Ce travail montre que la classe faisant l'hypothèse d'une dynamique lente donne des résultats favorables en terme de robustesse. Cette démonstration est menée au niveau cellulaire et à l'échelle d'un réseau de neurones, tant pour des modèles à conductances que des modèles réduits.

Acknowledgements

First, I would like to thank my supervisor Professor Guillaume Drion who gave me the opportunity to work on this exciting subject. I am infinitely grateful for having supervised me during the whole year. His availability and his wise advices help me to lead this project to the end.

Moreover, I wish to emphasize my acknowledgements to Professor Rodolph Sepulchre who gave me the unique chance to realize an internship at the University of Cambridge. I would like to thank him for his precious help and all the interesting conversations we had. Many thanks to all the members of the Control Group who contribute to my work, especially Timothy O’Leary.

Then, I express a special thought to my mum for her patience and support during all these years and to my grand-father.

I am also thankful to François and my friends who supported me during this work and throughout my studies.

Finally, I would like to thank all members of the jury for devoting time and interest to reading this report.

Liège, June 8th, 2018

A handwritten signature in black ink, consisting of several overlapping loops and strokes, likely representing the name Kathleen Coutisse.

Kathleen Coutisse

Contents

1	Introduction	1
1.1	Motivations	1
1.2	Structure	2
I	Background	5
2	Elements of neurophysiology and neuronal modeling	7
2.1	The cell	7
2.2	The plasma membrane	8
2.2.1	Biological structure	8
2.2.2	Membrane Potential	9
2.2.3	Electrical Model	11
2.2.4	Neuron model seen by the control theory	15
2.3	Thalamus	17
2.3.1	Where is the thalamus? What does it consist in? What is its major role? . . .	17
2.3.2	State-Dependent Behavior	18
2.3.3	T-Type Calcium Current	19
2.3.4	Synaptic connections between neurons	20
2.3.5	Switch Between Two Firing Modes	22
2.3.6	Sleep and Population Rhythm	22
2.3.7	Summary	24
II	Conductance-based modeling	27
3	Conductance-based models of thalamic neuron at the cellular level	29
3.1	Models From the Literature	29
3.2	Thalamic neuron models in Julia	30
3.3	Activation of the T-type calcium channel: fast or slow?	34
3.3.1	Introduction	34
3.3.2	Is the fast activation of the calcium channels valid?	34
3.4	Thalamic Neuron Models: Robustness Analysis at the Single Cell Level	37
3.4.1	Procedure	37
3.4.2	Results	37
3.4.3	Discussion	38
3.5	Summary	40
4	Thalamic neuron models at the network level	41
4.1	Introduction	41
4.2	Impact of the instantaneous activation of the calcium channels on the synchronisation of two cells	41
4.3	ANALYSIS OF ROBUSTNESS	43
4.3.1	State-of-art	43

4.3.2	Computational Procedure	44
4.3.3	Results	47
4.4	ANALYSIS OF TUNABILITY	51
4.4.1	State-of-art	51
4.4.2	Procedure	51
4.4.3	Results	52
4.5	ANALYSIS OF HETEROGENEITY	56
4.5.1	State-of-art	56
4.5.2	Procedure	56
4.5.3	Results	57
4.6	Discussion	61
4.7	Summary	64
III	Reduced Modeling	65
5	From conductance-based models to hybrid models	67
5.1	Introduction	67
5.2	Reduced models	67
5.2.1	HH model	67
5.2.2	HH+Ca model	68
5.2.3	Phase portrait	68
5.3	Normal form and hybrid modeling	72
5.4	Summary	75
6	Hybrid models of thalamic neuron	77
6.1	Transcritical hybrid modeling of thalamic neuron	77
6.2	Hybrid models of thalamic neurons existing in the literature	80
6.3	Switch in Hybrid Models	81
6.4	Network Analyses	84
6.4.1	ANALYSIS OF THE ROBUSTNESS	84
6.4.2	ANALYSIS OF TUNABILITY	85
6.4.3	ANALYSIS OF HETEROGENEITY	87
6.5	Discussion	88
6.6	Summary	90
IV	Conclusion and Perspectives	93
7	Conclusion and Perspectives	95
7.1	Summary	95
7.2	Prospects	97
	Appendices	A1
A	Conductance-based models of thalamic neuron: detailed modeling	A1
A.1	Hodgkin and Huxley model [38]	A1
A.2	Huguenard and McCormick model [19]	A2
A.3	Destexhe model [22]	A5
A.4	Drion model [29]	A7
A.5	Rush and Rinzel model [56]	A8
A.6	Modified Rush and Rinzel model called RushCa	A10
A.7	Wang model [67]	A11
B	Julia pseudo-code of a thalamic neuron conductance-based model	A13

C	Additional results of conductance-based models at the network level	A17
C.1	Tunability cell E	A17
C.2	Spectrograms of the LFP of the E-cells population	A18
D	Complement on hybrid modeling	A19
D.1	Reduced HH model	A19
D.1.1	Nature of the fixed points	A19
D.1.2	Vector field	A20
D.2	Reduced HHCa model	A20
D.2.1	Nature of the fixed points	A20
D.3	Additional Network Analyses of hybrid model of thalamic neuron	A22
D.3.1	Paramters used for the simulations in Izhikevich and HYB models	A22
D.3.2	Rhythmic network activity computed with the off-centered nominal values . . .	A22
D.3.3	Tunability analysis	A23
D.3.4	Population rhythm analysis	A23
	Bibliography	A28

Chapter 1

Introduction

1.1 Motivations

The brain is a very complex organ which contains approximately 25 billions of neurons. This particular type of cells communicates to each other by generating a electrical signal called an action potential. The manner the information is encoded in the pulses train is called the firing pattern. Then, the information is transmitted to another part of the brain or to a specific body area . Each neuron is connected to the others by synapses, called synaptic connections [70]. The presence of neuromodulators, which are chemical components, can regulate the state of a neuron or a population of neurons. The electrical nature of the neuron activity originates the exchange of ions through the membrane which leads to the notion of ionic current.

Inside the brain, the thalamus is the relay-station for the sensory inputs travelling to the cortex. It presents a *state-dependent behavior*. During wakefulness, the thalamic neurons fire in tonic mode which corresponds to a regular train of electrical pulses. While during the sleep, they are bursting *i.e.* each neuron undergoes short bursts of high frequency spike generation followed by silence [18, 50, 57, 71]. At the network level, the transition to the sleep state is characterised by a noticeable synchronous slow waves on EEG (electroencephalogram) recordings. This network activity shift is correlated with changes in the thalamus responsiveness. During the EEG-synchronized sleep, the thalamus stops the information processing [50, 59, 63].

An abnormal situation occurs when synchronised sleep oscillations are developed into absence epilepsy during wakefulness, which corresponds to a brain disconnection from the external world [29, 62]. Moreover, brain rhythmicity changes play a role in learning, a property called sleep-dependent memory consolidation. [49].

Therefore, the development of a robust mode of thalamic neuron firing is necessary to deepen our knowledge of the thalamic behavior compatible with regulatory mechanisms through neuromodulation or synaptic plasticity.

In the early fifties, Hodgkin and Huxley developed a model of the neuron electrical activity . Based on a simple RC circuit with non-linear conductances, they reproduced very well the behavior of a squid neuron. It is called the conductance-based modeling of a neuron. Over the last fifty years, the increase of experimental data and the better knowledge in neuroscience leads to extended versions of the Hodgkin and Huxley's model to reproduce more elaborated neurons. For thalamic neurons, a particular ionic current, called T-type calcium current, plays a major role in the firing patterns. It were included in the modeling.

The increase of complexity leads to time-consuming simulations and so it hinders the computational experiments of larger neurons populations. This is why a common strategy reduction is to consider the T-type calcium current as a fast current. However, recent evidences have highlighted the critical role of the slow dynamics of calcium currents in the switch from spiking to bursting [29, 31, 35].

Accordingly, this thesis gathers the most used conductance-based models of thalamic neuron in the literature with or without the presence of the slow dynamics of the calcium current. It investigates the robustness of these models *at the cellular level* by verifying if the model is still able to reproduce the switch from tonic mode to bursting mode when it is subjected to perturbations. Then, the robustness and the modulation of these models are studied *at the network level* by reproducing the thalamic circuitry. The computational experiments aim to mimic the regulatory mechanisms present in the thalamus.

Then, the thesis studies the mathematical modeling of thalamic neurons. Indeed, the advantage of the conductance-based model is the great physiological interpretability, but they lead to high-dimensional non-linear equations and so time-consuming simulations. Reduced models are thus necessary. They capture the subthreshold dynamics of the neuron through differential equations and add a reset rule to mimic the all-or-none nature of the spike. This kind of reduced models are called hybrid models.

The last major contribution is the hybrid models comparison which integrate or not the slow dynamics of the calcium current. The same computational experiments as the ones performed on the conductance-based models are reproduced.

1.2 Structure

This thesis is divided into four main parts.

Part I introduces the biological framework from the neuron description to the thalamus functioning. Indeed, the thesis starts with the neuron electrical activity and the explanation of its modeling. Hodgkin and Huxley were the first scientists to describe the behavior of the neuron thanks to an electrical analogy. Understanding their work is necessary to deal with the modeling of more complex neurons such as thalamic neurons (see Section 2.2).

Then, the thalamus is described from its composition, its role, its state-dependent behavior to its neuron network. The T-type calcium current is the key player in this state-dependent behavior. The impact of this current is detailed at the neuronal level. Afterwards, the connection of thalamic neurons is also discussed in order to shed light on the role of the calcium at the network level. Finally, the population rhythm and the associated information processing are discussed (see Section 2.3).

Part II is dedicated to conductance-based modeling.

Chapter 3 focuses on the cellular level with the introduction of the existing thalamic neuron models in the literature and the software used to simulate them. Then, the strategy reduction applied on the dynamics of the calcium current is discussed.

The first contribution of this thesis is the robustness analysis of the five conductance-based models found in the literature (see Section 3.4). In addition, a model which lacks the slow dynamics of the calcium current is transformed. The new version is exactly the same as the previous one with the integration of the slow time-scale feature. They will highlight the impact of the presence of this current.

Chapter 4 studies the robustness of conductance-based models at the network level. The study is decomposed in three analyses; the robustness analysis of a 2-cells circuit, the analysis of the tunability and the analysis of the population rhythm. This investigation at the network level for these conductance-based models corresponds to the second main contribution of the thesis.

Part III of the dissertation focuses on reduced modeling.

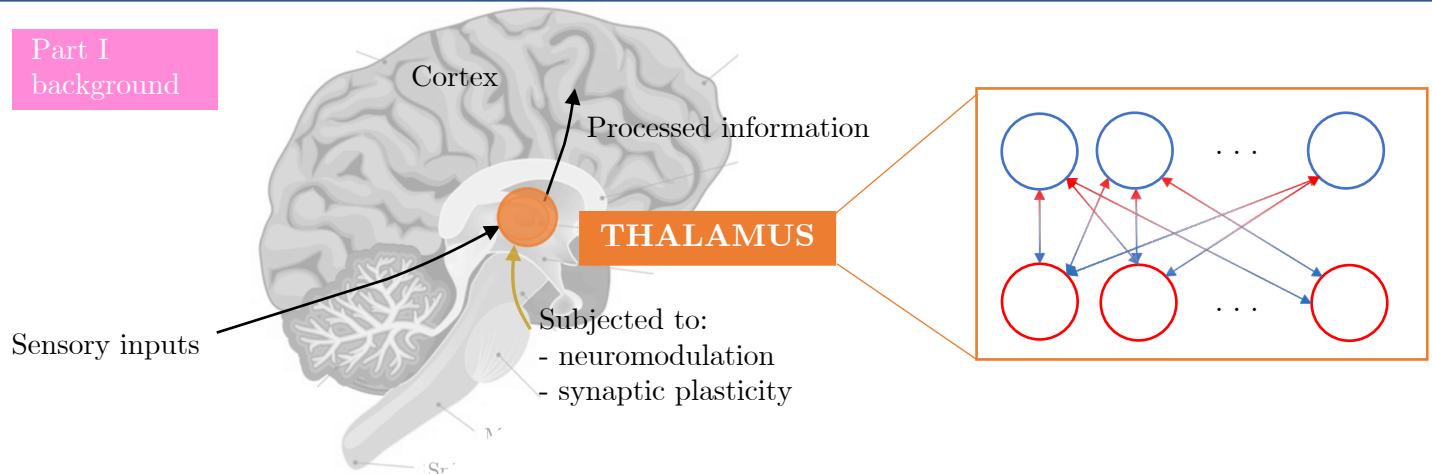
First, reduced modeling of a conductance-based model to a hybrid model is described with or without the integration of the calcium current (see Chapter 5).

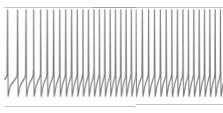
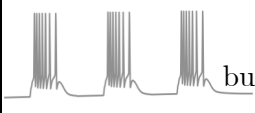
Then, two hybrid models of thalamic neurons are studied at the network level (see Chapter 6). Again, one of the two hybrid models lacks the slow dynamics of the calcium current. The same three analyses are performed; robustness, tunability and population rhythm. This corresponds to the third main contribution of the thesis; highlighting the impact of the calcium currents in hybrid models at the network level.

Part IV draws the conclusions about the importance of a current with slow dynamics current for a robust thalamic neuron and presents some applications of this research.

STRUCTURE & MOTIVATION

Part I background



State	Wakefulness	Sleep
Cellular level membrane potential	 tonic mode	 bursting mode
Network level	Asynchronous firing pattern	Cells synchronization → population rhythm
Role	Process the input information Relay them to the cortex	Block the information

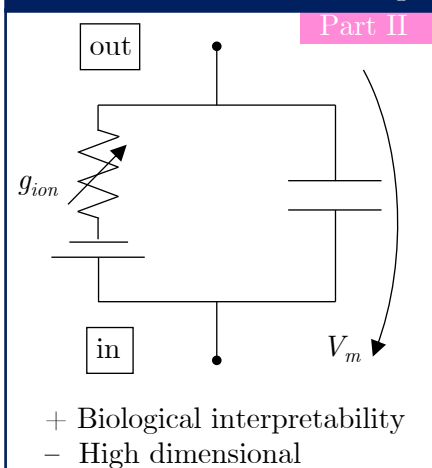
Key player: T-type calcium current

Which **kinetics** ensures the model robustness:
Slow or instantaneous ?

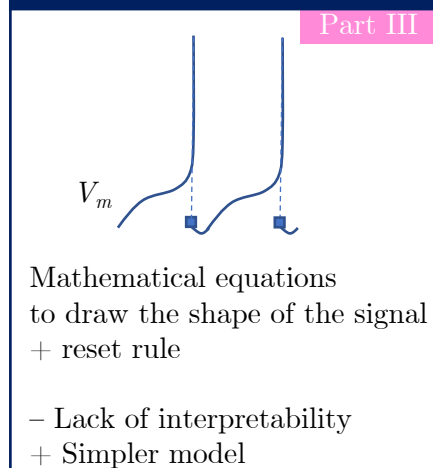
Computational experiments at cellular and network levels

In two types of neuron modeling

Conductance-based modeling



Hybrid modeling



PART IV - PERSPECTIVES

- Absence epilepsy
- Sleep-dependent memory consolidation

Part I

Background

Chapter 2

Elements of neurophysiology and neuronal modeling

2.1 The cell

The cell is the basic unit of life. There exists a large variety of types, but they share a common structure. An cell can be divided into several main components:

- the nucleus: the envelope that contains the genetic heritage,
- the cytoplasm: the intracellular medium,
- the plasma membrane: the barrier that isolates the intracellular medium from the extracellular medium,
- the organelles: the subunits of the cells having their specific functions (such as the mitochondrion)

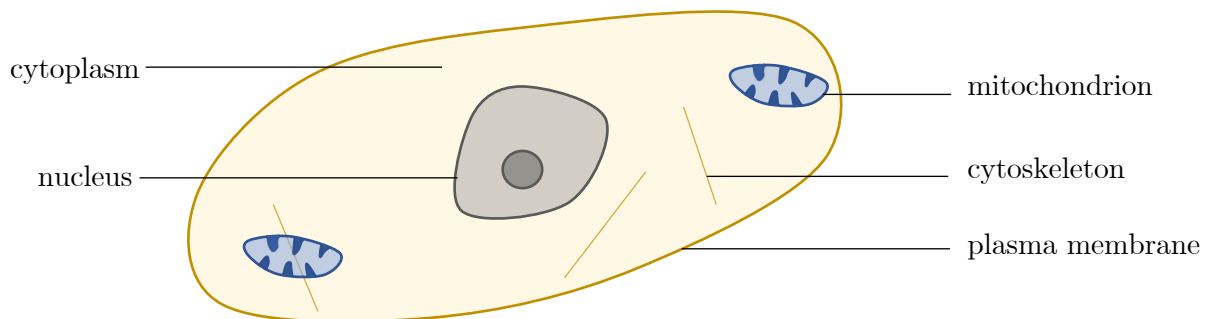


Figure 2.1 – Common cell structure - Besides different morphologies and functions, the cells exhibit this structure. They are composed of a nucleus (genetic heritage), cytoplasm (intracellular medium), a plasma membrane (envelope between the intracellular and extracellular medium), organelles (such as the cytoskeleton for the cell morphology and the mitochondrion for the cell respiration). [28]

Each cell has specific roles. For example, cells forming a tissue permit the body maintenance. This thesis focuses on a particular type of cells that is involved in signal processing, called *neurons*. A neuron receives, integrates and carries the information to another neuron or to the environment. The different types of neurons have their own role but they share a common structure as illustrated in Figure 2.2. The main components are the soma, the dendrites, the axon and the synapses.

Neurons communicate with each other by generating an electrical signal. The information is collected at the dendrites and then processed by the soma. If the input stimulation is large enough, an electrical signal (called action potential or spike) is generated. This impulse is propagated through the axon towards the other neurons. The axon is terminated by synapses where the electrical signal is transmitted thanks to electrical connections between the target neurons (i.e. electrical synapses) or by realising chemical components called neurotransmitters (i.e. chemical synapses). Each neuron is characterised by one or several neurotransmitter types. The dynamics of neurotransmitters releasing

is dictated by the way the synapses receive the action potential and then affects the target neuron responsiveness. Therefore, the key principle underlying the neurons communication is the manner the information is encoded in the action potential called *firing pattern* [28].

Neuron information processing relies on a cellular property called *excitability*. It allows to respond to a stimulation by rapid changes in membrane potential. This electrical origin comes from the ion fluxes across the plasma membrane [1].

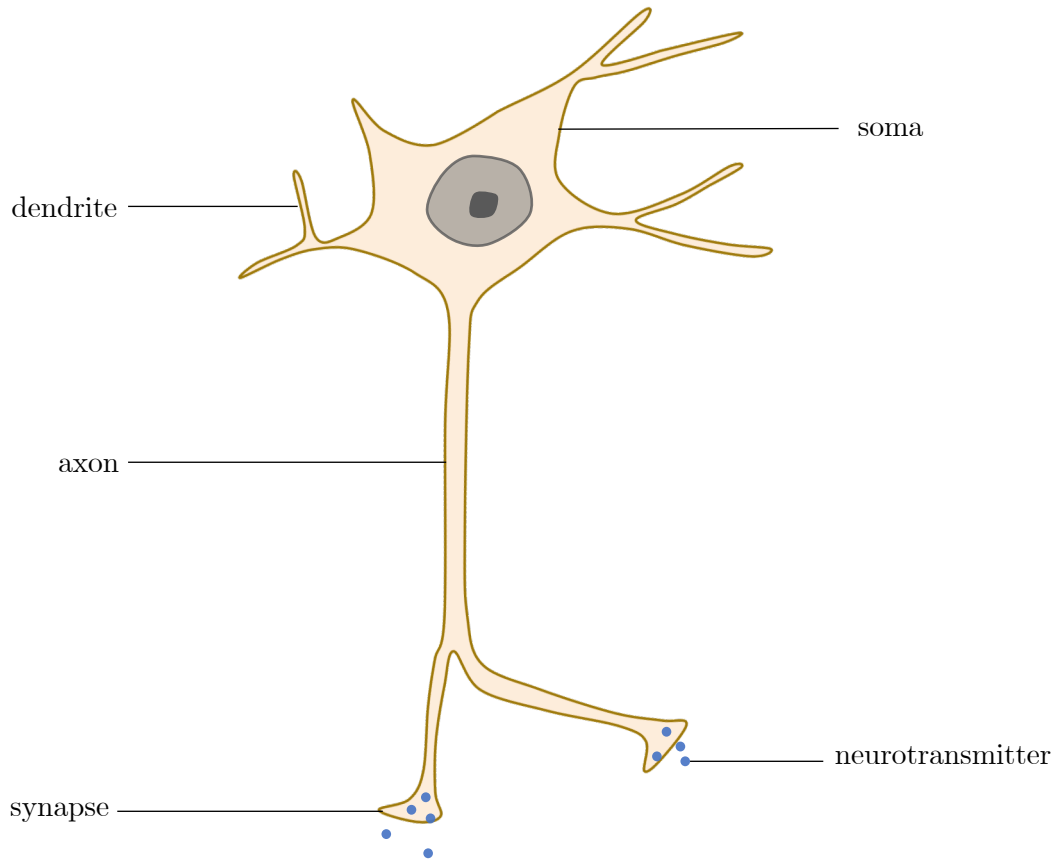


Figure 2.2 – General neuron structure - The main components are the dendrites, the soma, the axon, the synapses. The dendrites are connected to other neurons and collect the information. The input is integrated in the soma and then propagated in the axon to be transmitted to other neurons thanks to synaptic connections. A neurotransmitter corresponds to the chemical component released to the other neurons. [28]

2.2 The plasma membrane

2.2.1 Biological structure

The plasma membrane consists of a phospholipid bilayer that is permeable to small molecules and water but almost impermeable to ions or large molecules. The small molecules diffuse by following their concentration gradient and the water displacement is mostly dictated by osmosis. Ion and large molecules, which cannot diffuse, can cross it through proteins embedded in the membrane. These proteins are selectively permeable to one or a few substances. There are two groups of proteins which are relevant in this work: ion channels and active transporters [28].

Ion Channels

Ion channels are membrane proteins that act like modulated holes where selective ions such as sodium, potassium or calcium can flow through the membrane following their electro-chemical gradient. These

ion channels are proteins whose structure is able to move. This structure modification allows the channels to be open or closed.

Ion channels have a key role in signalling because they contribute to the charge repartition across the membrane. The channels density for a particular ion and their opening state define the permeability of the membrane to a specific ion. It is a dynamic variable [28, 37].

Active Transporters

The movement of a substance through the membrane against its electro-chemical gradient is feasible thanks to the active transporters using chemical energy for example under the form of ATP. Their presence is critical to sustain an unbalanced substances concentration, in particular for ions that determine the membrane potential.

2.2.2 Membrane Potential

The electrical behavior of neurons is based on the ion transfer across the membrane and the ions storage in the intra or extracellular spaces, mainly Na^+ , K^+ , Ca^{2+} and Cl^- . Their relative concentrations and their corresponding membrane permeability generate an electrical gradient across the membrane called the *membrane potential* ($V_m = V_{in} - V_{out}$).

For a theoretical example of a membrane only permeable to sodium, Figure 2.3 describes the ionic movement,

1. Na^+ moves following the concentration gradient *i.e* from the highest concentration medium to the lowest concentration medium; in this case, sodium enters the cell.
2. The intracellular medium becomes more positive.
3. The extracellular medium becomes more negative; the concentration of negative charges (such as Cl^-) becomes dominant.
4. The resulting electrical gradient resulting from the asymmetric distribution of charge molecules tends to oppose the entry of sodium ions into the cell.
5. The ions continue to move until the chemical force is perfectly counterbalanced by the electrical force.

This equilibrium corresponds to a specific value of the membrane potential called the Nernst potential ($V_m = V_{Na}$). This potential is defined by the Nernst law:

$$V_{Nernst} = \frac{RT}{zF} \ln \frac{[ion]_{out}}{[ion]_{in}} \quad (2.1)$$

where R is the gas constant, T is the temperature in kelvin, F is the Faraday's constant, z is the valence of the considered ion and $[ion]_{out}$ (resp. $[ion]_{in}$) is the extracellular (resp. intracellular) concentration.

Considering now the different major types of ions present across the membrane (sodium, potassium, calcium and chloride), Figure 2.4 shows their different ionic concentrations at both membrane sides and Table 2.1 sums up the typical nernst potentials for each ion (also called the reversal potentials).

Ion	$[ion]_{in}$ [mM]	$[ion]_{out}$ [mM]	Reversal potential [mV]
Na^+	18	145	$V_{Na} = 56$
K^+	135	3	$V_K = -102$
Ca^{2+}	10^{-4}	1.2	$V_{Ca} = 125$
Cl^-	7	120	$V_{Cl} = -76$

Table 2.1 – Ionic concentrations on both membrane sides and the corresponding reversal potential [28] and [37] Figure 5.2.

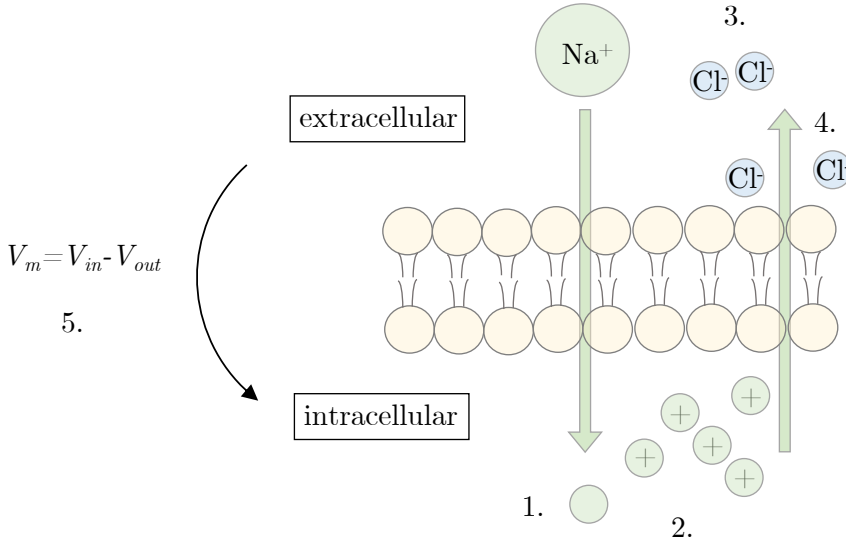


Figure 2.3 – Movement of sodium ions across a membrane only permeable only to these ions. 1- Movement of the sodium ions following the concentration gradient. 2- Intracellular medium is more positive. 3- The extracellular medium is more negative due to the presence of negative charges. 4- Presence of a resulting electrical gradient. 5- No more movement when the diffusion is counterbalanced by the electric force and the membrane potential V_m is equal to the reversal potential of the sodium V_{Na} (Figure 5.3 in [37])

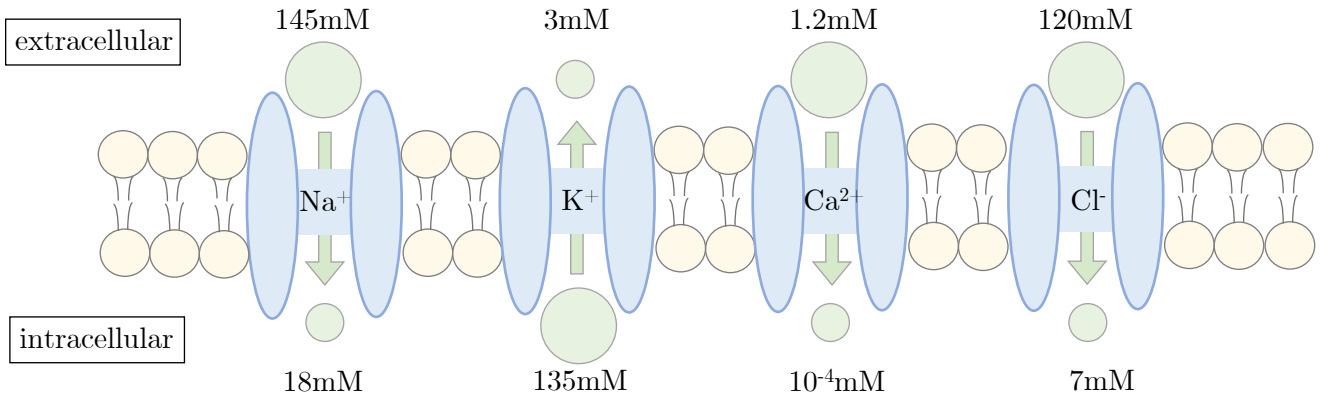


Figure 2.4 – Ionic concentrations on both membrane sides -This difference of concentration causes a voltage gradient giving the membrane potential V_m ([28] and Figure 5.2 in [37])

Finally, the resting membrane potential (V_m) comes from the repartition of these different ions whose distributions depend on the ion channels permeability. It follows the Goldman- Hodgkin-Katz equation (generalization of the Nernst equilibrium) :

$$V_m = \frac{RT}{F} \ln \left(\frac{P_{Na^+}[Na^+]_{out} + P_{K^+}[K^+]_{out} + P_{Cl^-}[Cl^-]_{in}}{P_{Na^+}[Na^+]_{in} + P_{K^+}[K^+]_{in} + P_{Cl^-}[Cl^-]_{out}} \right) \quad (2.2)$$

where P_{ion} is the ion relative permeability of the membrane (see [33]).

In summary, the neuron is an excitable cell that can respond to stimuli by generating an electrical signal. The origin of this electrical signal is studied at the membrane level whose structure lets ions cross it only through ion channels. These channels have a dynamic permeability. The variation of

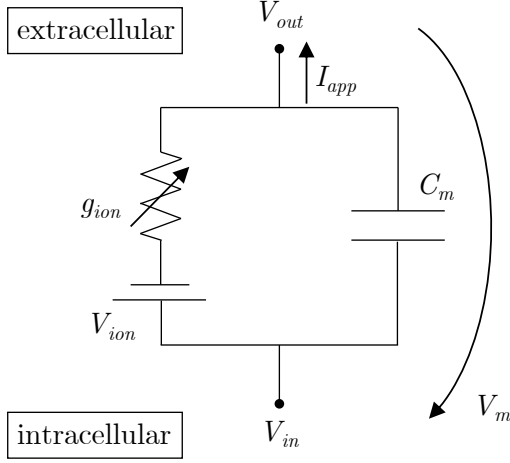


Figure 2.5 – Modeling of the membrane as an RC circuit. - The phospholipid bilayer is modelled as a capacitor C_m , an ion channel is assimilated as a variable conductance g_{ion} , the reverse potential is V_{ion} and the applied current I_{app} (Figure 7.1 in [37]).

this permeability regulates the ions flow and therefore the permeability changes are at the basis of the action potential.

2.2.3 Electrical Model

In the fifties, Huxley and Hodgkin were the first to record the membrane potential of a giant squid axon. They highlighted the role of sodium and potassium ions in the action potential generation and the presence of *voltage gated ion channels*. Besides, they provided a *mathematical modeling of action potential generation* by fitting their mathematical parameters to their recorded data [38].

Their model is based on an electrical analogy of the membrane. The phospholipid bilayer is considered perfectly impermeable to ions and allowing the charges accumulation in the intracellular and extracellular sides; its activity is modelled as a capacitor. The membrane and the cell morphology fix the capacitance C_m . The corresponding capacitive current I_C is defined by the variation of charge distribution across the capacitance :

$$I_C = C_m \frac{dV_m}{dt} \quad (2.3)$$

Concerning the proteins, each ion channel is assumed to be permeable to one specific ion which flows through the membrane following their gradient concentration. Each channel is assimilated as a resistor. Since the quantity of channels in open states for one specific ion is dynamically regulated, the corresponding conductance g_{ion} is a dynamic variable. The ion flow corresponds to the ionic current I_{ion} and according to the Ohm's law it is defined by:

$$I_{ion} = g_{ion}(V_m - V_{ion}) \quad (2.4)$$

where V_{ion} is the ion reversal potential.

Therefore, the membrane seen as an electrical component is a simple RC circuit (see Figure 2.5).

The variation of the membrane potential for n different ion channels is determined by applying the Kirchhoff's law on the electrical circuit with a negative sign for an inward current of positive ions by convention:

$$C_m \dot{V}_m = - \sum_{i=1}^n g_{ion,i}(V_m - V_{ion,i}) + I_{app} \quad (2.5)$$

where \dot{V}_m is the membrane potential variation per unit of time and I_{app} represents the applied current.

This equation emphasizes the key role of the dynamic permeability through the dynamic conductance in the variation of the membrane potential. Now, the modeling consists in defining this dynamic conductance g_{ion} .

Derivation of the conductance dynamics

According to Hodgkin and Huxley, the ion channel is voltage and time dependent and it can be seen as a regulated hole with two moving gates (see Figure 2.6). Therefore, the permeability is equal to 0 when either gate is closed and it varies to the maximum conductance of the ion \bar{g}_{ion} when both gates are open. This maximum value depends only on the channel density in the membrane.

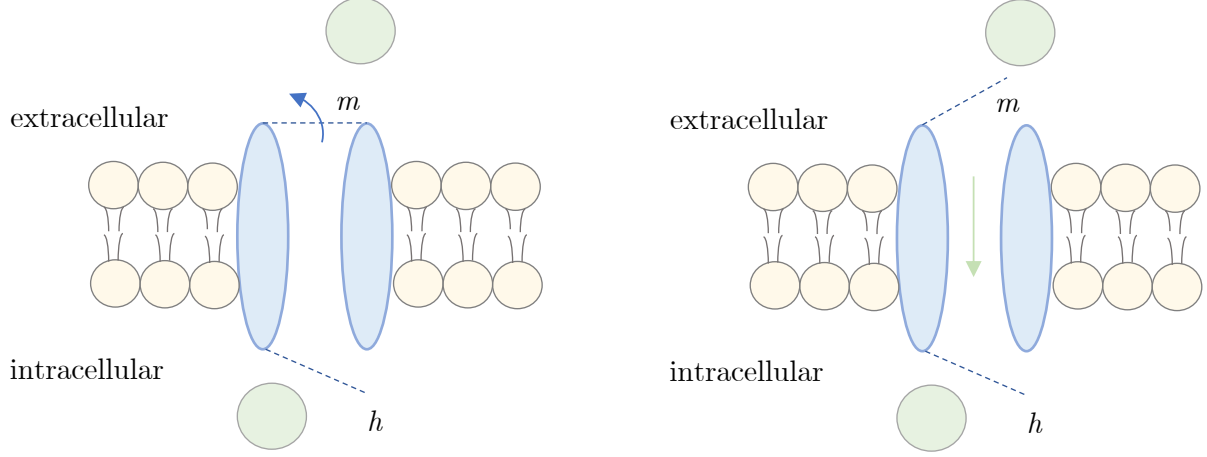
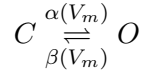


Figure 2.6 – Ion channel modelled with their activation and inactivation gates. - (left) The ion channel is closed because the activation gate is in closed state. (right) The ion channel is now open thanks to the opening of the activation gate and the inactivation gate has remained open. The ions can cross the membrane.

The dynamic variation of permeability follows the law of mass action. Schematizing the gate behavior



where C (resp. O) corresponds to the closed (resp. open) state and $\alpha(V_m)$, $\beta(V_m)$ are the voltage-dependent rate constants. Defining $n(V_m, t)$ as the fraction of open channels, the dynamic conductance is written as

$$g_{ion} = \bar{g}_{ion} n(V_m, t) \quad (2.6)$$

and the fraction variation of open channels over time is

$$\begin{aligned} \dot{n} &= \alpha(V_m)(1 - n) - \beta(V_m)n \\ &= (\alpha(V_m) + \beta(V_m)) \left(\frac{\alpha(V_m)}{\alpha(V_m) + \beta(V_m)} - n(V_m, t) \right) \end{aligned} \quad (2.7)$$

where $n \in [0; 1]$. Defining

$$n_{\infty}(V_m) = \frac{\alpha(V_m)}{\alpha(V_m) + \beta(V_m)} \quad (2.8)$$

$$\tau(V_m) = \frac{1}{\alpha(V_m) + \beta(V_m)} \quad (2.9)$$

where $n_{\infty}(V_m)$ is the fraction of open channels at steady-state and $\tau(V_m)$ is the channel time constant. Finally, the fraction variation of open channels is

$$\dot{n}(V_m) = \frac{n_{\infty}(V_m) - n}{\tau_n(V_m)} \quad (2.10)$$

The equations (2.8), (2.9) and (2.10) are characteristic for each type of ion channels and are determined

by experimental recordings [37].

As previously said, the channel is a regulated hole with moving gates. There are two types of gates: the *activation gate* which opens with a *depolarisation* (*i.e.* increasing membrane potential) of the cell and the *inactivation gate* which closes with a depolarisation of the cell. They are respectively expressed by an activation gate variable m and inactivation gate variable h . The fraction of open channels n can be replaced by the two gates and the conductance is written as

$$g_{ion}(V_m) = \bar{g}_{ion} m_{ion}^a h_{ion}^b \quad (2.11)$$

where a and b are coefficients to be tuned to fit with the experimental recordings. The kinetics of the gate variables is the same as equation (2.10)

$$\dot{m}_{ion} = \frac{m_{ion,\infty}(V_m) - m_{ion}}{\tau_{m_{ion}}(V_m)} \quad \text{and} \quad \dot{h}_{ion} = \frac{h_{ion,\infty}(V_m) - h_{ion}}{\tau_{h_{ion}}(V_m)} \quad (2.12)$$

The steady-state variables are sigmoid functions of the membrane potential and the time constants follow a unimodal function of the membrane potential (see respectively Figure A.1 and Figure A.2 in Appendix A.1).

Action potential generation

The electrical model of the membrane is entirely described, and the movement of the gates permits to understand the generation of the action potential.

Hodgkin and Huxley recorded that the action potential is composed of a fast depolarisation (*i.e.* increase of the membrane potential) followed by a slower hyperpolarisation (*i.e.* decrease of the membrane potential). A neuron contains sodium and potassium channels and the generation of the action potential relies on the different dynamics of the channels gates. The sodium channel has two gates: a *fast* activation gate and a *slower* inactivation gate. The potassium channel has only an activation gate that has the *same time scale* as the inactivation sodium gate [37].

The mechanism of the action potential generation can be decomposed into four steps [28] (see Figure 2.7):

- A. Resting state: the membrane potential is at its resting value. The only open gate is the inactivation sodium gate. The two others are closed. Almost no ion can cross the membrane.
- B. Depolarisation: an external excitatory current is applied. Two situations are possible: the stimulus is not large enough, the cell recovers its resting state or the stimulus is large enough to activate the sodium channels while the other gates do not move. Sodium rapidly enters the neuron which results in a depolarisation. This increase in membrane potential opens more sodium channels and so on (phase B'). It corresponds to a positive feedback where V_m is tending to the sodium reverse potential (V_{Na}), that it can never exceed.
- C. Hyperpolarisation: the activation gate of the potassium channel has a slower dynamics, it opens with a delay. Meanwhile, the inactivation sodium gate starts to close due to the depolarisation. Then in C', Potassium moves out of the cell resulting in a hyperpolarisation. The membrane potential is tending towards the potassium reversal potential (V_K).
- D. Repolarization: this last step corresponds to the return to the resting state. The sodium activation gate is closed then the potassium activation gate is closing and the sodium inactivation gate is opening. The membrane potential recovers its steady-state value.

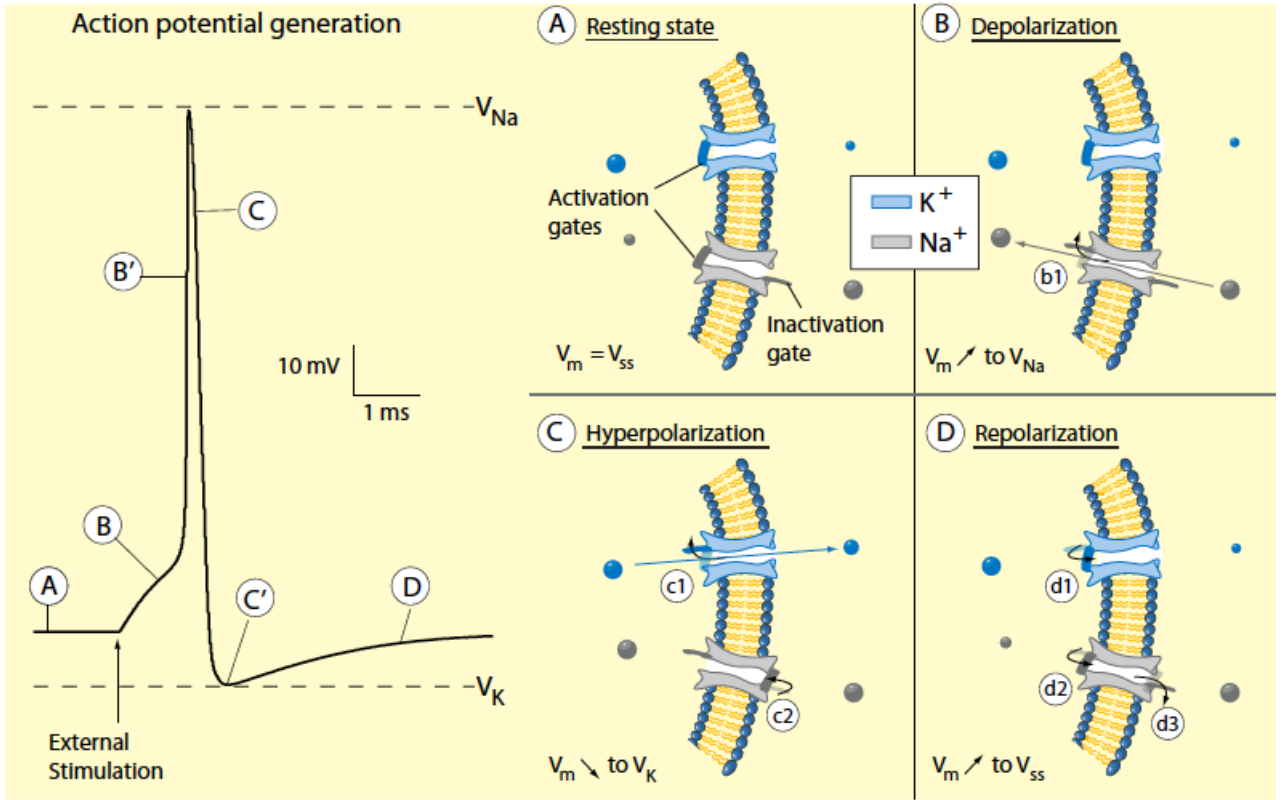


Figure 2.7 – Decomposition of the action potential. (left) time evolution of the membrane potential) for an external stimulation and (right) corresponding gating movements - A. At the resting, the membrane potential is around -70[mV]. Only the inactivation sodium gate is open. B. An external stimulation is applied, the membrane is depolarised and the activation sodium gate opens which increases again the membrane potential generating the fast upstroke (B') to reach almost the sodium reversal potential. C. The potassium activation gate is opening and the sodium inactivation is closing. The potassium goes out of the cell and (C') the membrane potential converges towards the potassium reversal potential. D. The potassium activation gate is closing and the sodium inactivation gate is opening. The membrane potential recovers its steady-state value [28].

Hodgkin and Huxley's Model = HH model

HH model includes three types of currents: a sodium current, a potassium current and a leak current [38]. This leak current accounts for the passive ionic exchange. Following the formalism of the equation (2.12), the model is defined by

$$\begin{aligned}
 C_m \dot{V}_m &= -\bar{g}_{Na} m_{Na}^3 h_{Na} (V_m - V_{Na}) - \bar{g}_K m_K^4 (V_m - V_K) - g_L (V_m - V_L) + I_{app} \\
 \dot{m}_{Na} &= \frac{m_{Na,\infty}(V_m) - m_{Na}}{\tau_{m_{Na}}(V_m)} \\
 \dot{h}_{Na} &= \frac{h_{Na,\infty}(V_m) - h_{Na}}{\tau_{h_{Na}}(V_m)} \\
 \dot{m}_K &= \frac{m_{K,\infty}(V_m) - m_K}{\tau_{m_K}(V_m)}
 \end{aligned} \tag{2.13}$$

where m_{Na} (resp. h_{Na}) is the activation (resp. inactivation) variable of sodium channels and m_K is the activation variable of the potassium channels. The kinetics of the entire model is given in Appendix A.1.

Figure 2.8 shows the response of the HH model to a step current. The membrane starts to oscillate due to the mechanism of the action potential generation described above. The evolution of the gate variables highlights the fast opening of the sodium channels when the membrane is depolarised (blue curve in Figure 2.8 (bottom)). Then, the inactivation gate of the sodium channel closes with the depolarisation but at the slower time scale (orange curve). Similarly, for the opening of the potassium channel (yellow).

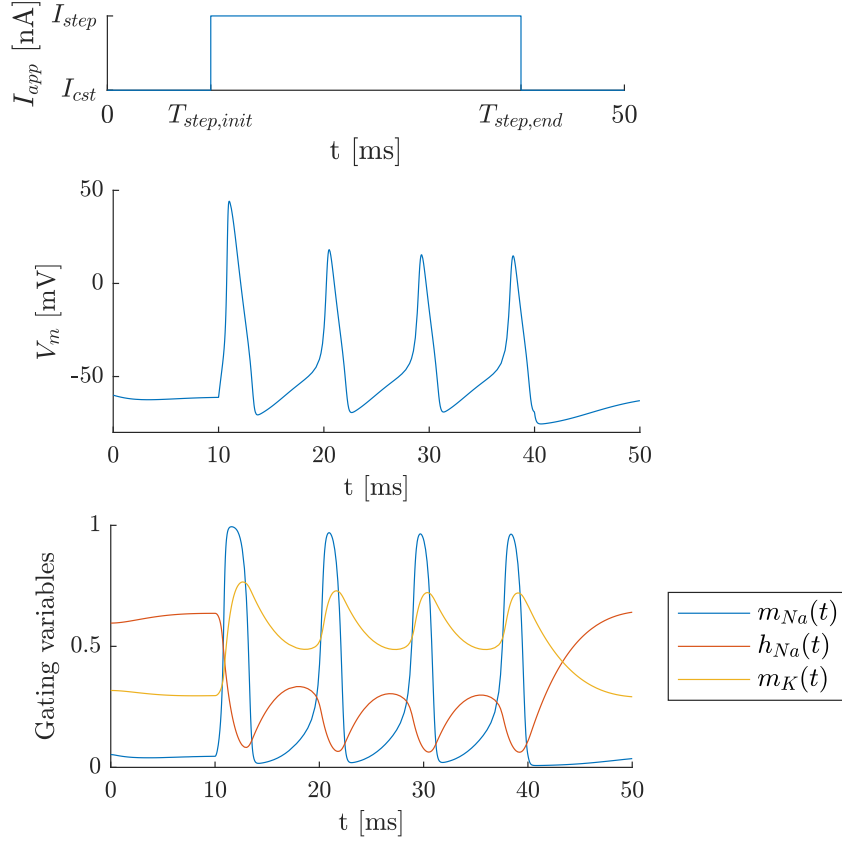


Figure 2.8 – Time evolution of the membrane potential (middle) for a step depolarising current (top) and the time evolution of the associated gating variables (bottom) [28, 37].

2.2.4 Neuron model seen by the control theory

The membrane has been modeled as an electrical circuit. The voltage-dependent conductances are non-linear elements present in this circuit. However, based on [27], this model can be studied from a control theory point of view. It is drawn as a *closed loop system* where the input is the applied current and the output is the membrane potential.

The evolution of the membrane is dictated by the difference of the applied current and the internal current (I_{ion}). This internal current is itself the sum of all the ionic currents present in the model. They respond to the Ohm's law, as previously explained, and they are driven by the output V_m . Representing the model as a closed *feedback loop* is a nice tool to highlight the voltage-dependency of the conductances as well as the role of the neuromodulation. The maximum conductances are subjected to neuromodulation which is seen as an external actor who can change the behavior of the closed loop.

Hodgkin and Huxley model is nicely represented by the block diagram (see Figure 2.9). Furthermore, this closed loop system can be easily extended to higher-dimensional models which include other ionic currents. Each new ionic current is simply added in parallel in the closed loop [27].

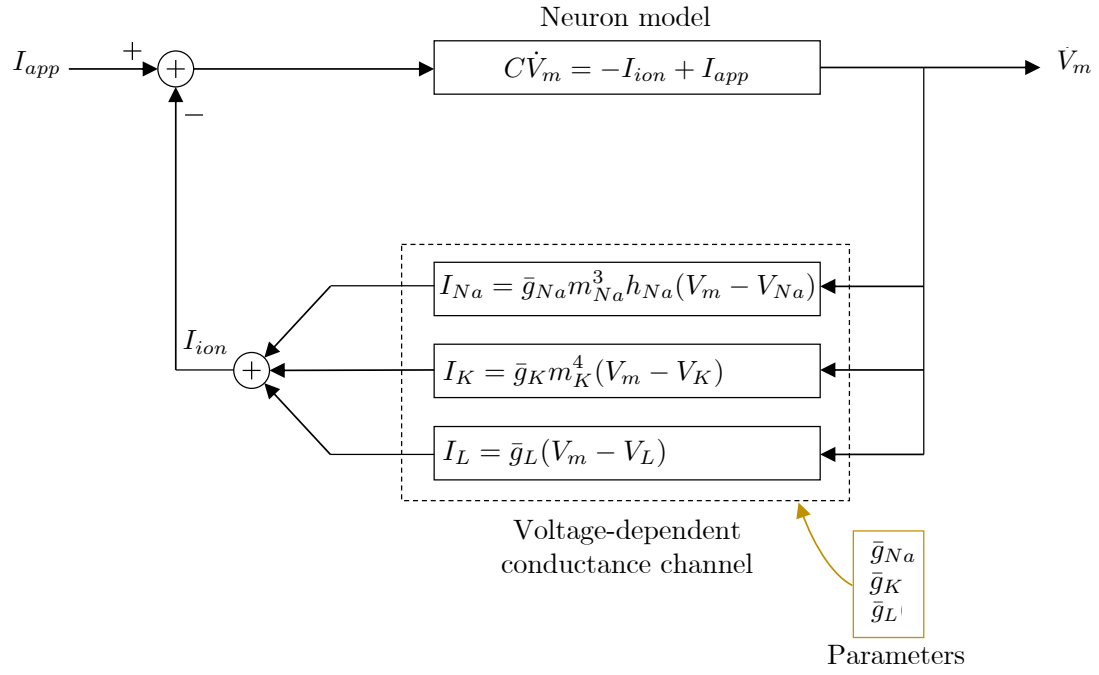


Figure 2.9 – Block diagram of the closed loop system corresponding to the electrical RC circuit of the membrane - The input (resp. the output) is the applied current I_{app} (resp. the membrane potential V_m). The ionic current I_{ion} is the sum of the parallel block associated to each ionic current present in the model. Neuromodulation can be seen as an external actor (in yellow) who changes the maximum conductance values.

2.3 Thalamus

The thesis focuses on thalamic neurons. Therefore, this section aims to introduce the thalamus, its role and its associated neurons network.

2.3.1 Where is the thalamus? What does it consist in? What is its major role?

The thalamus is situated in the middle of the brain below the cortex, above the hypothalamus and the brain stem as shown in Figure 2.10. It is the *relay station* for the information that is travelling to the cortex. Almost all the sensory information is proceeded through it. The olfaction is the only sensory input that does not pass through it. Then, the cortex receives the filtered information and can continue the processing (see Figure 2.11).

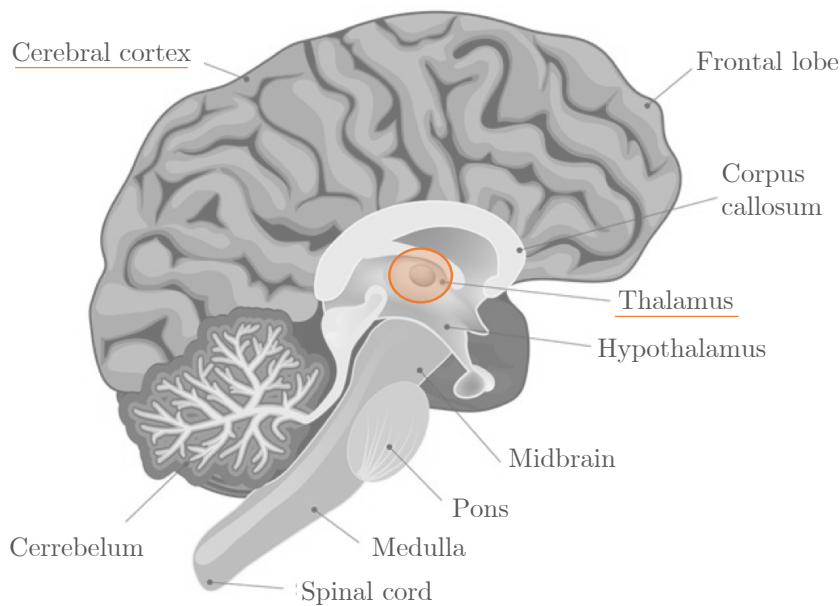


Figure 2.10 – Vertical cut of a human brain - The thalamus corresponds to the orange area shaped as an rugby ball connected to the cerebral cortex [4].

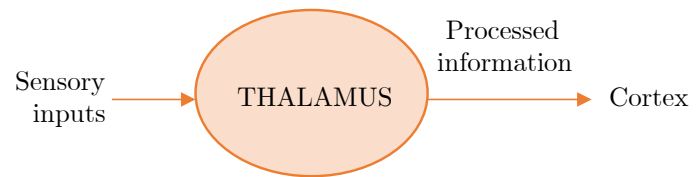


Figure 2.11 – Schematic of the thalamus input-output connections - The sensory information is firstly processed by the thalamus and then transmitted to the cortex.

Shaped like an rugby ball, the thalamus is composed of many different *nuclei*. Some of them consist of thalamic relay neurons (see Figure 2.12) . These relay neurons are *excitatory* neurons that transfer the information arriving from different brain areas to the cortex. Each nucleus has its own specialisation. For example, the medial geniculate nucleus and the lateral geniculate nucleus are used as relays for auditory and visual information respectively [14, 58].

There also exist nuclei that contain *inhibitory* neurons. For example, the perigeniculate nucleus which plays a role in the human visual system. The *thalamic reticular nucleus* contrasts from the other nuclei. It looks like a thin sheet surrounding the other nuclei. It is linked to them with *inhibitory* connections. As a reminder, the difference between excitatory and inhibitory neurons comes from the generation of excitatory or inhibitory neurotransmitters. An excitatory (resp. inhibitory) neuron produces a neurotransmitter which depolarises (resp. hyperpolarises) the membrane of the following neuron by opening sodium channels for example the AMPA glutamate receptor (resp. open chloride channels for example the GABA type A receptor).

The inputs of thalamic neurons are drivers or modulators. On the one hand, drivers correspond to the input representing the information being transmitted to the cortex. And on the other hand, modulators are inputs from other brain areas and are used to modify the drivers communication. They come from inhibitory neurons in the thalamus, in the thalamic reticular nucleus or from feedback from the cortex.

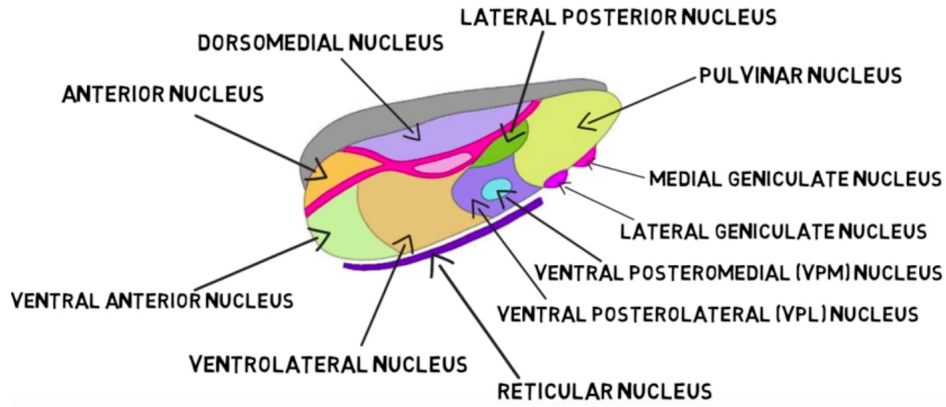


Figure 2.12 – A few nuclei of the thalamus [14]

This thesis will focus on a small network describing the interaction between the thalamic relay cells and the thalamic reticular nucleus as illustrated in Figure 2.13.

1. The relay cells in thalamic nuclei are excited by external inputs (such as the sensory information).
2. These cells transmit the information to the cortex and on the way, they send excitatory inputs to the inhibitory neurons of the thalamic reticular nucleus.
3. In response, the thalamic reticular nucleus sends back inhibitory connections to the thalamic relay cells.

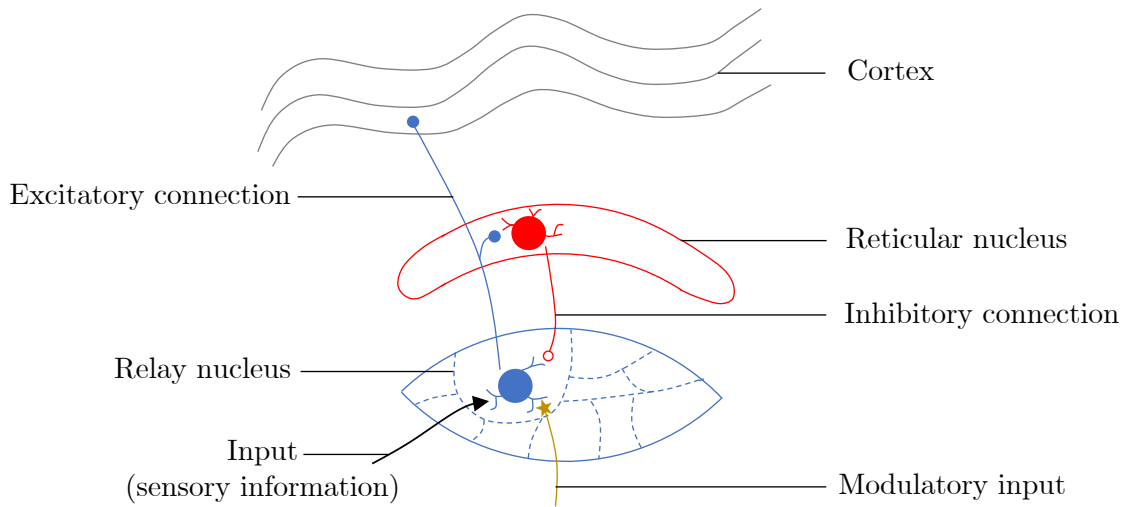


Figure 2.13 – Schematic of the interconnection between a thalamus relay nucleus and the reticular nucleus - The input (black arrow) excites a relay neuron (in blue) which transmits the information to the cortex and the thalamic reticular nucleus through a excitatory connection. A reticular neuron (in red) sends back the signal to the relay nucleus thanks to a inhibitory connection. A modulatory input (yellow arrow) can interact with this excitatory-inhibitory network [3].

2.3.2 State-Dependent Behavior

The thesis inquires on the thalamic mechanisms because it has a *state-dependent* behavior. Indeed, the shift from an aroused state to a sleeping state corresponds to a shift in the brain responsiveness. The thalamus, being the first station for the incoming information, blocks the path to the cortex during sleep [63]. Calton, in 1887, is the first investigator who recorded the activity in the cortex of a mammal and noticed the dependence between the firing pattern and the state of the animal [12].

The Electroencephalographic recording (EEG) reveals different types of rhythms depending on the state; a low amplitude and a high frequency rhythm for the aroused state which shifts to a larger

amplitude and a lower frequency for sleeping state (see Figure 2.14A). These activities are generated in the thalamus and the cortex.

To understand the origin of these two rhythms, intracellular and extracellular recordings of thalamic neurons are necessary. They exhibit different firing patterns depending on the state. When the brain is awake, the low amplitude and high frequency rhythm revealed on the EEG corresponds to a tonic firing mode at the cellular level *i.e.* a train of action potential. By contrast, during the sleep, the large amplitude and low frequency EEG waveform correspond to the synchronisation of burst firing present at the cellular level *i.e.* each neuron undergoes short bursts of high frequency spike generation followed by silence [18, 57, 71].

Figure 2.14 shows the EEG (on the top) and cellular recordings (on the bottom) of McCormick in 1997 [50].

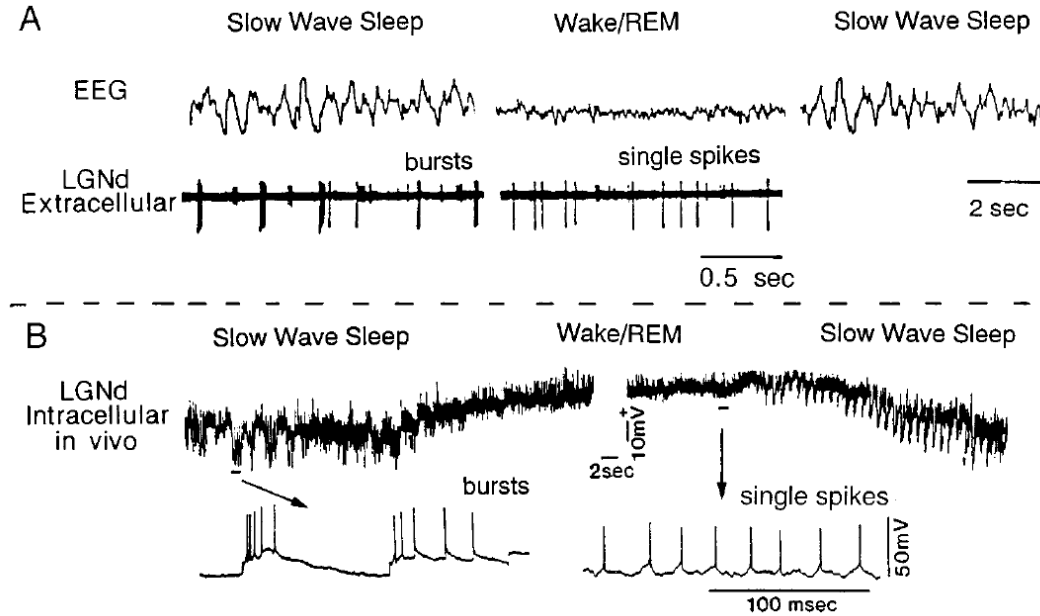


Figure 2.14 – Extracellular and intracellular recordings of lateral geniculate relay neurons during sleep and wakefulness [50]. (A) During periods of slow-wave sleep, the EEG displays synchronous slow waves and the extracellular recording exhibits burst of action potentials. During waking or REM (*i.e.* Rapid-Eye-Movement) sleep, the EEG displays a smaller amplitude. The extracellular recording shows the tonic mode. (B) The intracellular recording in vivo highlights a bursting activity during the sleep followed by a depolarisation of the membrane by 10-20 [mV] and the generation of single spikes.

2.3.3 T-Type Calcium Current

Thalamic neurons are able to fire in bursting mode thanks to an additional ionic current. In vitro recordings and voltage clamp analysis revealed the presence of a calcium current, known as the low-threshold or transient Ca^{2+} current (often written I_T or I_{CaT} in the literature) [43, 44]. The corresponding calcium channel has both an activation gate and an inactivation gate. The activation gate is rapidly open (resp. closed) by depolarisation (resp. hyperpolarisation) whereas the inactivation acts in the opposite way. It opens (resp. closes) by hyperpolarisation (resp. by depolarisation). But its dynamics is much slower; it takes about 100[ms]. The gating mechanism is similar as the sodium channel gating mechanism except that the time scale is larger for the calcium and the membrane operating range is smaller than -65[mV] (see Figure 2.15) [63].

Therefore, the following scenario is helpful to see the impact of this channel. If the cell undergoes an inhibition and the membrane potential is hyperpolarised during 100 [ms]; the calcium inactivation gate opens. If the neuron is then suddenly depolarised; the calcium activation gate will rapidly open. Since the dynamics of the inactivation gate is much slower, the gates are simultaneously open during a

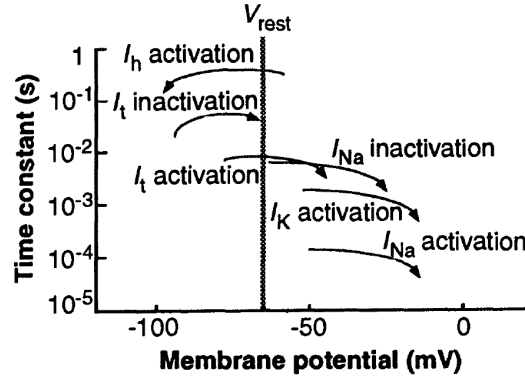


Figure 2.15 – Diagram of the activation and inactivation of the ionic currents present in the thalamocortical cell with their associated time constant. The activation (resp. inactivation) starts on the left side of the arc and is completed on the right side. The current I_h is an exception and activates with a hyperpolarisation [63].

certain amount of time. Calcium can enter the cell and depolarises it. It triggers a sequence of action potentials (sodium-potassium spikes generation) until the inactivation gate is entirely closed. Then the membrane potential decreases. This sequence describes a *bursting activity*.

The other scenario is associated to a membrane potential initially depolarised, the calcium current is inactivated and so there is no more calcium spike. If the membrane is depolarised around -55 [mV], the classical mechanism of action potential generation (sodium-potassium spikes generation) is triggered and it results in a tonic mode. Figure 2.16 A illustrated the different firing patterns in both scenarios [3, 50].

Thalamic Cell Behavior

McCormick described the behavior of a thalamic neuron at the membrane level *i.e.* by describing the interactions between the different ionic currents such as the low-threshold calcium current I_T , a hyperpolarization-activated cation current I_h and the classical combination between sodium and potassium currents (see Figure 2.16). These ionic currents have their own activation and inactivation voltage dependency and specific time scale (Figure 2.15).

The burst in a thalamocortical neuron is decomposed into four steps:

- i. When the membrane potential is around -65[mV], the T-type calcium current is activated. Calcium enters the cell and the cell is depolarised.
- ii. Around - 55[mV], the mechanism of action potential generation described in Section 2.2.3 occurs.
- iii. The I_T inactivation is much slower than its activation. After 100-200 [ms], the channel becomes closed and no more calcium enters the cell. This implies a decrease of the membrane potential and so no more Na-K spike can be generated.
- iv. This hyperpolarisation activates I_h . It results in a slow depolarisation and therefore another calcium spike can be generated (see step i.).

The rate of this sequence depends on the interaction between the ionic currents and the kinetics of the calcium current.

2.3.4 Synaptic connections between neurons

The thalamic relay neurons can switch from one mode to another thanks to the interaction with other components of the thalamocortical system; either by the inhibitory input of the thalamic reticular nucleus or by modulatory input. For example, in Figure 2.16, McCormick mimics the switch by injecting a depolarising current which closes the inactivation calcium gate. He also describes the synaptic connections between neurons as following [50]:

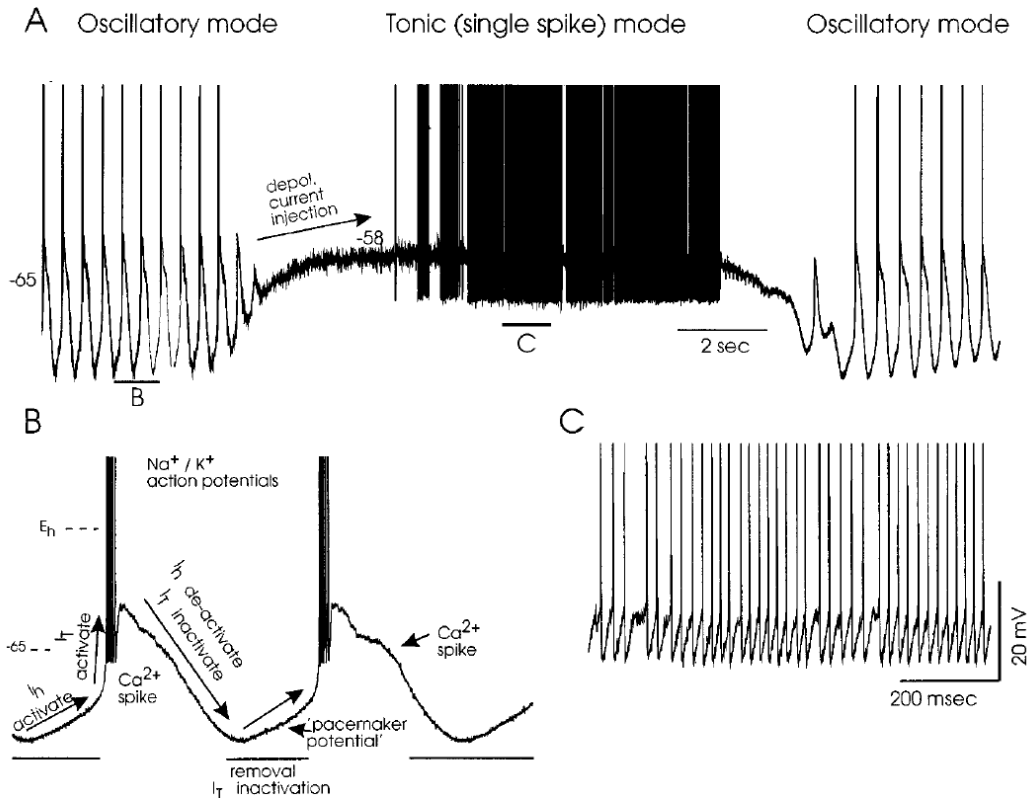


Figure 2.16 – Thalamocortical neurons recordings in bursting mode and in tonic mode and the ionic currents interaction. (A) The cat LGNd neuron generates a bursting activity at a rate equal to 2[Hz]. A external depolarising current injection switches the activity into the tonic mode. Finally, when the depolarising current is removed, the bursting mode is recovered. (B) Zoom on the oscillatory trace and the ionic current involved in the burst. Around -65[mV], I_T is being activated and depolarises the membrane potential to reach the membrane threshold for sodium-potassium action potential. I_h becomes deactivated and I_T inactivated provokes the repolarisation of the membrane followed by a hyperpolarising overshoot which activates I_h and de-inactivates I_T . (C) Zoom on the tonic mode which exhibits the classical sodium-potassium action potentials [50].

Inhibitory neuron to excitatory neuron (reticular cell to relay cell)

Activation of the thalamic reticular nucleus or the perigeniculate nucleus results in the activation of GABA receptors which give rise to inhibitory post synaptic potentials (IPSPs) in the relay neurons (see Figure 2.17).

There are two ways to activate the inhibitory neuron (for example the perigeniculate neuron (PGN)) [50]. The first one is the injection of a current pulse in the PGN neuron which generates a train of action potential. This induces a small IPSPs in the relay neuron (see Figure 2.17 B). Or the second way is performed at a lower potential, the injection of a current pulse in the PGN generates a burst firing mode which results in a larger IPSPs. This decreases more the membrane potential of the relay neuron and therefore opens the inactivation calcium gate of the relay neuron leading to a rebound Ca^{2+} spike (see Figure 2.17 C).

There are two types of GABA receptors; GABA_A and GABA_B . On the one hand, a GABA_A receptor causes the opening of chloride channels, which leads to the hyperpolarisation of the cell. On the other, a GABA_B receptor is coupled with a protein. When this receptor is activated, it indirectly opens potassium channels. The flow out of potassium ions also leads to a hyperpolarisation of the cell [13]. The hyperpolarisation due to the GABA_B receptors occurs at lower potential value than the first one and it is slower.

Excitatory neuron to inhibitory neuron (relay cell to reticular cell)

In a similar way, a single spike in the relay neuron induces excitatory post synaptic potentials (EPSPs) while a burst firing mode results in a larger amount of EPSPs leading to an increase value of the membrane potential in the reticular neuron (respectively illustrated in Figure 2.17 E and F).

This depolarisation originates from the presence of AMPA receptors which allows sodium to flow in [50].

The reciprocal connections between a relay neuron and a reticular neuron

This loop connection can be decomposed into several steps of interactions (see Figure 2.17 H):

- i. A current pulse in the PGN neuron (which is an inhibitory neuron) produces a burst firing activity.
- ii. This burst activity induces a rebound burst firing in the relay neuron.
- iii. The relay neuron in burst induces feedback EPSPs in the PGN.

The delay between the burst and the return of EPSPs in the PGN neuron is due to two reasons: the duration of the GABA_A- IPSPs in the relay neuron and the necessary delay for the generation of a calcium spike.

The loop can be studied from the relay neuron in a similar way such as a bursting activity in the relay neuron results in a feedback of IPSPs through a generation of a burst of action potential in the PGN neuron (see Figure 2.17 I) [50].

2.3.5 Switch Between Two Firing Modes

Thalamic relay cells can fire in two different modes, as explained earlier. Each mode has been associated with a specific state: tonic firing occurs during wakefulness and burst firing is limited during the sleep. In 2001, Sherman enlarged the state-dependent behavior of thalamic neurons. He brought to light that burst firing can also appear during wakefulness and plays a role in the information transmission [59].

What is the difference for the information relay between tonic and bursting mode ?

The responsiveness to sinusoidal visual stimuli applied on the geniculate nucleus is different depending on the state. The response is more sinusoidal in tonic mode than in bursting mode. The tonic mode offers a better reconstruction of the visual stimulation while the bursting mode focuses on the signal detection. In other words, the tonic firing is used as a *linear* mode and the burst firing is used for the *detectability*. This has led to the "wake-up call theory" of thalamic function . A representative example of this duality between the two firing modes occurs when an object suddenly appears in the visual field. This stimulus triggers bursting in thalamic neurons. The object is detected and roughly analysed. Then, the cells switch in tonic mode and the object is carefully examined. The switch from tonic to burst firing in the awake state originates in non-retinal inputs and controls the inactivation of I_{CaT} [57, 59, 69].

2.3.6 Sleep and Population Rhythm

The interest in thalamic neurons partly comes from that state-dependent behavior of the thalamus. The switch from the wakefulness to the sleep is characterised by a switch between tonic and bursting mode at the cellular level. Then, McCormick has described the interconnection between a relay neuron and a reticular neuron. This explanation for a 2-cell network helps to understand the oscillations recorded at a larger scale. Indeed, during the second stage of the sleep, the typical oscillations are called the *spindle waves* (recordings shown in Figure 2.18).

This corresponds to a train of oscillations which wax and wane in amplitude and last 0.5-3 [s] [63, 53]. This activity is attributed to the interconnection between the thalamic relay cells and the reticular cells as described in Figure 2.17 (G-I). Therefore, the sleep is characterised by a *synchronisation of the population* which leads to a population rhythm [21, 48]. The frequency of the waxing-and-waning

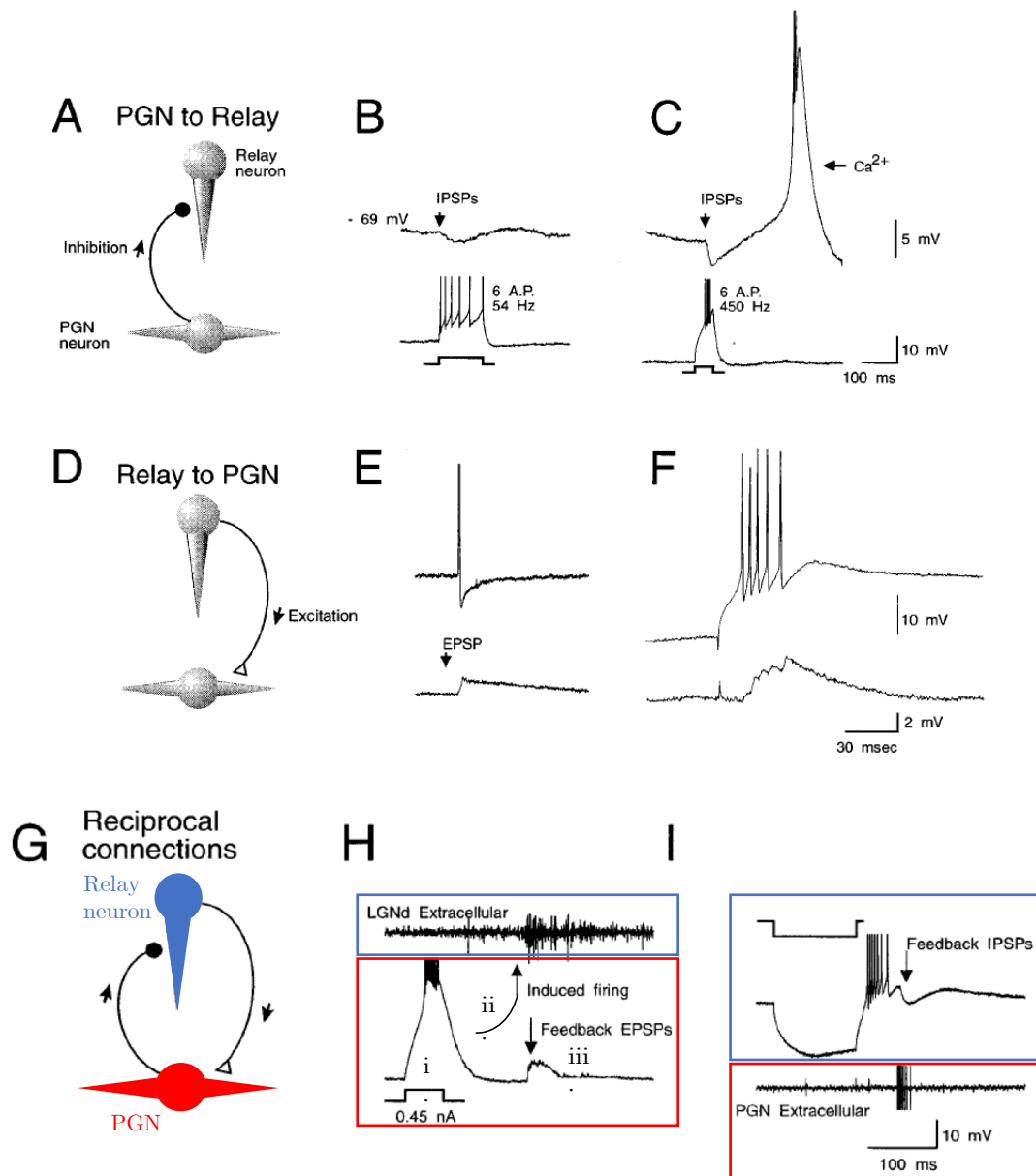


Figure 2.17 – Synaptic interconnection between a relay neuron and a perigeniculate (PGN) neuron. The first column is the connection schematic between the two cells. The second and the third columns correspond to the evolution of the membrane potential in both cells. - (A) Schematic of the inhibition induced by the PGN neuron to the relay neuron. (B) The injection of a current in the PGN cell causes action potential in the cell. This results in inhibitory post synaptic potentials (IPSPs). (C) At a lower membrane potential of the PGN, the injected current induces a burst firing which results in a larger IPSPs and a rebound calcium spike in the relay neuron. (D) Schematic of the excitation induced by the relay cell to the PGN neuron. (E) Excitatory post synaptic potentials (EPSPs) in the PGN neuron is the consequence of a single spike in the relay cell. (F) Larger amount of EPSPs in the PGN neuron is the consequence of a burst firing in the relay neuron. (G) Schematic of the excitatory-inhibitory connection between the relay cell and the PGN. (H) A current pulse in the PGN neuron drives the cell in bursting mode. This induces a rebound burst firing in the relay cell. In return, the relay cell generates EPSPs. (I) The injection of a hyperpolarised current in the relay cell leads to a rebound calcium spike. This bursting activity induces a burst mode in the PGN neuron and so a return of IPSPs in the relay cell [50]

field potentials is around 7-16 [Hz]. This is associated to the time required for one loop realisation of the excitatory-inhibitory neurons interconnection. Figure 2.19 highlights the sleep waves at different scales. The EEG is the largest scale characterised by the presence of the spindle. Then, the filtered EEG shows the wax-and-wane oscillation inside the spindle. Zooming on the spindle wave reveals the presence of the burst mode at the cellular level in the relay cell and the thalamic reticular cell.

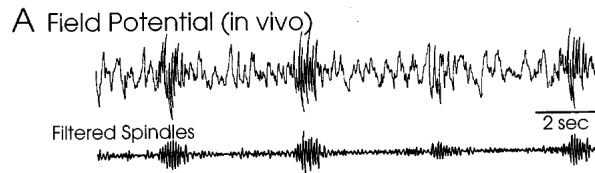


Figure 2.18 – Field potential recording in a cat thalamus (top) and its filtered signal (bottom). The wax-and-wane oscillation of the spindle wave is strongly revealed in the filtered signal. - [50] Figure 5A.

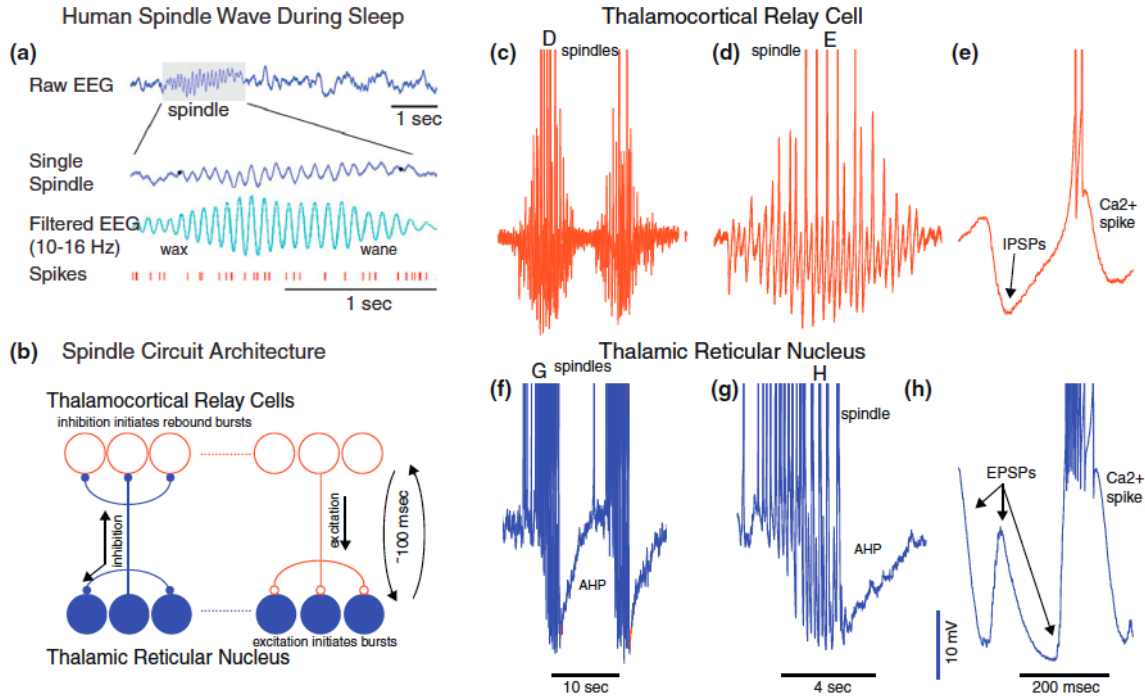


Figure 2.19 – Spindle waves: from the EEG recordings to the network mechanism underlying their generation - (a) During the sleep, typical oscillations characterised by a waxing and waning of 7-16 [Hz] rhythm. (b) Spindle waves result in the interaction of relay cells and reticular cells with this associated circuit architecture. - page 136 [51]

2.3.7 Summary

Table 2.2 gathers the main characteristics of the thalamus sorted as a function of the firing mode.

The interest for the brain rhythmicity increases with the desire of understanding how the sleep could affect different properties of our behavior such as for example the neuronal development, the memory consolidation or the maintenance of the sleep [49, 53]. In order to deepen the understanding of such mechanisms, a *robust* conductance-based model combined with a modeling of the synaptic connections is necessary. The main advantage of the conductance-based model is the presence of parameters which are physiologically relevant.

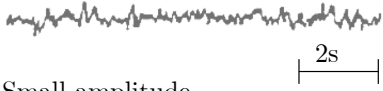

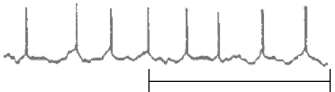
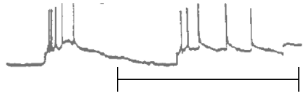
Firing mode Characteristics	TONIC FIRING	BURST FIRING
EEG	 <p>Small amplitude High frequency</p>	 <p>Large amplitude Small frequency</p>
Intracellular recordings	 <p>T-type calcium channel is inactivated</p>	 <p>T-type Ca channel is open</p>
<u>State</u> Role	<u>During the wakefulness:</u> information is transmitted to the cortex (linear analysis)	<u>During the wakefulness:</u> Detectability <u>During the sleep:</u> Information is blocked

Table 2.2 – Main characteristics of the thalamus sorted as a function of the firing mode; recordings of thalamic neurons [50] (EEG and intracellular waves) and distinction of the state-dependent.

Part II

Conductance-based modeling

Chapter 3

Conductance-based models of thalamic neuron at the cellular level

Thalamus has been proved to have an important role in the generation of the brainwave rhythmicity. The connection between relay and reticular cells can generate spindle waves. These oscillations originate from the T-type calcium current. Therefore, researchers developed *computational models* in order to understand the behavior of this current and, at a larger scale, to mimic the population rhythm.

In the nineties, experimental data have been collected to characterise the current [11, 16]. Carbone (1987) and Coulter (1989) started to describe the kinetics of the I_{CaT} current. Then, scientists used this kinetics analysis to model the electrophysiological properties of thalamic neurons. Almost all researchers followed the procedure described by Hodgkin and Huxley and created a conductance-based model fitting with the recordings.

Computational models provide a lot of valuable tools such an easy access to different ionic currents or the study of varying parameters in the time-course membrane voltage, for example. However, it is only a computational form of a conceptual model derived from scientists [52]. Indeed, they choose the different variables and their values according to the data but they decide how many different channels they model and the precise values of each parameters.

The aim of this part is to study conductance-based models of thalamic neuron and their robustness. The first step consists in gathering the most used models in the literature. With the selected models, we reproduce the relevant firing patterns at the cellular level. Then, we enter the core of the project by analysing their robustness at the cellular level and in the next chapter at the network level.

3.1 Models From the Literature

This section gathers five conductance-based models that are often used through the literature. Most of them were developed between 1990 and 2000. These models have the same architecture as Hodgkin and Huxley model with additional currents. Therefore, in order to highlight the main characteristics they are described in a similar manner (from Table 3.2 to Table 3.6);

- Name of the scientists and the related paper,
- Year of the paper describing the model,
- Origin and motivation to create the model,
- Equation of the evolution of the membrane potential written in the general form:
 $C_m \dot{V}_m = - \sum I_{ion} + I_{app}$ where I_{app} is the excitatory current,
- Number of conductances and number of leak currents,
- Simulations of the model provided in the paper,
- Generation of three firing patterns: tonic firing, PIR *i.e.* post-inhibitory rebound, HIB *i.e.* hyperpolarisation-induced bursting.

Note that to obtain different firing patterns, the excitatory current I_{app} is adapted according to Figure 3.1. This excitation is decomposed as a constant applied current I_{cst} and a step current I_{step}

such as $I_{app} = I_{cst} + I_{step}$. The detailed equations, parameter values and stimulation for each model are given in A.

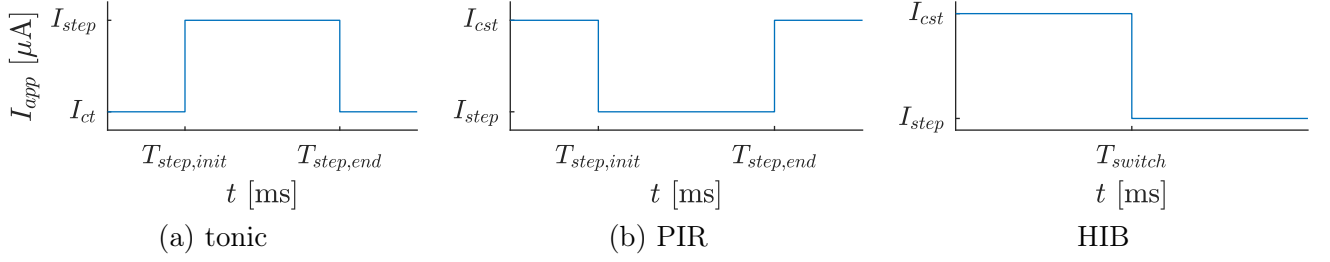


Figure 3.1 – Excitation current I_{app} pattern in order to generate the different firing patterns

The T-type calcium current has been proven to play a crucial role in the switch from tonic mode to burst mode. Therefore, we are particularly interested in the modeling of this current. Among the five listed models, we can classify them in two categories based on the kinetics of the activation gate (m_{CaT}) of this T-type calcium current (which respect the HH formalism); either the activation is *slow* or *instantaneous* (see Table 3.1).

Slow activation	Instantaneous activation
Huguenard and McCormick (1992) Destexhe (1998) Drion (2017)	Rush and Rinzel (1994) Wang (1994)
$I_{CaT} = g_{CaT} \mathbf{m}_{CaT}^a h_{CaT}^b (V_m - V_{Ca})$ $\dot{m}_{CaT} = \frac{m_{CaT,\infty} - m_{CaT}}{\tau_{m_{CaT}}}$	$I_{CaT} = g_{CaT} \mathbf{m}_{CaT,\infty}^a h_{CaT}^b (V_m - V_{Ca})$

Table 3.1 – Classification of the conductance-based models according to the kinetics of the activation gate of the T-type calcium current; slow activation (blue column) or instantaneous (gray column).

Each model is implemented in **Julia**. The equations of the neuron and their associated parameters values are retrieved from the paper. Then, they are solved numerically with Euler’s method and some parameters values are adapted to obtain the different firing patterns.

3.2 Thalamic neuron models in Julia

The five conductance-based models are translated in a Julia code. For Drion’s model, the files are available in [29]. For the other models, the different equations are extracted from the paper and translated in **Julia** language.

The architecture of the code is the same for each conductance-based model. Only the kinetics and the parameters need to be adapted separately from each model.

The simulation of a conductance-based model is divided into two files; **TC.jl** and **Simu_TC.jl**.

TC.jl

This file contains all the kinetics of each gate, the equation corresponding to the derivative of the membrane potential, the differential equations of each gate and the resolution of the various differential equations following the Euler Method. The pseudo-code is given in Appendix B.

Simu_TC.jl

This file contains all the parameters constants and simulation values. It calls **TC.jl** to obtain to time evolution of the membrane potential. The pseudo-code is given in Appendix B.

Choice of the Language

At the network level, the resolution of all the differential equations is time-consuming. Compared to Matlab, this language is much faster.

Furthermore, it was an opportunity to learn a new programming language.

Table 3.2 to Table 3.6 summarise the main characteristics of the five conductance-based models found in the literature.

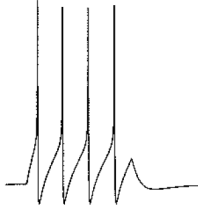
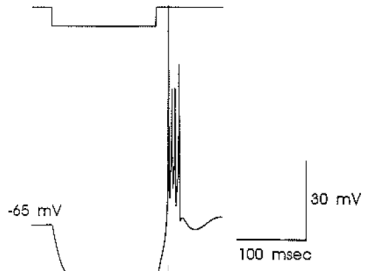
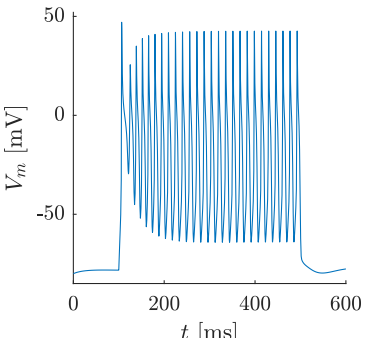
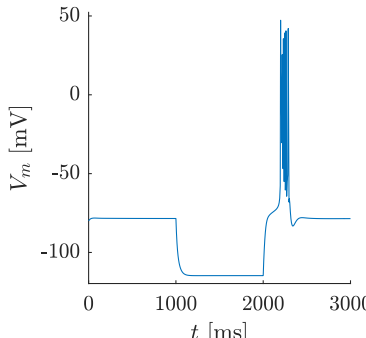
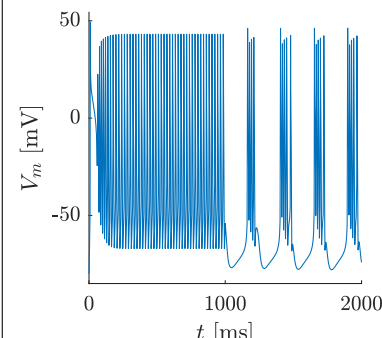
Name	HUGUENARD AND MCCORMICK [19]		
Year	1992		
Motivation	An detailed model in order to analyse each ionic contribution separately.		
Equation	$C_m \frac{dV_m}{dt} = -I_{Na} - I_{Nap} - I_L - I_{CaT} - I_C - I_A - I_{K2}$ $-I_{Kleak} - I_{Naleak} + I_{app}$ <p> I_{Nap}: depolarisation-activated sodium current I_L: high-threshold calcium current I_A: transient and depolarisation-activated potassium I_{K2}: slowly inactivating and depolarisation-activated potassium I_C: calcium-activated potassium current </p>	Nbr of conductances Nbr of leak currents	9 2
Paper simulations	<div style="display: flex; justify-content: space-around; align-items: center;"> <div style="text-align: center;"> <p>Tonic firing</p>  </div> <div style="text-align: center;"> <p>PIR</p>  </div> </div>		
Firing patterns	<p style="text-align: center;">TONIC</p> 	<p style="text-align: center;">PIR</p> 	<p style="text-align: center;">HIB</p> 

Table 3.2 – Description of the Huguenard and McCormick model - in the further sections; this model is called HM

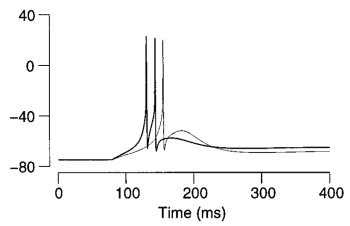
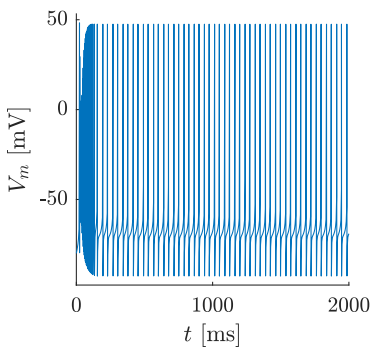
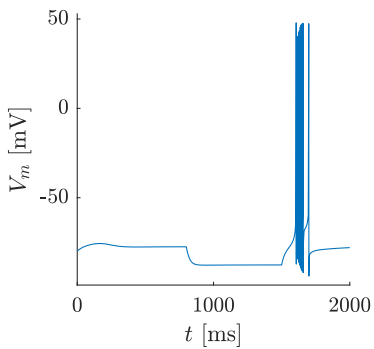
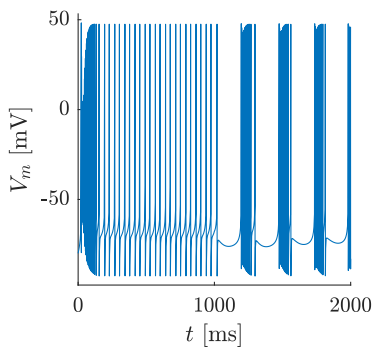
Name Year	DESTEXHE [22] 1998		
Motivation	<ul style="list-style-type: none"> - The kinetics of the Na^+ and K^+ currents are retrieved from the Traub's model. [65] - The kinetics of the T-type calcium current I_{CaT} is inspired from Huguenard and McCormick [19] but slightly modified to take into account new recording data. 		
Equation	$C_m \dot{V}_m = -I_{Na} - I_K - I_{CaT} - I_{leak} + I_{app}$	Nbr of conductances Nbr of leak currents	3 1
Paper simulations	<p>Generation of a low threshold current spike in a relay cell (Fig. 11B4 in [22])</p> 		
Firing patterns	<p>TONIC</p> 	<p>PIR</p> 	<p>HIB</p> 

Table 3.3 – Description of the Destexhe model


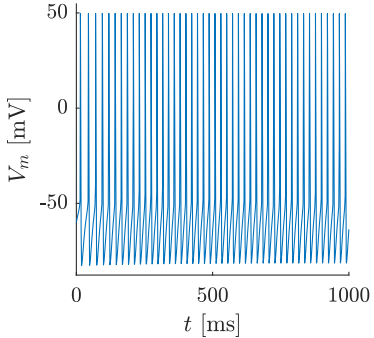
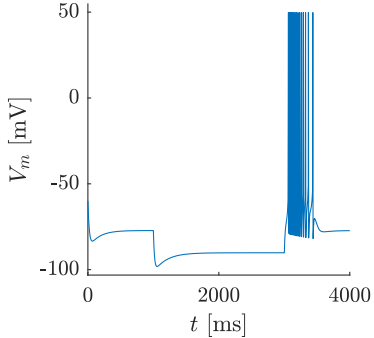
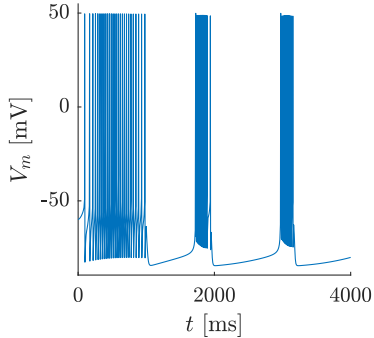
Name Year	DRAIN [29] 2017		
Motivation	Model based on phase plane analysis and the current time-scale studies		
Equation	$C_m \dot{V}_m = -I_{Na} - I_K - I_{CaT} - I_{K,Ca} - I_H - I_{leak} + I_{app}$ $I_{K,Ca}$: calcium-activated potassium current I_H : hyperpolarisation-activation cation current	Nbr of conductances Nbr of leak currents	5 1
Paper simulations	<p>PIR RB HIB</p> 		
Firing patterns	<p>TONIC</p> 	<p>PIR</p> 	<p>HIB</p> 

Table 3.4 – Description of the Drion model

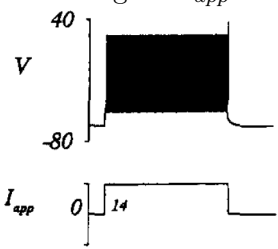
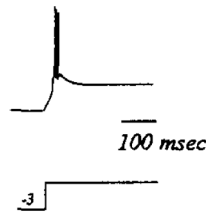
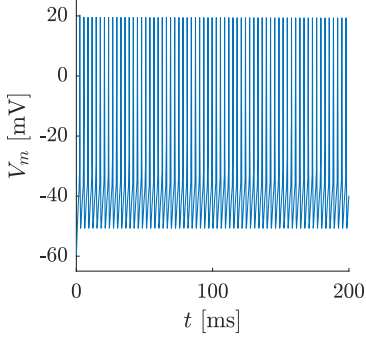
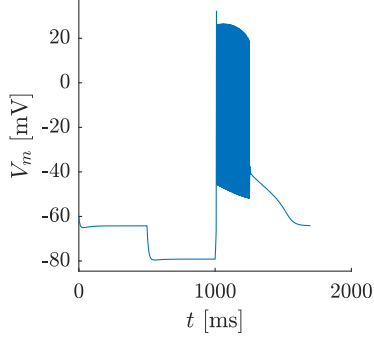
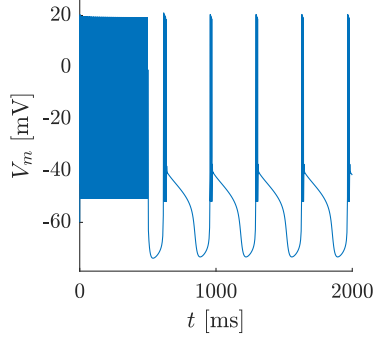
Name Year	RUSH AND RINZEL [56] 1994		
Motivation	<ul style="list-style-type: none"> - T-type calcium current realised by Wang in 1991 [68] - The activation of the T-type calcium is set at its steady-state value ($m_{CaT,\infty}$). 		
Equation	$C_m \dot{V}_m = -I_{Na} - I_K - I_{CaT} - I_{Nleak} - I_{Kleak} + I_{app}$	Nbr of conductances Nbr of leak currents	3 2
Paper simulations	<p>Tonic firing for $I_{app} = 14$</p>  <p>PIR for I_{app} switching from -3 to 0</p> 		
Firing patterns	<p>TONIC</p> 	<p>PIR</p> 	<p>HIB</p> 

Table 3.5 – Description of the Rush model - in the further sections; this model is called Rush



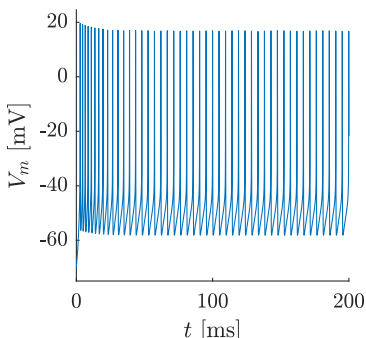
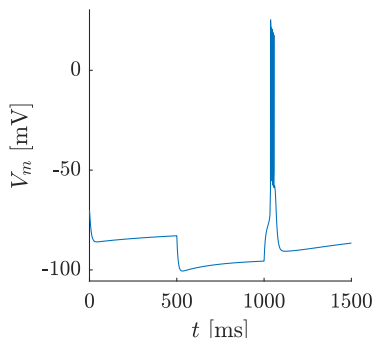
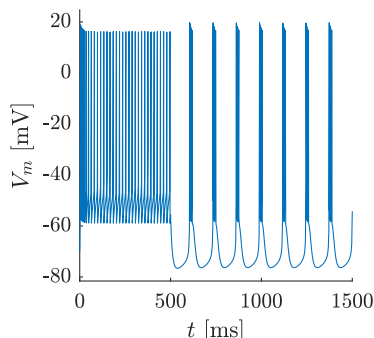
Name Year	WANG [67] 1994		
Motivation	<ul style="list-style-type: none"> - T-type calcium current realised by Wang in 1991 [68] - The activation of the T-type calcium is set at its steady-state value ($m_{CaT,\infty}$). 		
Equation	$C_m \dot{V}_m = -I_{Na} - I_K - I_{CaT} - I_h - I_{Nap} - I_{leak} + I_{app}$ I_h : hyperpolarisation-activated cation current I_{Nap} : non-inactivating sodium current	Nbr of conductances Nbr of leak currents	5 1
Paper simulations	<p>Tonic firing for $I_{app} = 3$</p>  <p>Burst firing for $I_{app} = 0.8$ (4 spikes/period)</p> 		
Firing patterns	<p>TONIC</p> 	<p>PIR</p> 	<p>HIB</p> 

Table 3.6 – Description of the Wang model

3.3 Activation of the T-type calcium channel: fast or slow?

3.3.1 Introduction

The modeling of thalamic neurons follows the Hodgkin and Huxley's procedure and integrates calcium in order to reproduce the tonic mode, the bursting mode and the switch from one mode to the other one. As it is shown in the previous section, the five models can fire in both modes and switch by fixing the parameters to a specific set of values. Thus, they mimic well the neuronal behavior at the single cell level. Therefore, they are integrated in numerous scientific research. Just to name a few, which use HM or Destexhe, there are the explanation of the thalamic neuron modeling in NEURON software (1995, [52]), the analysis of the population frequency (1996, [47]), the comparison between some compartmental models (2005, [55]) or the discussion about slow-wave sleeps (2012, [8]).

In this way, the major applications of a thalamic model are either to understand the thalamus activity at a higher level in order to study the brain rhythmicity or to deepen the knowledge in this field by applying complex mathematical tools.

However, working at a network level implies time-consuming computations which leads to a compromise; the model has to mimic the intrinsic properties of the neuron but it has to be fast and efficient. Accordingly, a *common reduction strategy* is to fix *the activation of the calcium channels to its steady-state value*. In other words, it means the activation is considered to happen very fast such as it reaches instantaneously its steady-state value.

This assumption *originates* to the comparison between the activation of Ca channels which is faster than the inactivation of Ca channels.

The major *reasons* to apply this assumption are:

- the decrease of the model complexity,
- the interest in a more quantitative description of the model rather in a qualitative one,
- the phase plane analysis requires reduced models.

Through the five selected models, Rush-Rinzel and Wang have made the assumption of the instantaneous activation of the calcium channels. After exploring the literature, Destexhe himself also wanted a minimal conductance-based model able to reproduce the different behaviors of the thalamic neuron. This minimal model follows the common reduction strategy by using the steady-state activation of the calcium current. Then, he integrated it with other minimal neuron models [54]. The motivation behind this combination of neurons is to model the entire brain which is a hot topic called the Human Brain Project [2].

Another example to highlight the tendency for quantitative models is Amarillo who studied the different physiological currents involved in the thalamus in 2014. For this biological analysis, he used an adapted version of HM and Destexhe models [7]. One year after, he wanted to perform quantitative studies and phase plane analysis [6]. He reduced his model by using the common reduction strategy. Then, he displayed similar results as Izhikevich's model which is a purely mathematical model of a neuron [42]. Likewise, Elijah illustrated the interest of applying complex mathematical tools to study thalamic neurons. He used the Wang's model in 2015 to compute the mutual information encoded in the neuron by applying Shannon's formula [32].

Browsing the different models and studies performed on the thalamic neuron through the literature shows the interest in simpler models which require *assumptions*. Nowadays scientists are working on these models, they are performing new analysis and tend to be more quantitative. However, we should take a step back and ensure that assumptions made on the models are valid.

3.3.2 Is the fast activation of the calcium channels valid?

This thesis only focuses on the assumption about the activation of the T-type calcium channels and it aims to answer the question; can we use the steady-state value of this activation or is its slow kinetics necessary in the thalamic neuron modeling?

In other words, do we have "good" thalamic neuron models? Are they able to mimic the right behavior of a thalamic neuron? Are they able to perform this particular biological feature *i.e.* to switch from tonic mode to burst mode? Do these models have a *robust* switch?

This leads to the next question: what is a robust model? According to [35], robustness means a small variation of the parameters does not disrupt the bursting pattern and the switch is not affected. In contrary, a model is fragile when small deviations from the nominal set of parameters leads to large modifications in the bursting pattern.

Franci, Drion and Sepulchre have investigated the impact of a fast or a slow kinetics of the calcium channels in a STG¹ model *at the single-cell level* [35]. The robustness property is explained with the decomposition in *negative and positive conductances at different time scales* thanks to a voltage-clamp² computational experiment.

The voltage is maintained at a constant value, then a small voltage step perturbation is applied ΔV_m at $t = 0$. The local conductance appears in the current step response $\Delta I_m(t)$ such as $\Delta I_m(t)/\Delta V_m$. It corresponds to the conductance at a given time and at a given voltage.

The STG model has a slow kinetics for the activation of the calcium channel. In the parameter space of two of the seven conductances of the model, the set of parameters corresponding to the situation (a)(resp. (b)) generates a tonic mode (resp. bursting mode) as shown in Figure 3.2 (top). When the time constant decreases (moving from the left to the right) to reach an instantaneous activation, the model is no longer able to generate a burst [35].

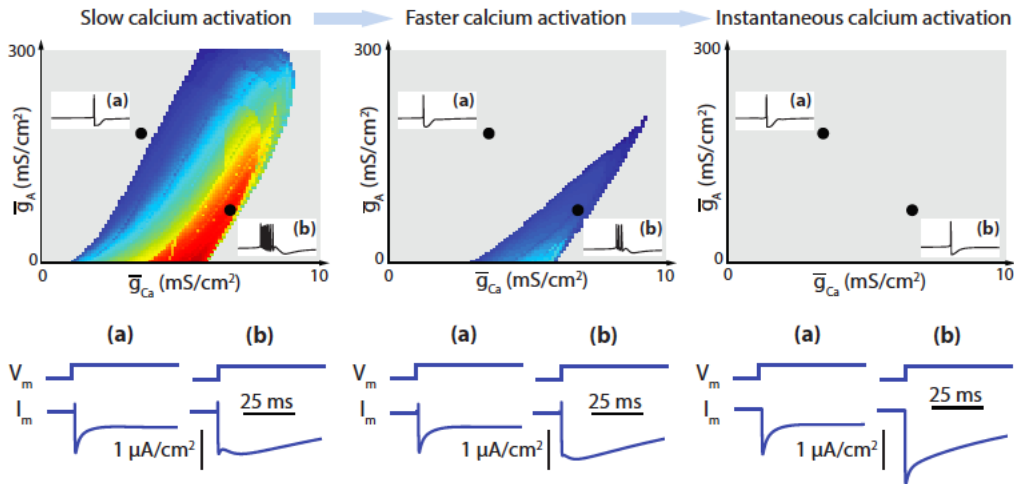


Figure 3.2 – Top: Evolution of the parameter chart as a function of the parameters \bar{g}_A and \bar{g}_{Ca} for a decreasing calcium current activation time constant. Bottom: Associated voltage-clamp experiment with the voltage step and the corresponding current response. - The region corresponding to the burst mode decreases when the time constant is reduced. For an instantaneous activation, there is only the tonic mode. The current response shows that the slow negative conductance merges with the fast negative conductance. [35]

On the current response (see Figure 3.2 (bottom)), the difference between the two modes is the presence of this *slow negative conductance*. In the tonic mode, the current step response shows a fast negative conductance followed by a slow positive conductance. It respectively corresponds to the fast activation of an inward current (sodium current) followed by the slow inactivation of sodium channels and the slow activation of an outward current (potassium current). In the bursting mode, a slow negative conductance is present resulting from the slow activation of the calcium channels. This slow negative conductance becomes faster and the slow inverse response is no more distinct from the fast

¹stomatogastric ganglion. The conductance based model contains the transient sodium current, I_{Na} , a fast depolarizing current, and the delayed-rectifier potassium current, i_K , a slower hyperpolarizing current, plus a leak current, I_L , the low-threshold T-type calcium current, I_{CaT} , the hyperpolarisation-activated cation current, I_H , and the calcium-activated potassium current, I_{KCa} .

²This technique permits to measure the ion channel kinetics. The membrane potential is fixed to a constant value and so the ionic currents can be recorded. By setting \dot{V}_m to; $I_{app} = \sum I_{ion,i}$.

one as shown in Figure 3.2 (bottom). Similarly, Figure 3.3 highlights the contribution of each current with their activation and inactivation and the corresponding time-scales. When the activation of the calcium channel is fast, it merges with activation of the sodium channel [35].

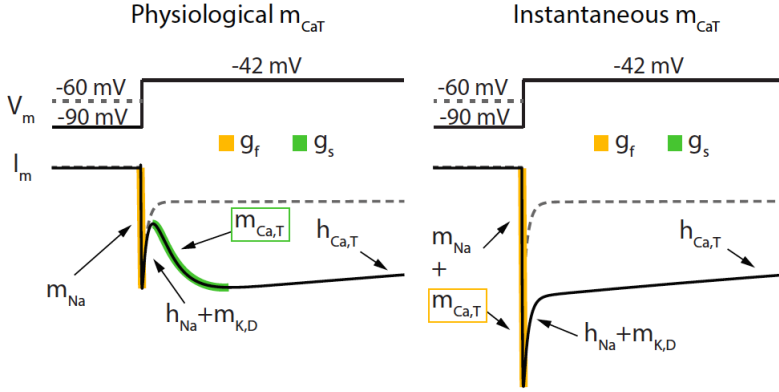


Figure 3.3 – Voltage step and its associated current response of the voltage-clamp experiment performed on the Drion's model when the activation of the calcium current is slow (left) or instantaneous (right) . When the activation of the calcium current is considered as instantaneous, The distinction between the slow negative conductance and the fast negative conductance associated to the fast activation of the sodium channel disappears [29]

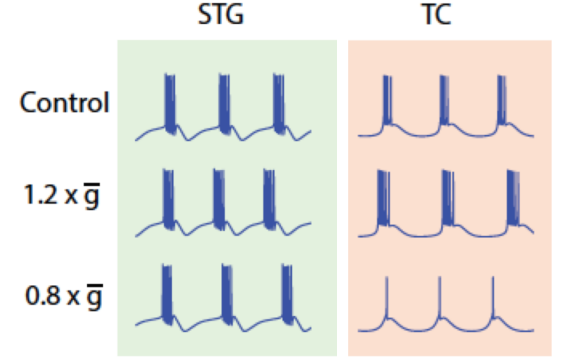


Figure 3.4 – Time evolution of the membrane potential in a burst mode for the STG model (on the left) and for the Wang model (on the right). The maximal conductances are scaled *i.e.* the capacitance value is changed to -20% and +20% - The STG model is robust to this perturbation; his firing pattern is maintained. The Wang's model which lacks of a slow negative conductance cannot handle this perturbation. His bursting pattern is destroyed [35]

This slow negative conductance is necessary to have a *robust* bursting model *i.e.* when some parameter perturbations are added to the model, it still generates the same bursting patterns. To illustrate this property, the STG and Wang's models, which generate burst for the nominal parameter set, undergo a simple computational experiment. A uniform scaling of all maximal conductances is added. Mathematically it is equivalent to scale the capacitance C . Figure 3.4 displays the evolution of the bursting pattern subjected to parameter perturbations for the STG and the Wang's models (TC). This thalamic model lacks the slow negative conductance (as described in Section 3.1) and it is no more able to reproduce its initial bursting pattern by contrast to the STG model [35].

3.4 Thalamic Neuron Models: Robustness Analysis at the Single Cell Level

This thesis is dedicated to thalamic neuron models. Therefore, we reproduce the same computational experiment which has been carried out on the STG model and Wang model on Destexhe, Drion, HM and Rush-Rinzel models. The goal is to discover the robustness or the fragility of each model at the single cell level when it is subjected to a uniform scaling of all maximal conductances.

3.4.1 Procedure

Each model is simulated with the capacitance equal to +20% and - 20% from its initial value, all the other parameters being conserved. For example, if $C_m = 1$, the model is simulated with $C_m = 0.8$ and $C_m = 1.2$.

3.4.2 Results

According to Figure 3.5, Destexhe, Drion and HM are still able to fire in tonic mode and then to switch in burst mode. They are robust to the perturbation. Unlike Rush and Rinzel model, there is no more firing pattern when the capacitance C_m is increased of 20%. Wang's model also loses its ability to burst when the capacitance is decreased of 20% (see Figure 3.4). So, these models cannot handle a small perturbation.

In order to highlight the responsibility of the fast negative conductance in the fragility of Rush-Rinzel's model, we create a *modified version* of this model called RushCa (see Table 3.7). The assumption of an instantaneous activation of the calcium channel ($m_{CaT,\infty}$) is removed and the activation recovers a slow activation. It means that two new equations are added; one for the dynamics of the activation gate m_{CaT} and another for its associated time constant $\tau_{m_{CaT}}$. As explained in Section 3.1, Rush-Rinzel used the T-type calcium current of the Wang's model (1991, [68]) and changed the slow activation to a fast one. The modified model conserves the primarily version without the common strategy.

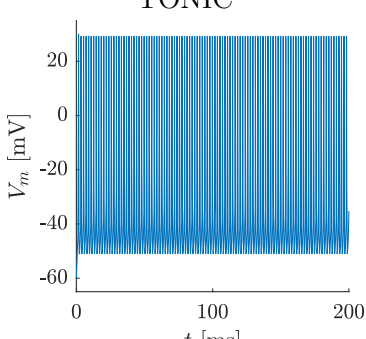
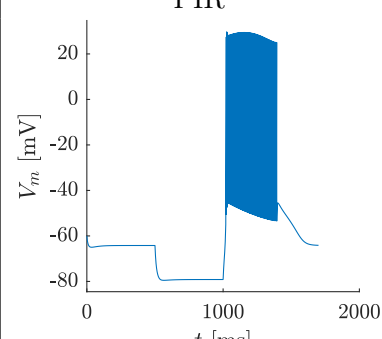
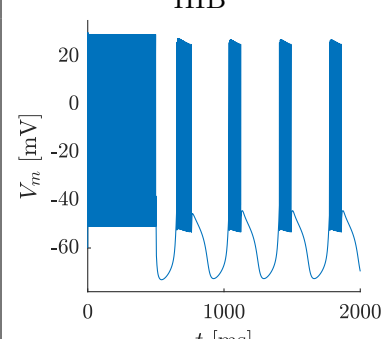
Name	RushCa		
Year	2018		
Motivation	- Rush and Rinzel's model with the initial slow activation of the T-type calcium from Wang's model in 1991 [68]		
Equation	$C_m \dot{V}_m = -I_{Na} - I_K - I_{CaT} - I_h - I_{Nap} - I_{leak} + I_{app}$	Nbr of conductances	5
		Nbr of leak currents	1
Firing patterns	<div style="text-align: center;">TONIC</div> 	<div style="text-align: center;">PIR</div> 	<div style="text-align: center;">HIB</div> 

Table 3.7 – Description of the RushCa's model

This small alteration is sufficient to make the model robust to a small perturbation. Indeed, the new version of the Rush-Rinzel model still switches and the firing pattern is not affected by the perturbation, contrarily to the initial model.

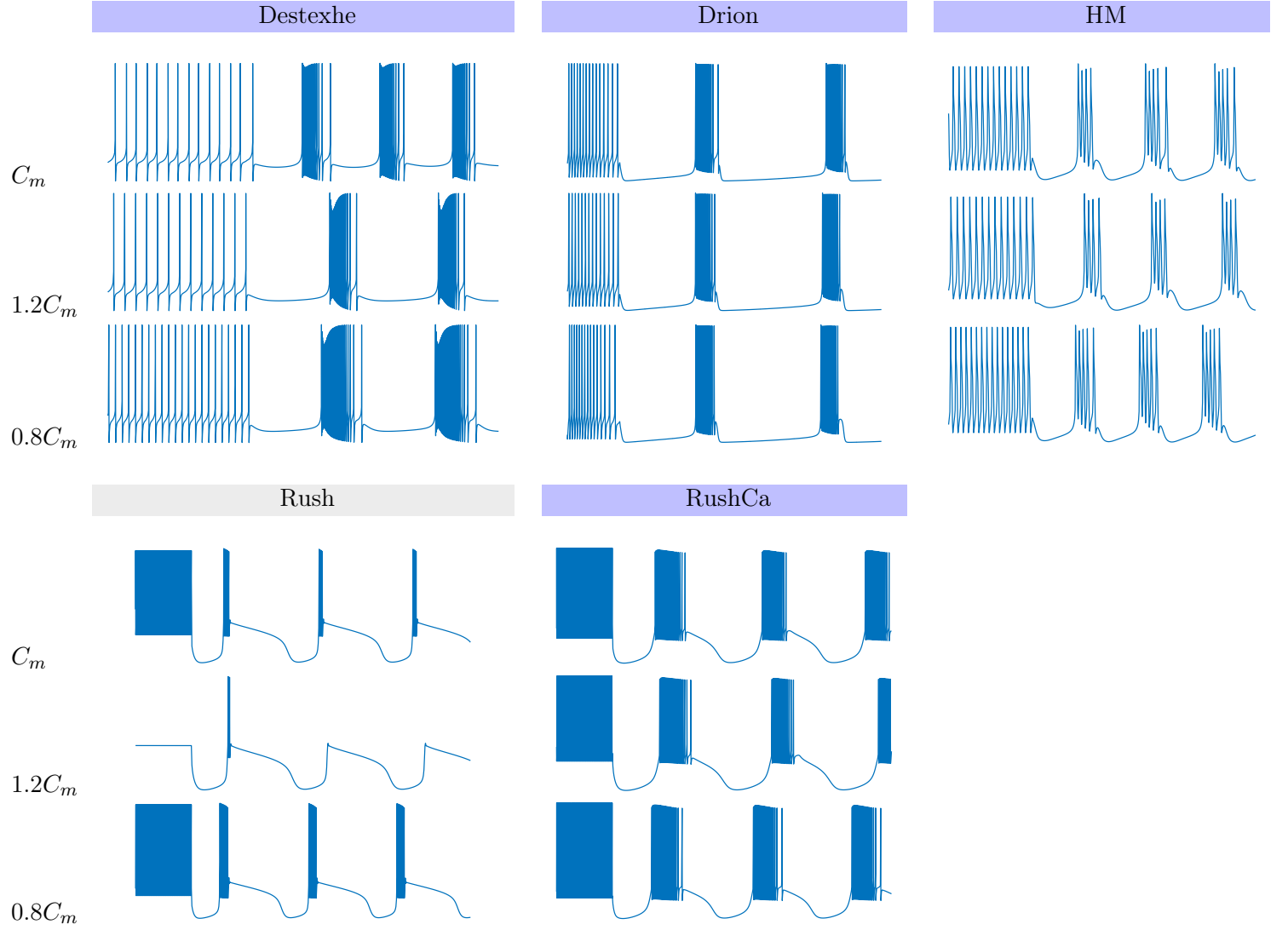


Figure 3.5 – Time evolution of the membrane potential in HIB when all maximal conductances are uniformly scaled *i.e.* when the capacitance is modified. Top: C - Center: $1.2C$ - Bottom: $0.8C$. A blue cell corresponds to a model which integrates the slow activation of the calcium channel while the gray cell indicates the model which lacks the slow kinetics.

Rush model which lacks the slow negative conductance is the only fragile model. RushCa model has turned the instantaneous activation of the calcium current into a slow activation, and it is robust to the perturbation.

3.4.3 Discussion

The slow activation of the T-type calcium current is mandatory in thalamic neuron model in order to have a *robust* model at the single cell level.

Through the literature, it has been shown that the calcium current is considered as a *slow* current. In 1987, Carbone recorded the calcium current in rat cells and fitted an activation time constant from his experiments [11]. Similarly, in 1989, Coulter claimed that this T-type calcium current is modelled in an analog manner as the sodium current but with a slower kinetics [16]. Indeed, as shown in Figure 3.6, the activation fitted by Carbone is around 10-50 [ms] for low voltage value.

Nowadays, this slow activation is often disregarded. Indeed, it is widespread that the activation of calcium channels is considered in the same time scale as the activation of sodium channels, for example in Izhikevich's book [42]. It is a common strategy to reduce the number of variables and so decrease the computation time and the complexity of the model.

However, this *computational experiment* highlights the robustness of HM, Drion and Destexhe models and the fragility of Rush-Rinzel and Wang models. This experiment is based on the scaling of the maximum conductances. It can be seen as a *neuromodulation* study. In reality, neuromodulators modulate the firing pattern by varying the density of ion channels [66]. Therefore, a "good" model has to handle the impact of neuromodulators. The most remarkable result is the robustness improvement for Rush-Rinzel's model when the slow activation is recovered.

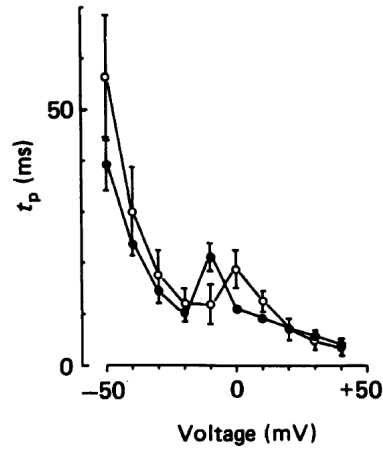


Figure 3.6 – Recordings of the activation of the T-calcium current as a function of the voltage in two different animal cells [11]

3.5 Summary

STATE OF ART

Model	Destexhe	Drion	HM	Rush	Wang
year	1998	2017	1992	1994	1994
Nbr. conductances	3	5	9	3	5
Nbr. Leak currents	1	1	2	2	1
m_{CaT}	slow	slow	slow	steady-state	steady-state
Firing patterns	Each conductance-based model is able to reproduce a tonic mode, PIR and HIB.				

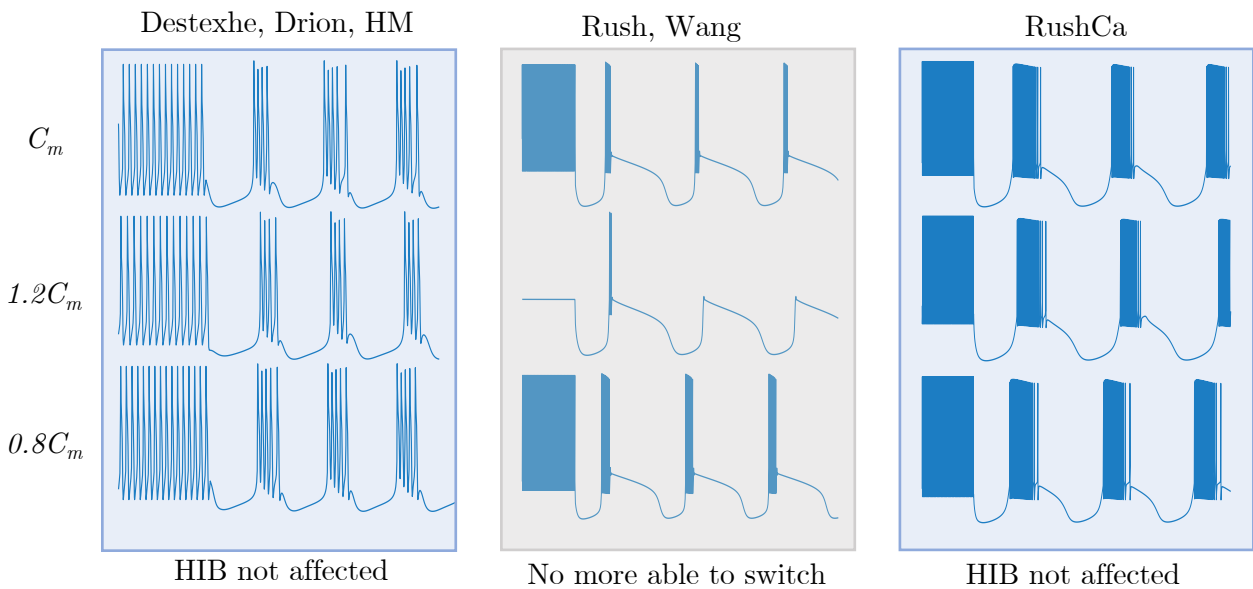
Activation of the T-type calcium current: slow or fast ?



Slow activation brings cellular robustness

CONTRIBUTIONS

Cellular robustness analysis: Alteration of the capacitance



Creation of a modified version of Rush:

The steady-state activation $m_{CaT,\infty}$ is changed by a slow activation

Chapter 4

Thalamic neuron models at the network level

4.1 Introduction

As described in Section 2.3.2, the thalamus is state-dependent, exhibiting population waves with a small amplitude and a high frequency during wakefulness in contrast with the high amplitude and small frequency signal during sleep. The difference from one state to another originates from the tonic to burst switch at the cellular level which is manifested by the hyperpolarise-induced bursting. This biological feature leans on the switching "on" of the slow negative conductance in the model which corresponds to the *slow deinactivation* of the T-type calcium channels (as discussed in Section 2.3.3) [29].

The behavior of the neurons *population* relies on their connections. These connections correspond to an excitatory inhibitory (E-I) network as displayed between the relay cells and the reticular nucleus cells for example (see Section 2.3.4). The cellular switch induces a rhythmic synchronisation in this larger population. The neuronal excitability switches from greatly reactive to synaptic inputs ("awake state") to favorable to synchronisation ("asleep state") [29].

The previous section has focused on the single cell level. The *slow* activation of the calcium channels has been recognised necessary to generate a *robust* switch [35]. This section is dedicated to study the impact of this kinetics at the network level and so to investigate the robustness of the thalamic neurons models. Moving to a larger scale, the robustness signification has to be enlarged. Indeed, in network, the neurons are submitted to perturbations such as neuromodulation and the synaptic plasticity. Therefore, studying the robustness of a model at the network level requires computational experiments which reproduce this variability present in real networks.

4.2 Impact of the instantaneous activation of the calcium channels on the synchronisation of two cells

Drion continues the analysis concerning the kinetics of the activation of the calcium channels at the network level in [29]. The rhythmicity of the network is studied in *his* model with or without this slow kinetics. To do so, a 2-cells network is created with two different cells from his model *i.e.* both cells follow his model dynamics but have a different maximum conductance of the T-type calcium current. When the cells are not connected, they are both able to generate a hyperpolarisation-induced bursting as illustrated in Figure 4.1. However, the two cells generate different rhythms and fire at different instants [29].

Then, the two neurons are connected in an E-I circuit thanks to two synaptic connections (AMPA and GABA_A). The network displays a strong *synchronisation* in the bursting mode; the burst firing occurs at the same instant in both cells (see Figure 4.2 on the left). In order to highlight the role of the slow activation of the calcium channel, this activation is set at its steady-state (the other kinetics

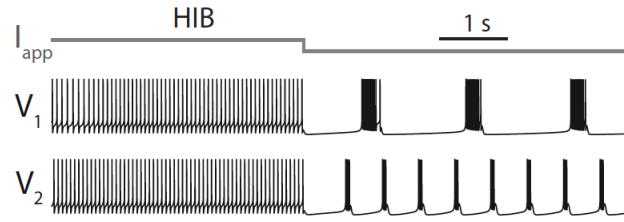


Figure 4.1 – HIB response of two cells for different parameters values [29].

and parameters being the same). The outcome is strongly affected; the burst synchronisation does not exist any more (see Figure 4.2 on the right) [29].

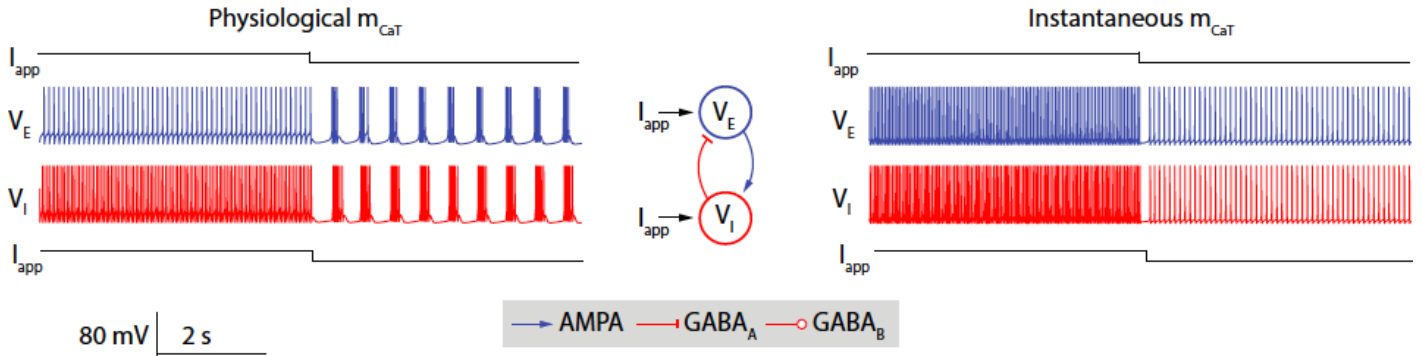


Figure 4.2 – 2 cells connected with two synaptic connections ($AMPA$ and $GABA_a$) to obtain a E-I network are excited by a hyperpolarised current. - The model which lacks the slow activation of the calcium current (right simulations) does not switch from tonic to burst) [29]

The second experiment is to connect the two same cells in a E-I network with three synaptic connections ($AMPA$, $GABA_A$ and $GABA_B$) and to only stimulate the inhibitory cell with a hyperpolarised current. This hyperpolarisation leads to a switch in the network activity and a synchronisation (see Figure 4.3 on the left), while when the activation of the calcium channel is instantaneous, there is no more synchronisation (see Figure 4.3 on the right) [29].

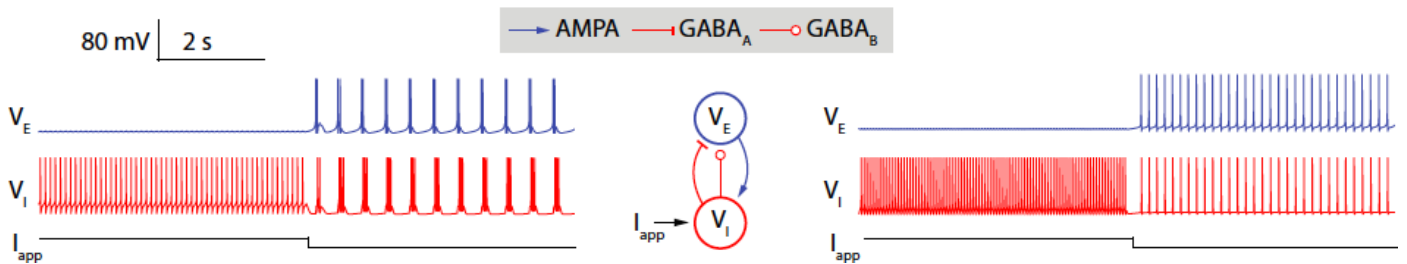


Figure 4.3 – 2 cells are connected with three synaptic connections ($AMPA$, $GABA_a$ and $GABA_b$) to obtain a E-I network. A hyperpolarised current is applied to the inhibitory cell. - The model which lacks the slow activation of the calcium current (right simulations) does not switch from tonic to burst[29].

These two figures highlight the crucial role of the slow kinetics of the activation of the calcium channels in this model. It guarantees a network switch and a synchronous bursting. In other words, it ensures a *rhythmic network activity*. Therefore, this thesis aims to extend this analysis to the other conductance-based models found in the literature.

4.3 ANALYSIS OF ROBUSTNESS

4.3.1 State-of-art

At the cellular level, the robustness of a thalamic neuron model is studied through its ability to generate the switch while it is subjected to perturbations. The bursting pattern must not be affected by the uniform scaling of the maximal conductances (see Section 3.4).

At the network level, the neurons are exposed to regulatory mechanisms such as *neuromodulation* or *synaptic plasticity*. On the one hand, neuromodulators vary the membrane properties. And on the other hand, the synaptic plasticity affects the synaptic strength between the cells. However, the switch and the synchronisation of the cells coexist with these phenomena [29].

From a modeling point of view, a robust model integrated in network must be able to handle theses regulatory mechanisms and continue to switch and synchronously burst. The robustness to neuromodulation will be studied by adding some perturbations on the maximal conductances and the capacitance *i.e.* on the *intrinsic parameters*. Similarly, the robustness to synaptic plasticity will be studied by adding some perturbations on the synaptic connections *i.e.* on the *extrinsic parameters*.

Drion performs this computational experiment in order to study the robustness of his model. He keeps the same 2-cells E-I circuit for 1000 networks and he adds variability on the maximal conductances of the ionic currents and on the synaptic conductances [29].

From a simulation point of view, the intrinsic perturbation means that each cell is not computed from the nominal maximal conductance value but with new maximal conductance value chosen randomly with a uniform distribution in the range given in [29]. Then, the extrinsic perturbation corresponds to the variability applied on the synaptic conductances. The synaptic current representing the connection is described by the following equation:

$$I_{syn} = g_{syn} m_{syn} (V_m - V_{syn}) \quad (4.1)$$

where g_{syn} is the synaptic weight, m_{syn} corresponds to the kinetics of AMPA, GABA_A and GABA_B connections and V_{syn} is the receptor reversal potential. The synaptic weights are taken randomly following a uniform distribution around a central value: $\bar{g}_{syn} = \bar{g}_{syn,central} \pm \bar{g}_{syn,central}/8$. The receptor reversal potentials are respectively $V_{syn,AMPA} = 0[\text{mV}]$, $V_{syn,GABA_A} = -70[\text{mV}]$ (equal to the chloride reversal potential) and $V_{syn,GABA_B} = -85[\text{mV}]$ (equal to the potassium reversal potential) (see Section 2.3.4 as a reminder).

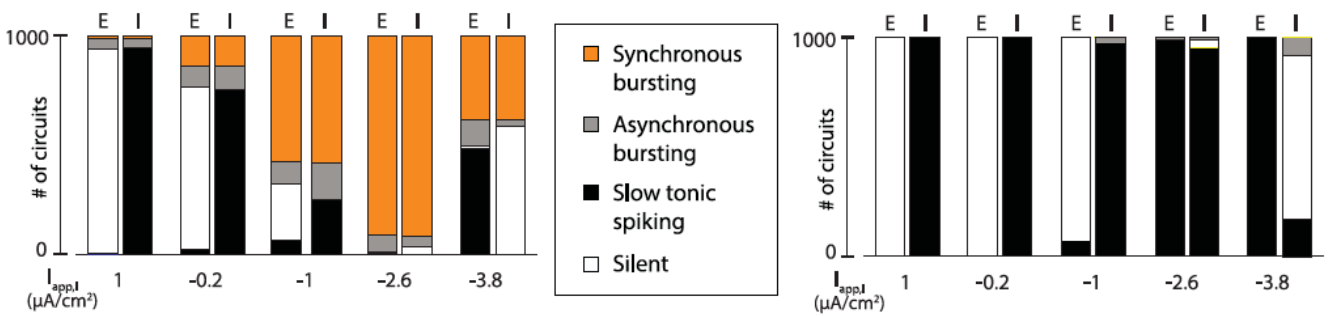


Figure 4.4 – Number of rhythmic network activities for 1000 networks subjected to variability on the conductances and on the synaptic connections. For five different values of the excitatory current, the firing pattern of the 2 cells is determined; cells are either silent (white), spiking slowly (black), bursting asynchronously (grey) or involved in a synchronous bursting rhythm (orange). - Comparison between the firing patterns of the same model with and without the slow activation of the T-type calcium channel. The model which has an instantaneous activation never display a network which switches in synchronous bursting mode. [29]

The result between the Drion's model with or without the slow kinetics of the activation of the calcium channels is once again more marked. Figure 4.4 shows that when the injected current is equal to $1 [\mu\text{A}/\text{cm}^2]$, the inhibitory cell is depolarised and so in tonic mode while the excitatory cell is

silent (the same behavior as in Figure 4.3). Then, the injected current is reduced which leads to the hyperpolarisation of the inhibitory cell. In the case where the physiological activation of the calcium channels is taken into account (see Figure 4.4 (left)), both neurons start to synchronise. For example, for $I_{app} = -2.6 [\mu \text{ A/cm}^2]$, more than 90% of networks have switched and are synchronous bursting. Therefore, the *circuit rhythm* in this model is well independent on the intrinsic and extrinsic parameters since it is almost *blind* to the variability. On the contrary, in Figure 4.4 (right), the model which has set the activation to its steady-state value is fragile and the robustness is lost. There is no network rhythmic activity found for the explored range of parameters [29].

Drion has shown the robustness of his model by emphasizing the critical role of the physiological activation kinetics of the T-type calcium current. He has also shown the fragility of his modified model when the activation is instantaneous.

4.3.2 Computational Procedure

Based on [29], the major contribution of this thesis is to reproduce a similar computational experiment for the conductance-based models selected in the literature. Therefore, the models of Destexhe, Drion, HM, Rush, RushCa and Wang will be subjected to intrinsic and extrinsic perturbations. The expected result is to highlight the robustness of Destexhe, HM and RushCa’s models like Drion’s model in contrast with the fragility of Rush and Wang like the modified version of Drion’s model.

For each model, two cells are connected in an E-I network and are subjected to extrinsic and intrinsic perturbations. Then, among 100 networks, the number of networks which have switched and have been synchronously bursting are computed *i.e.* the *rhythmic network activity* is analysed.

Each model can be summarised with its main equation:

$$C_m \dot{V}_m = -I_{ion} + I_{app} + I_{syn}$$

where the intrinsic perturbations act on C_m and on the maximum value of the n conductances $\bar{g}_{ion,i}$ in $I_{ion} = \sum_{i=1}^n \bar{g}_{ion,i} m_{ion,i}^a h_{ion,i}^b (V_m - V_{ion,i})$ and the extrinsic perturbations act on g_{syn} in $I_{syn} = g_{syn} m_{syn} (V_m - V_{syn})$

Following the Julia code used in [29], the conductance-based model of Drion is replaced by the tested model. Then, the *synaptic connections* as well as the *extrinsic perturbations* are exactly the same as in the paper. In this experiment, the synaptic perturbation is *always* present.

The *intrinsic perturbations* chosen in [29] must be adapted. Indeed, these perturbations come from the random choice of the maximal conductances in ranges subjected to different relative variability (see Table 4.1). Drion has chosen these ranges to have a wide exploration of the parameters. Since the

Conductance $g_{ion,i}$	g_{Na}	g_K	g_{CaT}	g_{KCa}	g_H	g_{leak}
Nominal value [mS/cm^2]	170	40	0.55	4	0.01	0.3025
Range	[135, 205]	[20, 60]	[0.375, 0.725]	[3, 5]	[0.0095, 0.0105]	[0.0475, 0.5575]
Relative variability [%]	20.6	50	31.8	25	5	84.3

Table 4.1 – Nominal values of the conductances used in [29], their associated ranges of variation and the relative variability.

models differ in terms of number of ionic currents, kinetics and parameter values, keeping the ranges chosen by Drion is impossible. For example, HM has more conductances than Drion and so the question would be; which value of the relative variability should be used for these new ionic currents. Therefore, in order to reproduce the same general procedure in all the models, the maximal conductance values $\bar{g}_{ion,i}$ and the capacitance C_m are picked randomly following a uniform distribution in ranges subjected to same *relative intrinsic variability*, noted γ and expressed in %. This change in parameters values corresponds to the *intrinsic variability*.

The robustness comparison through all the models is achieved by deriving the evolution of the percentage of networks that have *switched from tonic to bursting and generated a synchronous bursting* (noted y in %) for a increasing relative intrinsic variability (noted γ in %). This variability is applied on all the maximal conductances and the capacitance while the extrinsic variability always exerted on the synaptic connections. In other words, the robustness of each model is brought to light by computing the evolution of the *number of rhythmic network activities* (y) as a function of the intrinsic relative variability (γ).

The procedure to obtain the percentage of rhythmic network activities (y) is the following:

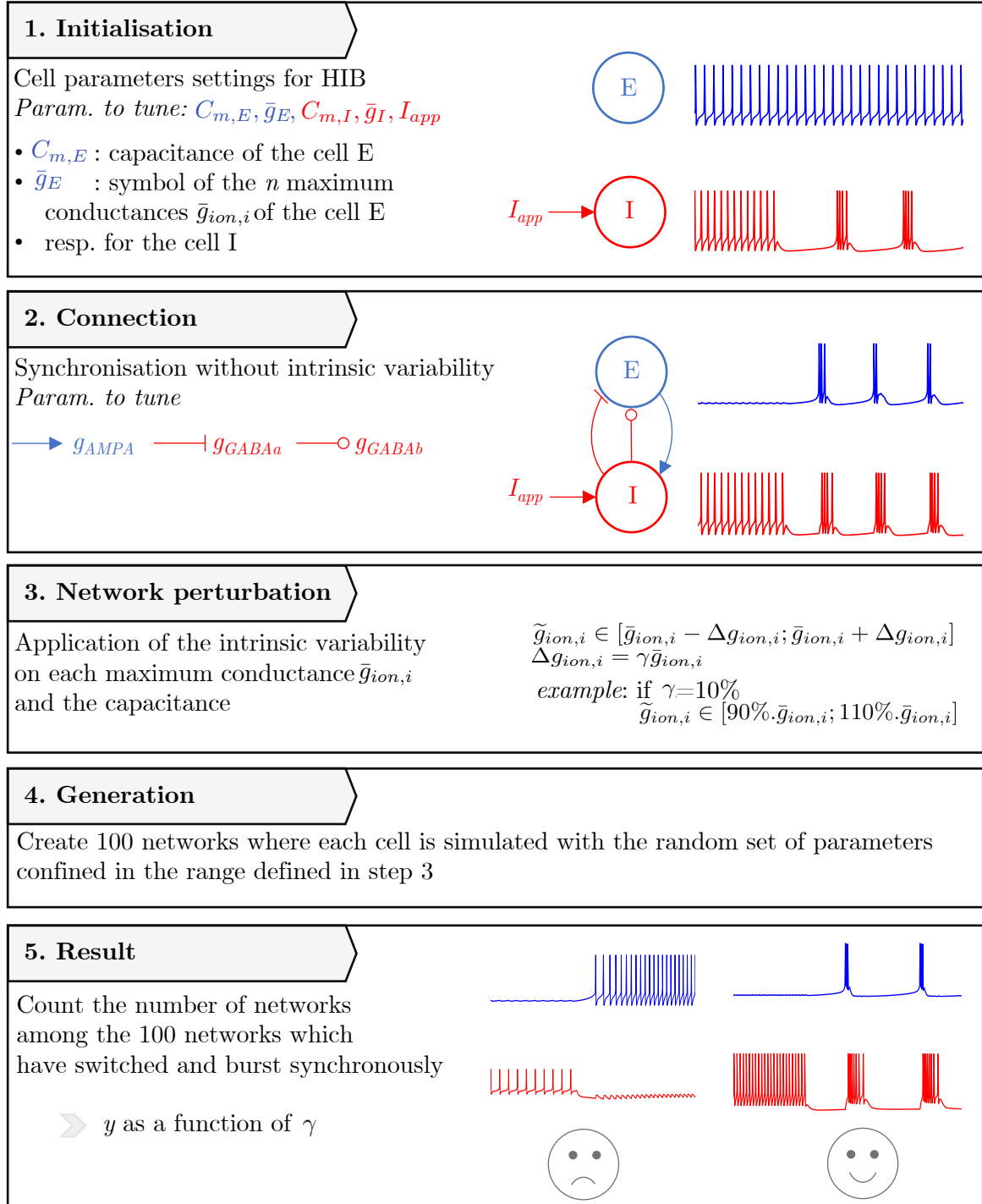


Figure 4.5 – Procedure to obtain the percentage of rhythmic network activities decomposed into 5 steps.

This procedure can be seen as an exploration in the set of parameters. For a hypothetical model with three maximum conductances ($\bar{g}_1, \bar{g}_2, \bar{g}_3$), the exploration of parameters due to the applied relative variability on the nominal values can be drawn as a sphere¹ (see Figure 4.6). The orange area corresponds to the set of parameters which lead to a rhythmic network activity (*i.e.* a network able to switch and burst synchronously).

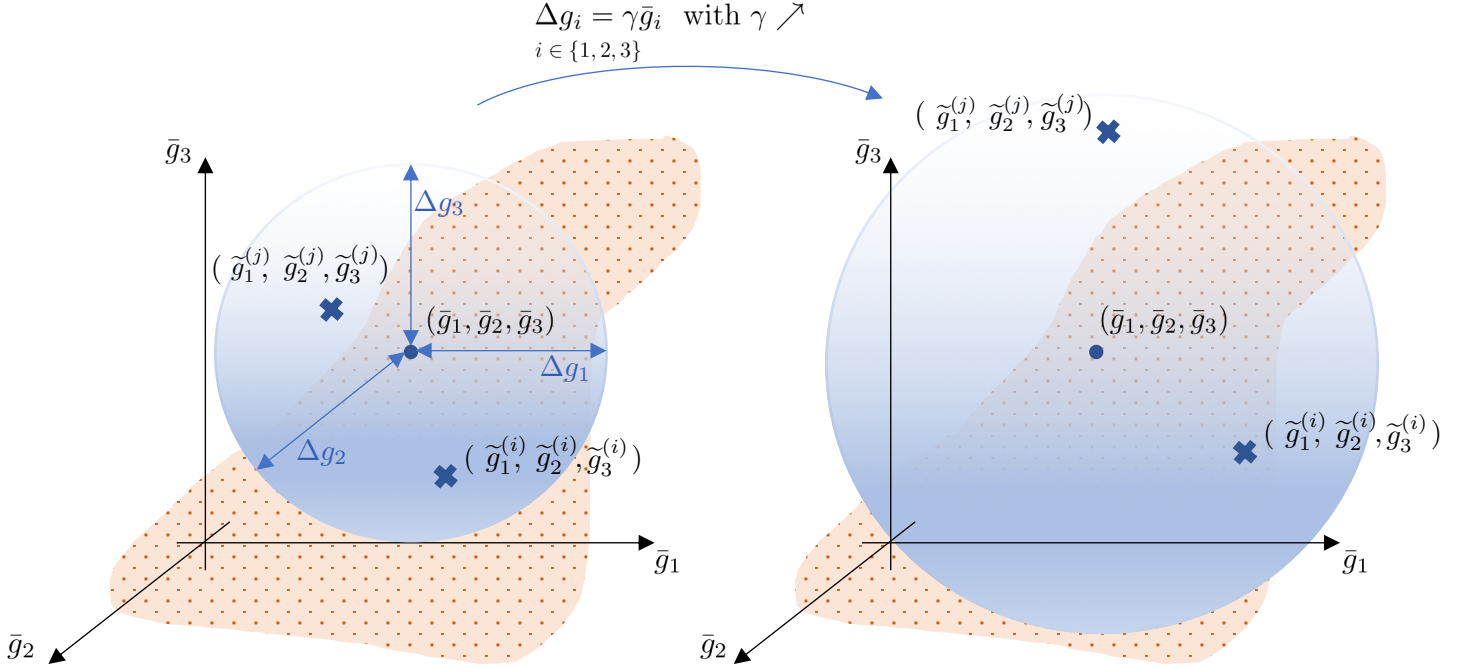


Figure 4.6 – Exploration of the parameters in a theoretical conductance based model with 3 conductances. The nominal value of each conductances is (g_1, g_2, g_3) . The exploration of the parameters is seen as an exploration inside the blue sphere. The chosen set for the network i (resp. j) is $(\tilde{g}_1^{(i)}, \tilde{g}_2^{(i)}, \tilde{g}_3^{(i)})$ (resp. $(\tilde{g}_1^{(j)}, \tilde{g}_2^{(j)}, \tilde{g}_3^{(j)})$). The orange area is the set of parameters which permits the network to switch and have a synchronised bursting mode. (On the right), the sphere grows due to the increasing intrinsic relative variability (γ).

Due to the randomness, the set can be located in the orange area. It corresponds for example to the network i computed for the set of maximal conductances $(\tilde{g}_1^{(i)}, \tilde{g}_2^{(i)}, \tilde{g}_3^{(i)})$. This network i will switch and it will synchronously burst. In a bad case, the set is located in a wrong zone (as the network j associated to the set $(\tilde{g}_1^{(j)}, \tilde{g}_2^{(j)}, \tilde{g}_3^{(j)})$). This network j will not switch or it will not generate a synchronously bursting mode.

When the relative variability increases, the sphere becomes larger. This allows a wider exploration of parameters sets. Therefore, a *robust model* corresponds to a model with a large orange area. Even for a large parameter exploration, the probability of picking a set in the orange area is high. In opposition, the orange area is small for a fragile model. When the variability increases, the network is more likely driven by a set of parameters which does not lead to a switch or synchronous bursting.

The conductance-based models studied are a higher dimensional order. Destexhe has 4 conductances, Rush and RushCa have 5, Drion and Wang have 6 and HM has 11, in addition to the capacitance. Therefore, the sphere in 3D becomes a higher dimensional solid.

The evolution of the percentage of networks that have made the switch to synchronous bursting as a function of the relative intrinsic variability is given in Figure 4.8. This result is analysed in the following section.

¹the sphere volume is used to ease the graphical representation. The possible 3D volume domain is a parallelepiped with the size of the edges equals to $\bar{g}_1, \bar{g}_2, \bar{g}_3$.

A question arises from this procedure: what is the influence of the nominal values of the maximal conductances and the capacitance ?

Using the 3D sphere illustration, Figure 4.7 shows the initial nominal values $(\bar{g}_1, \bar{g}_2, \bar{g}_3)$ and the same set but shifted (g_1^*, g_2^*, g_3^*) . The initial set is located too close to the boundary of the orange volume. Therefore with the added variability, a network has more chance to pick a wrong set and will not be able to switch or to produce a synchronous bursting. In the opposite, for (g_1^*, g_2^*, g_3^*) centered in the orange volume, the intrinsic variability will not disrupt the switch and the synchronous bursting. By consequent, in order to evaluate the impact of the nominal values; the steps 3 to 5 of the procedure are reproduced for *off-centered nominal values*. These new nominal values are randomly picked with a uniform distribution in a range of 5% from its initial values (denoted $g_{ion,i}^*$).

The maximal ionic conductances are now chosen in this interval: $\tilde{g}_{ion,i} \in [g_{ion,i}^* - \Delta g_{ion,i}^*; g_{ion,i}^* + \Delta g_{ion,i}^*]$ with $\Delta g_{ion,i}^* = \gamma g_{ion,i}^*$.

However, one constraint is fixed: the set of the off-centered nominal values must provide 100% of switching networks when there is no intrinsic variability *i.e.* $\gamma = 0\%$. Thus, hundred 2-cells networks are tested only with extrinsic variability and if the set gives at least one non-switching network, the set is rejected. In the sphere analogy, this ensures that (g_1^*, g_2^*, g_3^*) is in the orange area to start the analysis.

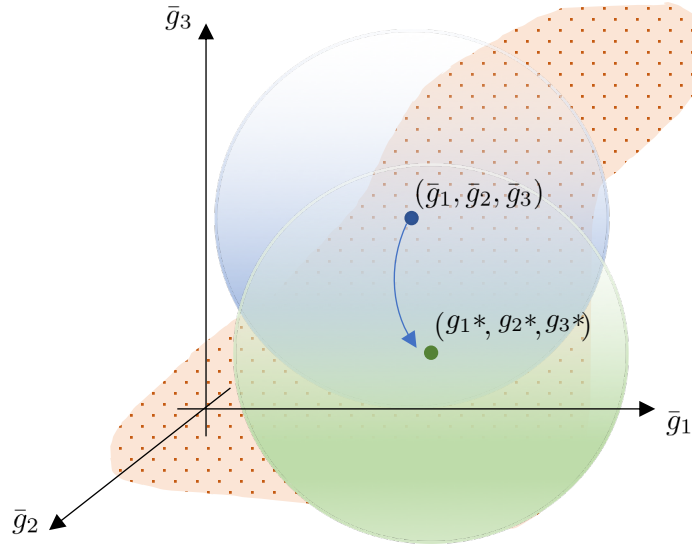


Figure 4.7 – The center of the blue sphere is the nominal set of conductances $(\bar{g}_1, \bar{g}_2, \bar{g}_3)$. By off-centering this set, the green sphere might be better located in the orange area with the off-centered set of parameters (g_1^*, g_2^*, g_3^*) as the new center.

This off-centering operation is repeated three times ² for each model and compared to the result obtained previously with the initial nominal values (see Figure 4.9).

Finally, the mean of the off-centering operation is computed in order to have one final curve per model. Figure 4.10 concludes the analysis of the rhythmic network activities when the intrinsic relative variability increases.

4.3.3 Results

Rhythmic network activity computed with the nominal values

This computational experiment shows as expected that the number of rhythmic network activities decreases with an increasing intrinsic variability (see Figure 4.8). However, depending on the model,

²Only three times because the experiment is time-consuming. It has to be reproduced in the six models. Obviously, to obtain more accurate results, more off-centering tests should be performed. However, three curves allow for a preliminary representation.

the diminution is greatly different. The rating according to the robustness between the different models for a low variability ($\gamma < 15\%$):

$$\text{Drion} > \text{Destexhe} > \text{Wang} > \text{RushCa} > \text{Rush} > \text{HM}$$

and for a high variability ($\gamma \in [15\%; 30\%]$):

$$\text{Drion} > \text{Destexhe} > \text{RushCa} > \text{HM} > \text{Rush} > \text{Wang}$$

The Drion's model is remarkably robust. Indeed, for a relative intrinsic variability equals to 30%, the percentage of rhythmic networks is above 90%. In contrast, for HM, Rush and Wang, less than one in five networks is still able to switch and burst synchronously.

An interesting feature happens when no intrinsic variability is added in the model, which corresponds to the point $\gamma = 0\%$. The six models have 100% of rhythmic networks even if they are subjected to synaptic variability. By consequent, the extrinsic perturbation does not really change the robustness of the model.

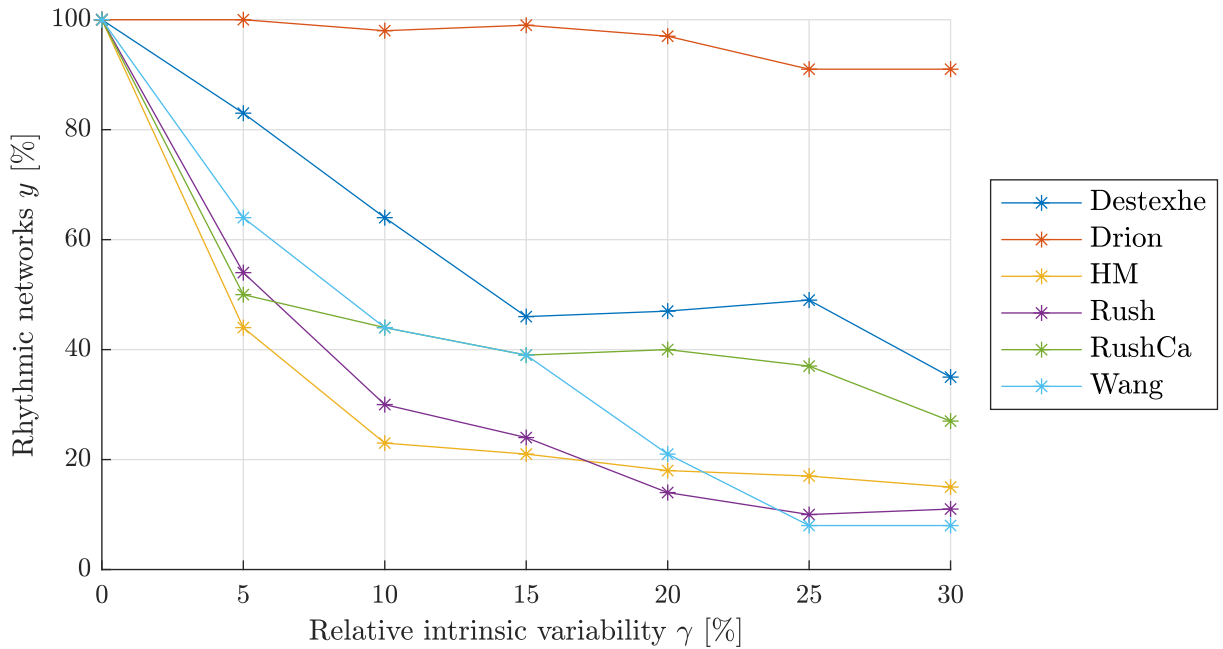
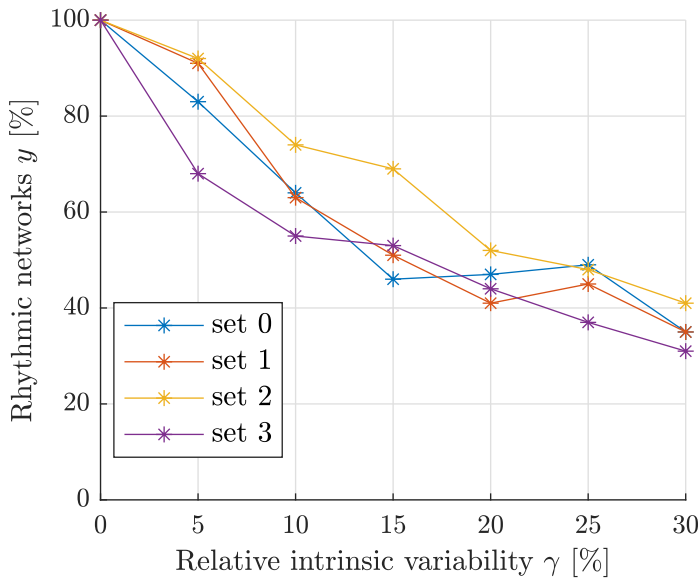


Figure 4.8 – Evolution of the percentage of rhythmic networks as a function of the relative intrinsic variability for the different conductance-based models computed with the nominal values of the intrinsic parameters.

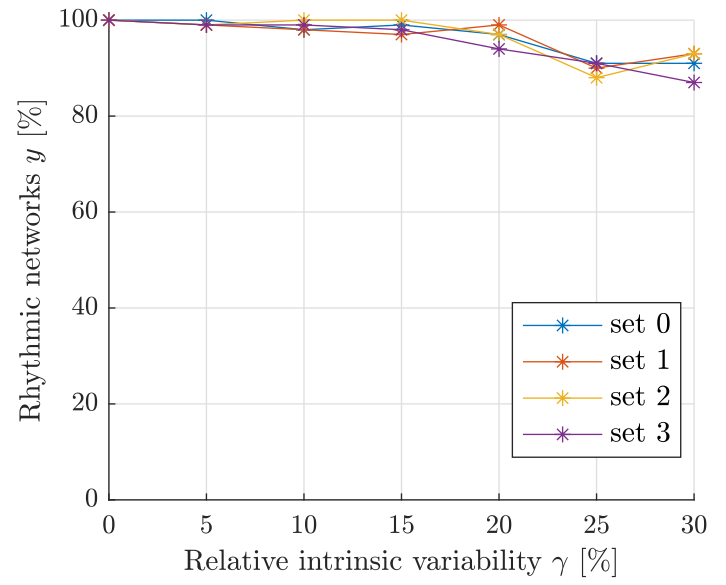
Rhythmic network activity computed with the *off-centered* nominal values

The models are simulated three times with off-centered nominal values. The evolution of the percentage of rhythmic networks for an increasing intrinsic variability is illustrated in Figure 4.9 for all the models. The blue curve is the same as the one drawn in Figure 4.8. The three other curves are computed for different off-centered nominal values (the off-centered values for each model are given in Appendix A).

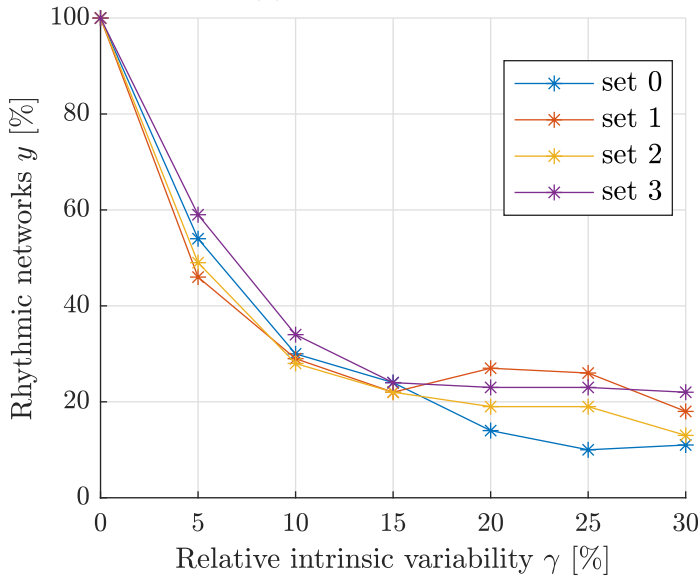
The major observation is that the off-centering does not really impact the profile. The percentage of rhythmic networks for one value of the relative variability is obviously different for each curve. This could be easily understood from the sphere analogy; the three sets (g_1^*, g_2^*, g_3^*) are randomly picked around the initial nominal. So maybe one set is closer than the boundary (resp. centered in the orange area) and provides worse (resp. better) results. But, globally, the tendency is maintained.



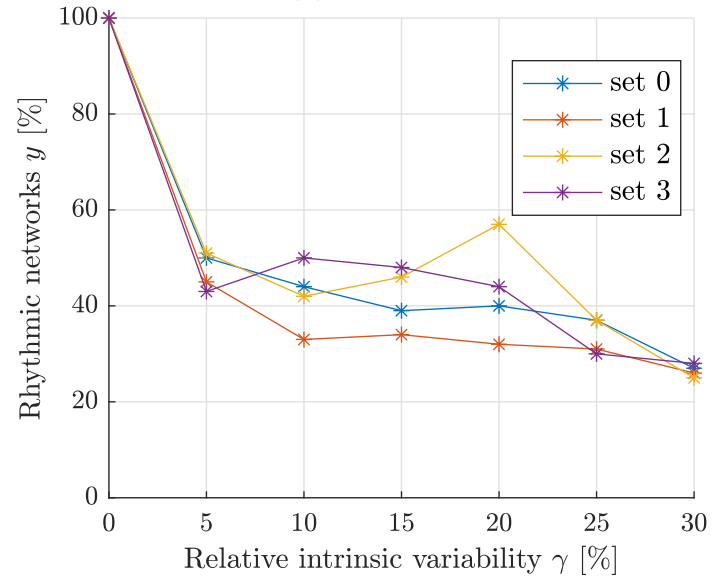
(a) DESTEXHE



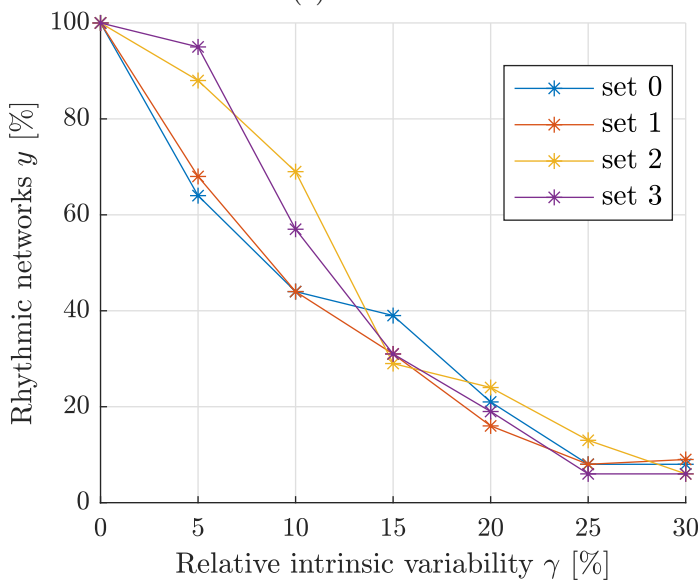
(b) DRION



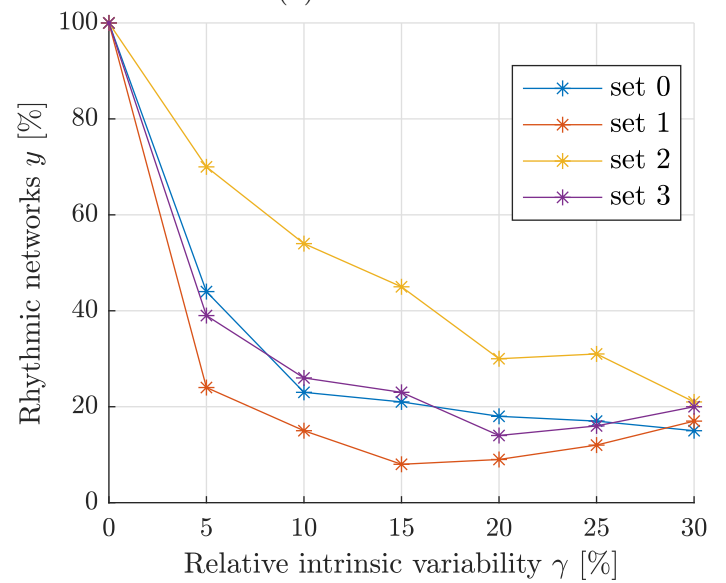
(c) RUSH



(d) RUSHCA



(e) WANG



(f) HM

Figure 4.9 – Evolution of the percentage of rhythmic networks as a function of the relative intrinsic variability for each model computed with the nominal values of the intrinsic parameters (called set 0) and three off-centering set of parameters (called set 1, set 2, set 3). The values of the parameters for each set are given in Appendix A

Averaged Rhythmic Network Activity

Figure 4.10 is the most important contribution for the network analysis of the conductances-based models. It corresponds to the mean of the four curves shown in Figure 4.9. The rating is almost the same as the one given for the initial nominal values;
for low intrinsic variability ($\gamma < 15\%$):

$$\text{Drion} > \text{Destexhe} > \text{Wang} > \text{RushCa} > \text{HM} \geq \text{Rush}$$

for high variability ($\gamma \in [15\%; 30\%]$):

$$\text{Drion} > \text{Destexhe} > \text{RushCa} > \text{HM} \geq \text{Rush} > \text{Wang}$$

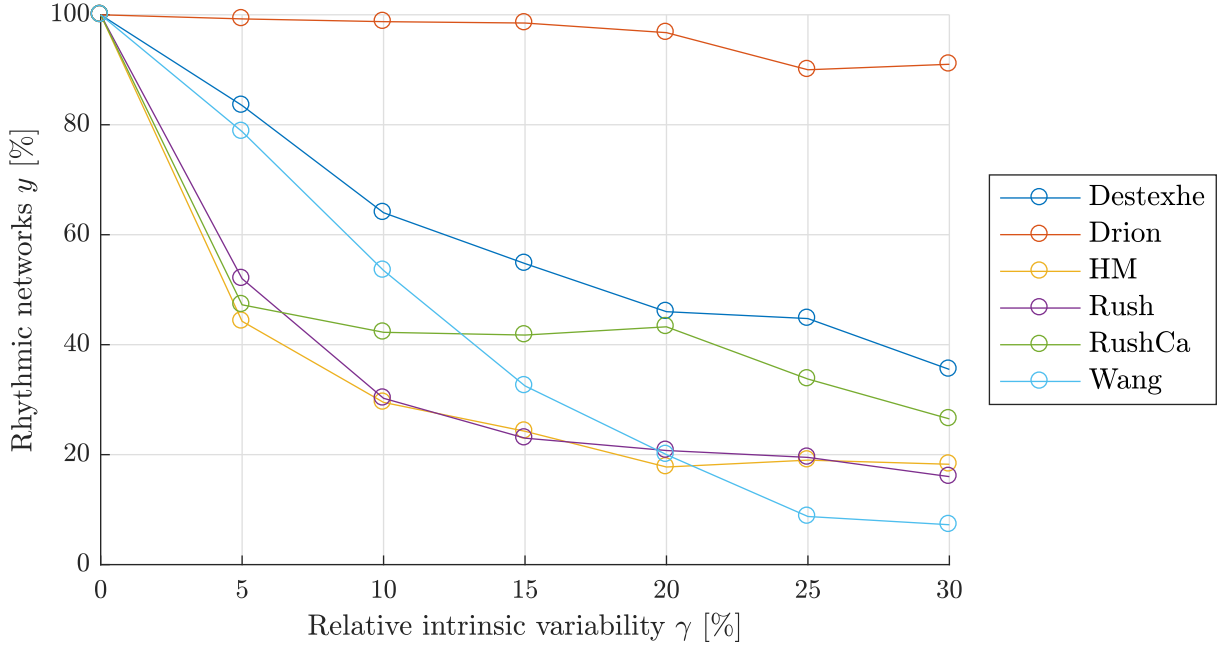


Figure 4.10 – Mean of the percentage of rhythmic networks for each set of parameters shown in Figure 4.9 as a function of the relative intrinsic variability for each conductance-based model.

The robustness of Drion's model must be again emphasized; almost all networks switch and burst synchronously. The gap with the other models is noticeable. Then, the second more robust model is Destexhe. One network over two is able to switch and bursts synchronously when the intrinsic relative variability is around 30%. Then, Rush and Wang lag behind. At low variability, Wang seems to be robust; but shrinks faster than Destexhe when the perturbations grow.

The last remarkable feature is the improvement of the Rush's curve when the activation is not more instantaneous; about 10% of augmentation.

4.4 ANALYSIS OF TUNABILITY

4.4.1 State-of-art

After studying the rhythmic network activity, the behavior of the cell in the network and the characteristics of its firing pattern are investigated. As shown in Figure 4.11, these characteristics are

- *tonic frequency* defined as the inverse of the time duration between two Na-K action potentials in tonic mode,
- *intraburst frequency* defined as the inverse of the time duration between two Na-K action potentials in a burst,
- *interburst frequency* defined as the inverse of the time duration between two burst onsets, also called *network frequency* [25],
- *duty cycle* defined as the ratio between the burst duration and the period, averaged over two neurons [25],

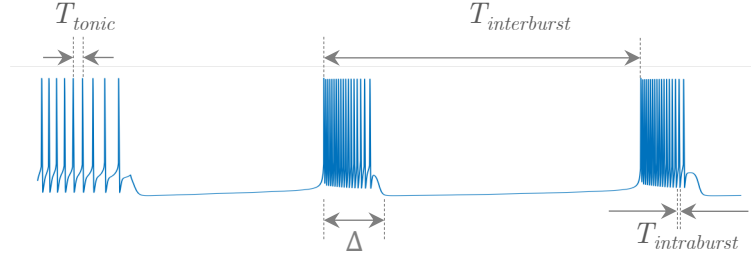


Figure 4.11 – Characteristics of a firing pattern (tonic period, interburst period, duty cycle (Δ) and intraburst period).

Physiological property

In addition to the robustness, it is interesting to verify if a model exhibits the *physiological property* of the hyperpolarisation-induced bursting [9, 50]:

$$f_{\text{tonic}} < f_{\text{intraburst}} \quad (4.2)$$

In [29], the tonic and intraburst frequencies of each network that has switched and bursts synchronously are exhibited and are linked by a line in Figure 4.12. For each network, the physiological property is verified; the intraburst frequency is higher, than the tonic frequency. It is confirmed by the positive slope of the line.

Tunability

A "good" model is not only robust but also *tunable* *i.e.* the characteristics of the firing pattern are modulated over a wide range of values, in opposition to a *rigid* model where the characteristics of the pattern are restricted to particular values.

Computing these features for each rhythmic network is a good indicator to assess the tunability of a model. Figure 4.12 shows that the Drion's model allows a large modulation for the explored range of parameters. The frequency of the rhythm and the duty cycle are modulated over a broad range [29].

4.4.2 Procedure

Physiological property

Similarly done [29], the physiological property of the HIB is studied. Therefore, for each model, we referred to Figure 4.9 and choose the simulation with the highest number of rhythmic networks. For example, for Destexhe's model, the set of conductances 2 gives the best result. Similarly, for Rush's model, the set of conductances 3. Among the 100 networks, the tonic frequency and the intraburst frequency are computed for each rhythmic network at each γ .

The evolution of these frequencies as a function of an increasing intrinsic variability γ is illustrated in Figure 4.13.

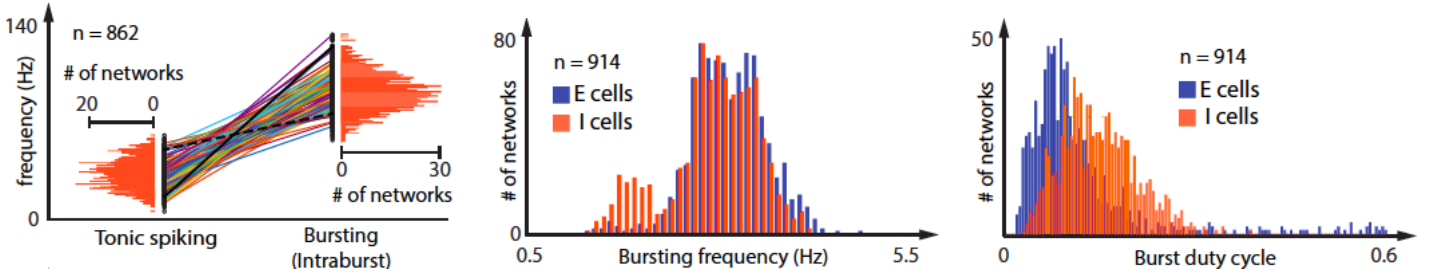


Figure 4.12 – (left) Relationship between the tonic frequency and the intraburst frequency in each rhythmic network. The covered range is large. (middle) Distribution of the interburst frequency and the duty cycle (right) in each rhythmic network. [29]

Tunability

Then, we are interested in the cellular behavior of the rhythmic networks for each model, the tonic, the intraburst, the interburst frequencies and the duty cycle of the firing patterns. These characteristics are computed when the model is subjected to the maximum value of the relative intrinsic variability γ which gives at least 40% of rhythmic network activities. In other words, we choose the maximum value γ_* such as $y \geq 40\%$ ³ in the best curve in Figure 4.9 (choosing the favorable situation). Table 4.2 gathers the value of γ_* for each model associated to the best curve (defined by the number of the associated set of conductances).

Model	Destexhe	Drion	HM	Rush	RushCa	Wang
set	2	0	2	3	3	2
γ_*	30%	30%	15%	5%	20%	10%

Table 4.2 – Value of the relative intrinsic variability which gives at least 40% of rhythmic network activities for a given set of parameters.

4.4.3 Results

Physiological property

Figure 4.13 shows the evolution of the tonic frequency and the intraburst frequency of the rhythmic networks when the intrinsic relative variability (γ) increases.

General observations through all the models can be extracted: when γ increases, the percentage of rhythmic networks obviously declines according to the observation given in Figure 4.10. The second general characteristic occurs at $\gamma = 0\%$; the synaptic variability provides a small modulation. Only a small range of frequencies are covered. When the intrinsic variability enters into account, the frequencies both in tonic or in bursting modes are modulated over a larger range. However, the width of the range is different depending on the model.

Only three models respect the physiological property; Destexhe, Drion and Wang for all values of γ . Rush loses this property when the relative intrinsic variability is higher than 10%. By contrast, HM and RushCa do not exhibit the property when there is only synaptic variability. When γ increases some networks verify it.

Therefore, for HM, Rush and RushCa, the cellular behavior of the cell is not biologically correct when he subjected to modulation either synaptic and neuromodulation.

Tunability

Figure 4.14 shows the mean and the standard deviation of the four features of the HIB *i.e.* the duty cycle, the interburst, the tonic and the intraburst frequencies of each model subjected to a maximum

³ y equals at least 40% allows to analyse more than 40 circuits characteristics with a value of $\gamma \neq 0$. For $y \geq 80\%$, for example, only Destexhe and Drion have a $\gamma \neq 0\%$.

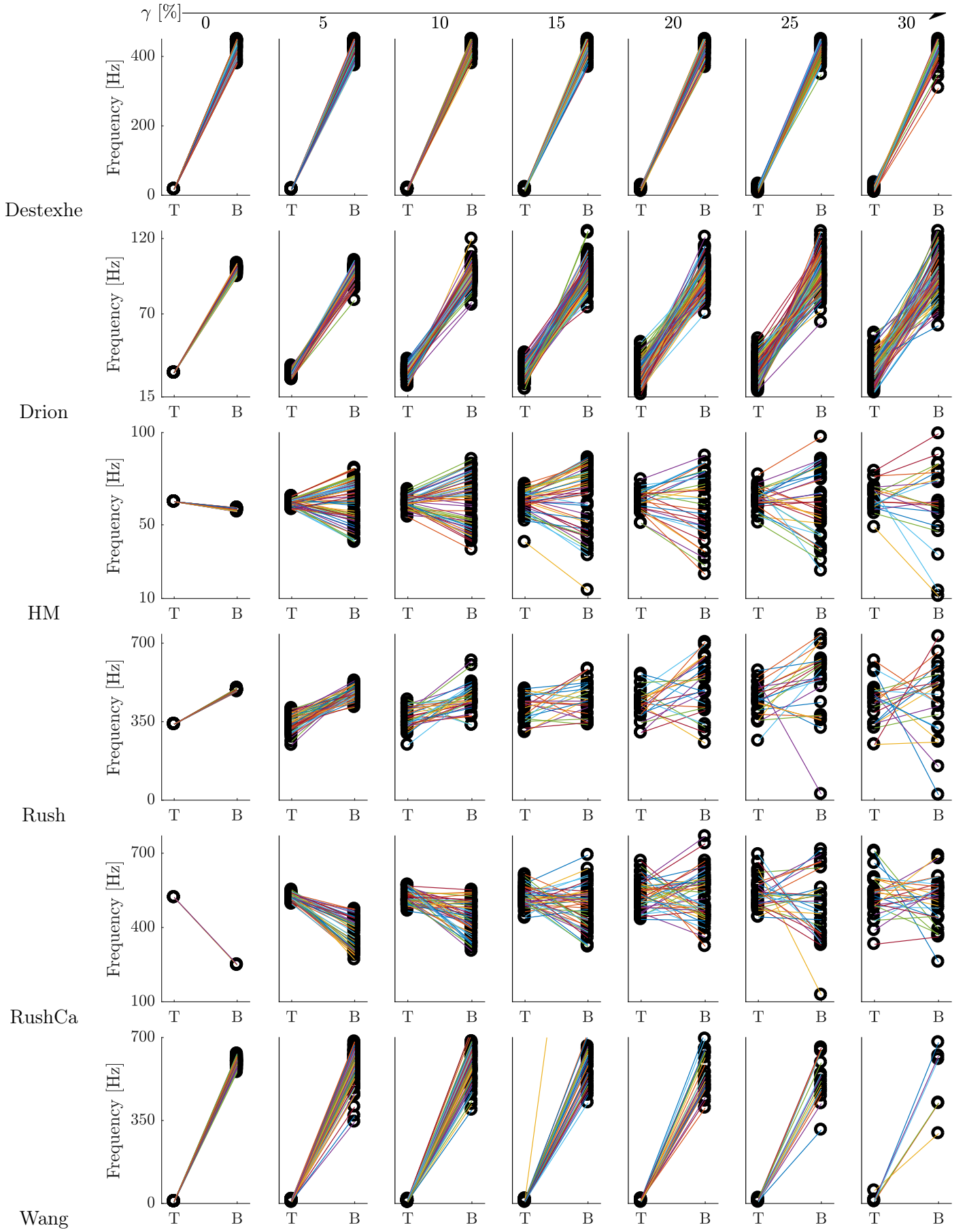


Figure 4.13 – Evolution of the relationship between the tonic frequency (T) and the bursting frequency (B) for each rhythmic network for an increasing relative intrinsic variability in each model.

intrinsic variability γ_* which leads to at least 40% of rhythmic networks. The characteristics of the inhibitory cells and the excitatory cells are almost the same (see Appendix C.1). Only the characteristics of the cells I are displayed.

- For the duty cycle, RushCa has a very high mean compared to the other models and its modulation is also more important than the others. On the contrary, HM presents a small mean and a small standard deviation. The four other models are approximately in the same range and size of modulation.
- For the interburst frequency, Wang covers the largest range compared to the others. HM is again restricted to the narrowest range.
- For the tonic frequency, Rush and RushCa have both a high mean and the largest range. It is so more interesting to zoom on the four other models. They display a similar modulation (see Figure 4.15).
- For the intraburst frequency, Destexhe, Rush, RushCa and Wang models have a high mean which is greater than 400 Hz. RushCa and Wang cover a larger range compared to the others. The standard deviation of HM and Drion are quite small.

In general, RushCa cover larger ranges, followed by Wang (excepted for the tonic frequency). Regarding HM, this model has always the smallest modulation. This analysis of tunability sheds light on the mechanism of the hyperpolarised induced bursting in a network of 2-cells. The same mechanism exists in very different rhythmic states [29]. However, it is important to stay close to the physiology and the different states must exist in reality.

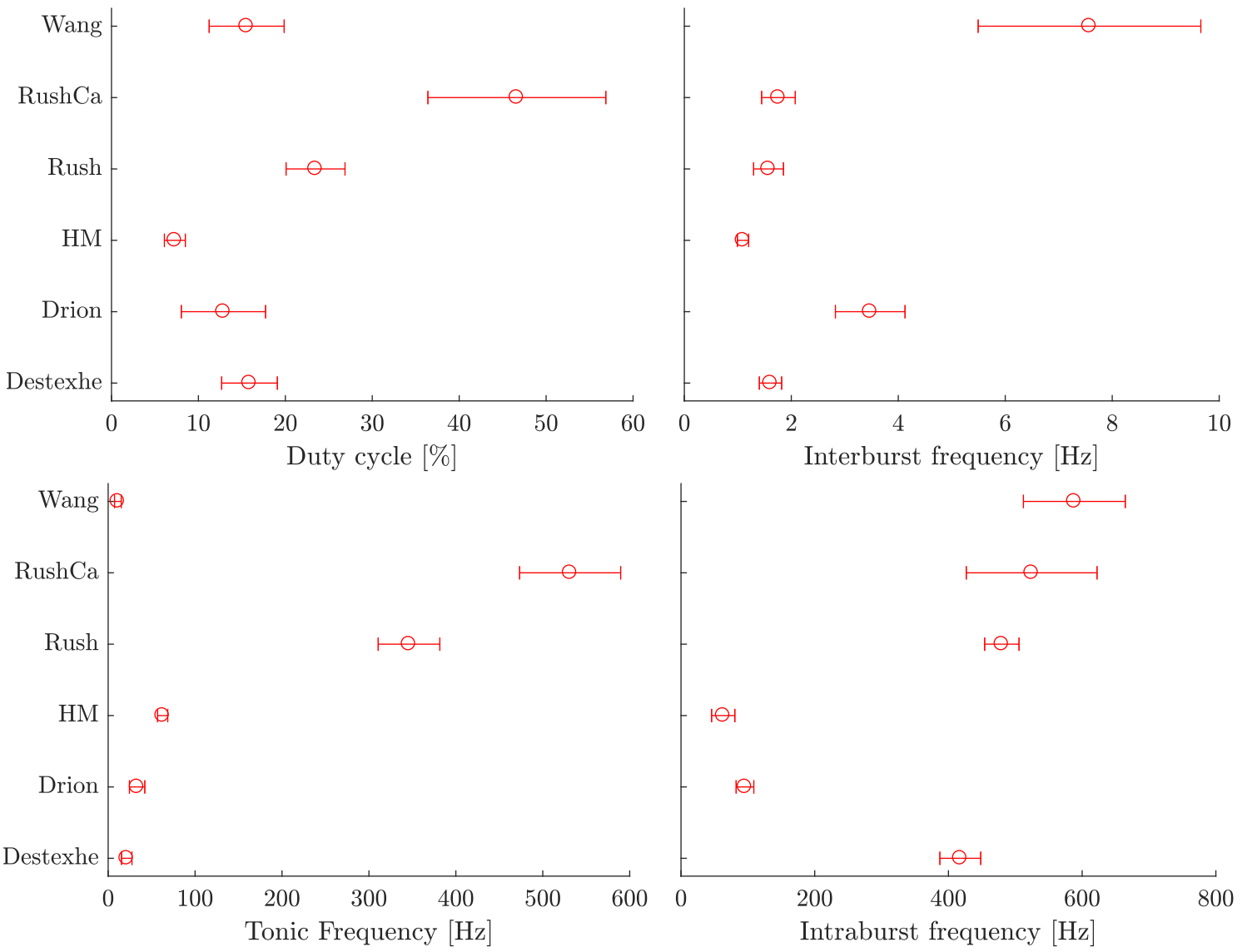


Figure 4.14 – Mean and standard deviation of the distribution of the four firing characteristics for the rhythmic networks in each model for the inhibitory cells computed for γ_*

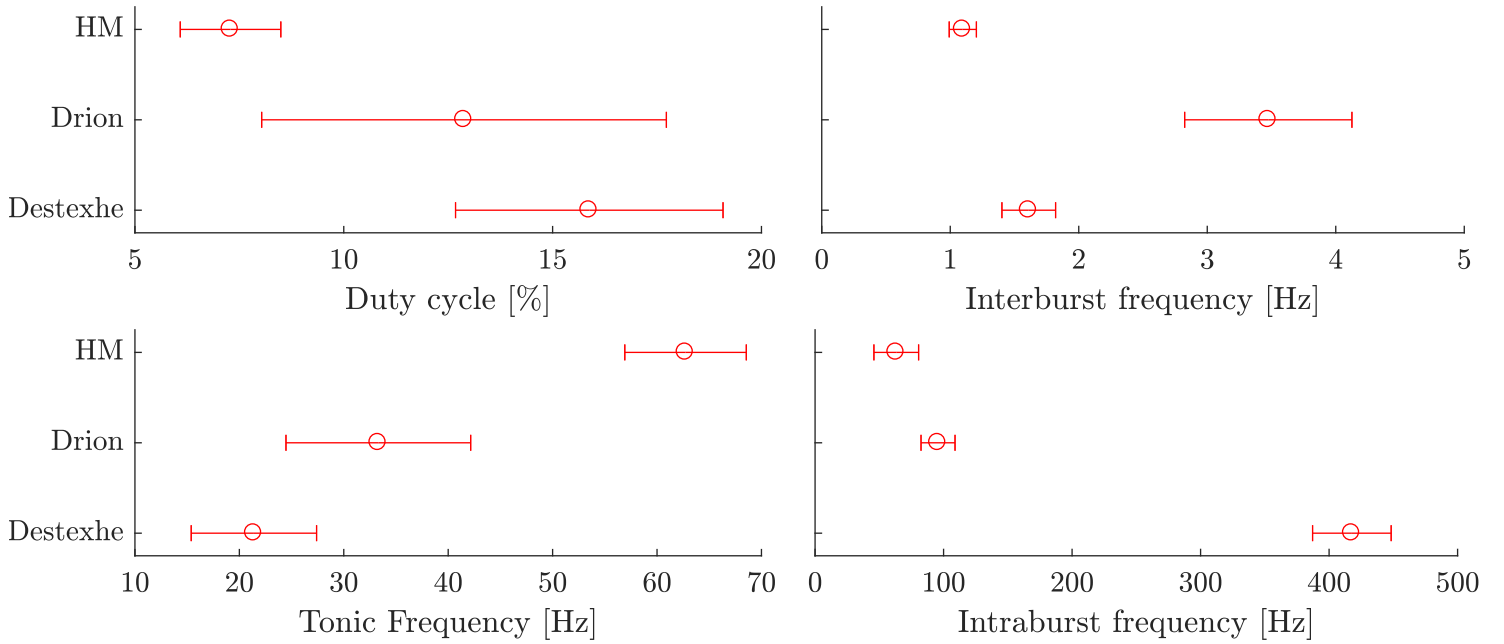


Figure 4.15 – Mean and standard deviation of the distribution of the four firing characteristics for the rhythmic networks in Destexhe Drion and HM for the inhibitory cells computed for γ_*

4.5 ANALYSIS OF HETEROGENEITY

4.5.1 State-of-art

The previous computational experiments are performed on 2-cells E-I network. In this section, we want to investigate the activity of a larger population and study the robustness to intrinsic and extrinsic variability.

In a real experiment, the activity of a larger population is recorded with micro-electrodes inserted in brain tissue and the recorded electric potential is called the *Local Field Potential* (LFP). It corresponds to the mean field measure of the average behavior of large numbers of interacting neurons [24]. It differs from the EEG which is recorded at the surface of the scalp [20].

To reproduce the experiment, the activity of the population corresponds to the synaptic activity of the neuronal population and so the LFP is computed by the normalised sum of the post-synaptic currents [23, 29]. In order to reflect this global activity in a time-frequency plot, the spectrogram of the LFP is computed.

The robustness of the switch in a 200-cells E-I network of the Drion's model is illustrated in Figure 4.16 A. The first and last parts are associated to the tonic firing at the cellular level while the central part (when the applied current is decreased) is associated to the bursting. The spectrogram brings to light the switch between the asynchronous behavior in tonic mode to the synchronous behavior in bursting mode (also described in [24]). Indeed, a high spectral power in a confined frequency band is revealed during the hyperpolarising current.

The key concept to remind of this computational experiment is the existence of a population even if at the cellular level, cells are *heterogeneous* and exhibit a *heterogeneous* behavior. Indeed, Figure 4.16 B displays cellular recordings of 4 excitatory and 4 inhibitory neurons. The *heterogeneity* means here that some neurons do not fire at the same period. They are not synchronised exactly at the same moment or they even do not present the same number of spikes per burst. However, considering the mean field, a rhythm emerges [29].

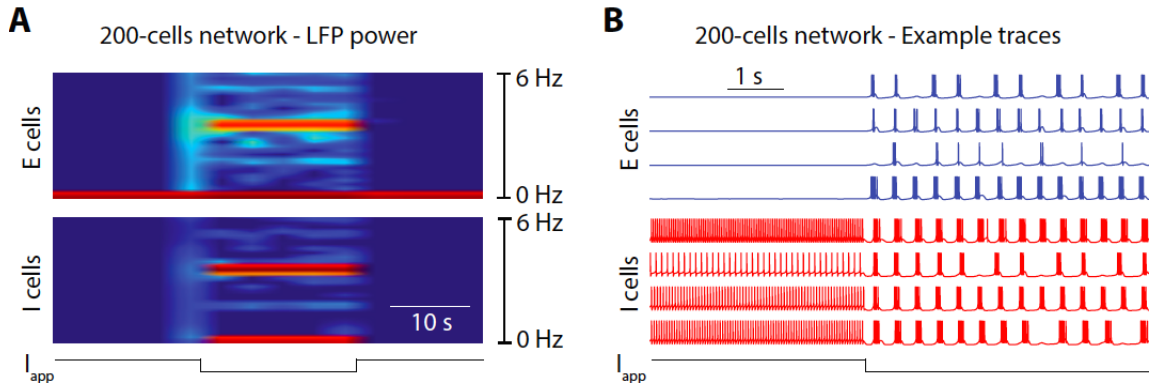


Figure 4.16 – E-I network of 200 cells excited by a hyperpolarised current. A. The spectrogram of the LFP in the excitatory cells and in the inhibitory cells. The hyperpolarisation leads a population rhythm represented by the high spectral power in a confined frequency band. B. Time-evolution of cellular activity of 4 excitatory cells and 4 inhibitory cells. The population displays heterogeneous a single cell activity but these cells are synchronised [29].

4.5.2 Procedure

The same computational experiment as done in [29] is performed for the six conductance-based models. The `Julia` code to obtain the LFP is kept.

The post-synaptic current from neuron i to neuron j is

$$I_{syn,ij} = -g_{k,i}(V_m - V_k)$$

k is the receptor type (*AMPA*, *GABA_a* and *GABA_b*). Then, the entire post synaptic current of the neuron j is the sum of the post-synaptic current of all the neighboring neurons. The sum over the N neuron is computed:

$$I_{syn,j} = \frac{1}{N} \sum_{i=1}^N I_{syn,ij}$$

N is the number of pre-synaptic neurons of the neuron j . Finally, to compute the local field potential, the sum of all the post-synaptic current of all the neurons are given by:

$$LFP = \frac{1}{M} \sum_{j=1}^M I_{syn,j}$$

where M is the number of post-synaptic currents in the population.

The population rhythm of the inhibitory cells are compared in two situations; either when only the synaptic connections are subjected to perturbations or both synaptic connections, the conductances and the capacitance are perturbed. In the second case, the LFP is computed for γ equals to 10%.

The spectrogram of the LFP is the time-frequency representation of the signal. The frequency content is estimated in time sections of the signal. There is a fundamental trade-off between the frequency resolution and the time resolution. To have a nice frequency resolution, the sections must be long. However, long sections fail to track frequency changes. In the case of the switch in the population, an accurate time evolution along all the simulation is not primordial, since a switch is expected when the hyperpolarised current is injected followed by a constant population rhythm.

4.5.3 Results

Figure 4.18 shows the spectrograms of the LFP recorded in a 200-cells E-I network where only the inhibitory cells are represented, similarly done in [29]. The spectrograms associated to the excitatory cells are displayed in Appendix C.2 and they approximately present the same rhythm.

At 20 [s], when the hyperpolarised current is injected in the inhibitory cells, a switch in the population is expected. Figure 4.17 reveals 6 cells of the network from the Drion's model with and without intrinsic variability. Without any intrinsic variability, only the synaptic connections are perturbed, the population switches from an asynchronous behavior to a synchronous spiking mode at the cellular level. With intrinsic variability, the firing pattern among the different cells is more heterogeneous. For example, the first excitatory cell has a twice higher interburst frequency compared to the two other excitatory cells. Among the inhibitory cells, the number of spikes per burst is very different. However, considering the whole network, a synchronisation phenomenon appears and leads to the population rhythm.

There are some differences in the population rhythm frequency and the power of the spectral band between the different models. Figure 4.20 displays the population rhythm frequency and the associated intensity of the spectral power band for each model.

When only the synaptic connections are perturbed, Drion and Rush have the highest spectral power in a confined frequency band followed by Wang. HM and Destexhe present a smaller intensity. Then, RushCa does not reveal a strong population rhythm.

The frequency of the population rhythm is different among the models. HM has a synchronous population around 1 [Hz], Destexhe, Rush and RushCa around 2 [Hz] followed by Drion at 4 [Hz] and Wang at 8.5 [Hz]. Besides, some supplementary bands appear in Destexhe, HM, Rush and RushCa. These bands seem to be the harmonics, but they could also represent a rhythm of a subpopulation present in the network.

Then, each cell is integrated in the network with perturbed values of the conductances and the capacitance in addition to the synaptic variability. Each value is randomly chosen in a uniform distribution in the range of 10% around the nominal value. Only Destexhe, Drion and Wang models still

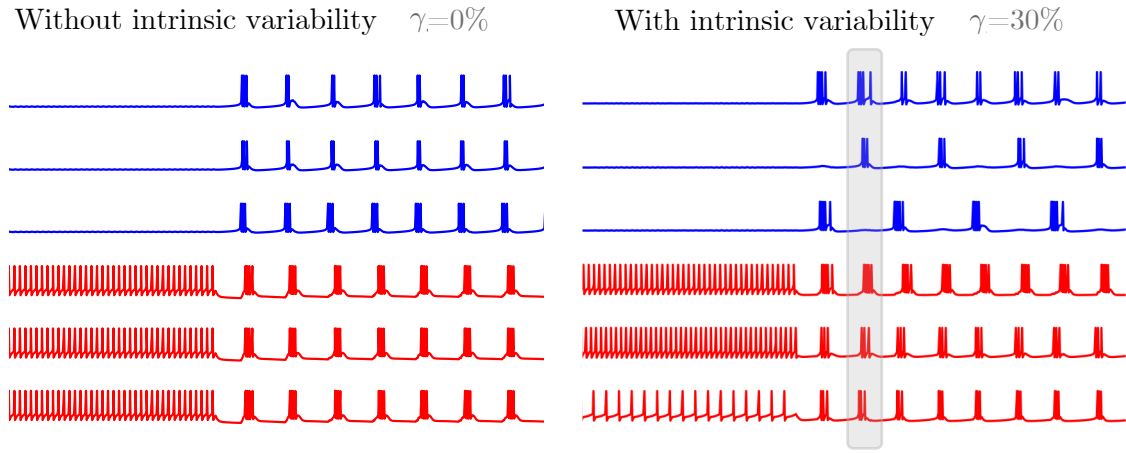


Figure 4.17 – Examples of time evolution of the membrane potential in 6 cells of the network with and without intrinsic variability. - Without variability, the cells exhibit a similar firing pattern and are synchronised. With variability, the cells have a heterogeneous behavior. The synchronous rhythm appears by taking into account all the cells in the network.

exhibit a population rhythm. Their respective frequency rhythm is not so much perturbed. Indeed, the parameter variability impact the unicellular rhythm but not the network interactions (as highlighted in Figure 4.17 for Drion's model). On the contrary, HM, Rush and RushCa do not have a synchronous population.

Then, to deepen the analysis, γ is set at 20%, the corresponding spectrograms of Destexhe, Drion and Wang models are shown in Figure 4.19. Wang does not show any more a population in opposition to Destexhe and Drion. According to Figure 4.20, the intensity of the power spectral band in Destexhe's model is slightly reduced.

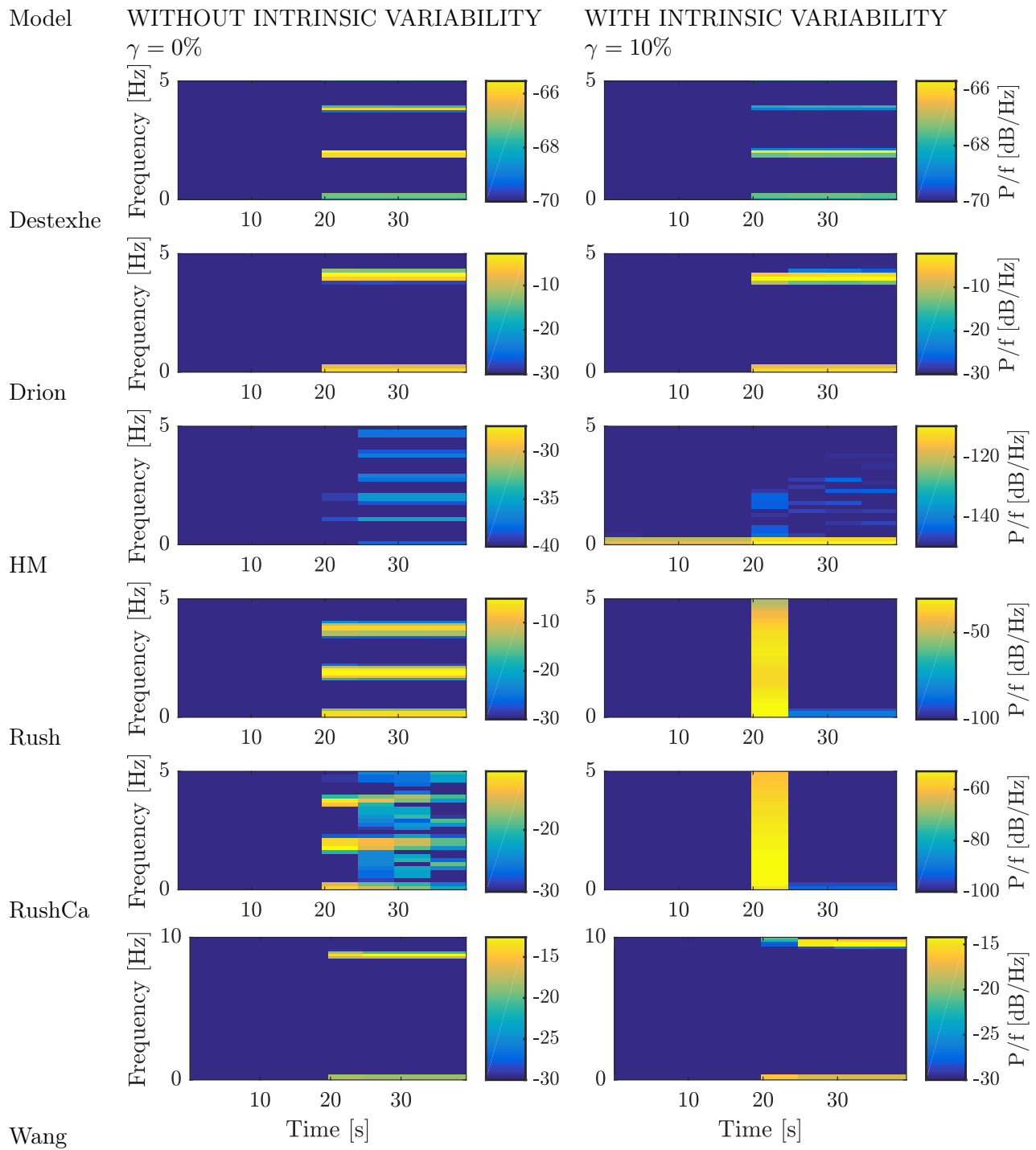


Figure 4.18 – Spectrogram of the LFP of the I-cells populations in a 200 network without intrinsic variability (on the left) and with a relative intrinsic variability of 10% (on the right) for each model. - The hyperpolarising current is expected to generate a switch in the population and revealed a population rhythm. Without intrinsic variability, all the models display a population rhythm except HM. With an intrinsic variability, only Destexhe, Drion and Wang maintain their rhythm.

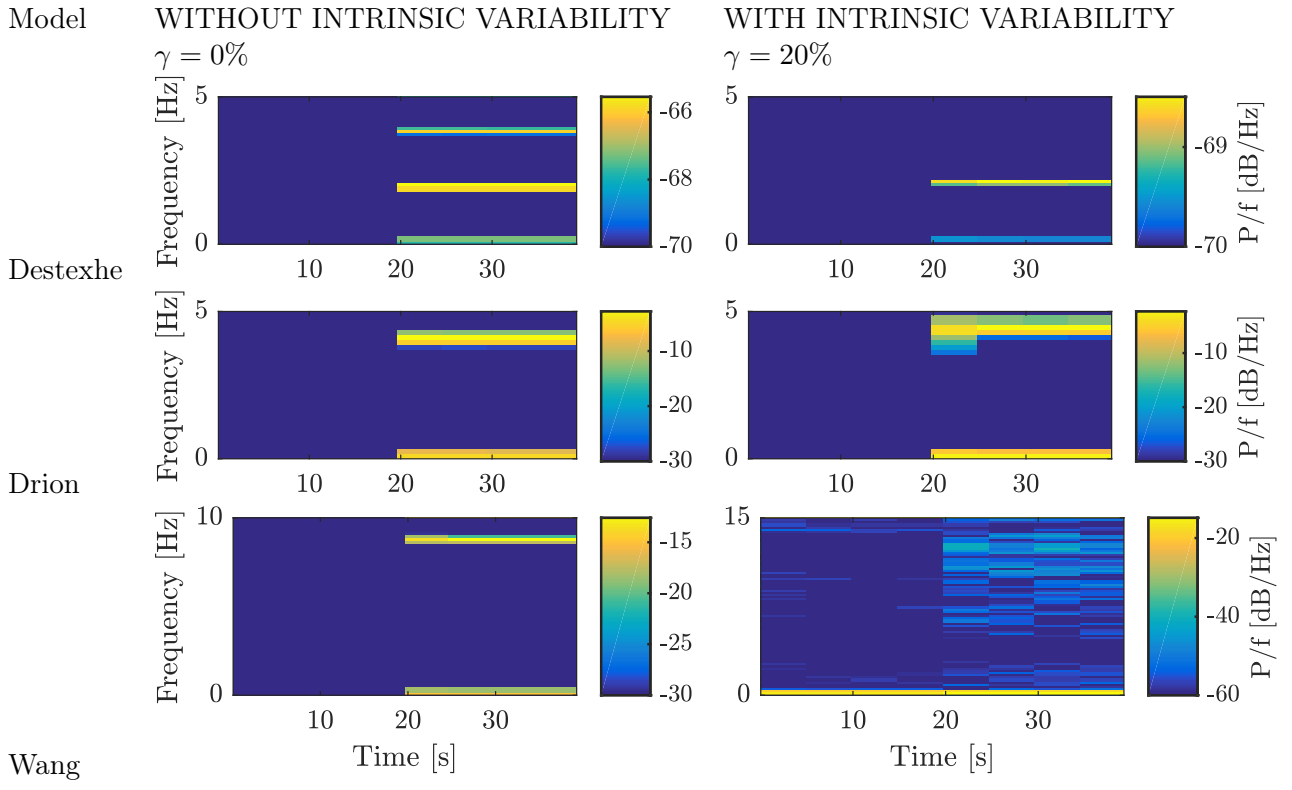


Figure 4.19 – Spectrogram of the LFP of the I-cells populations in a 200 network without intrinsic variability (on the left) and with a relative intrinsic variability of 20% (on the right) for each model. The intensity of the power spectral content is expressed in Power/Frequency, denoted P/f.- Only Destexhe and Drion maintain their population rhythm when perturbation is applied in the network.

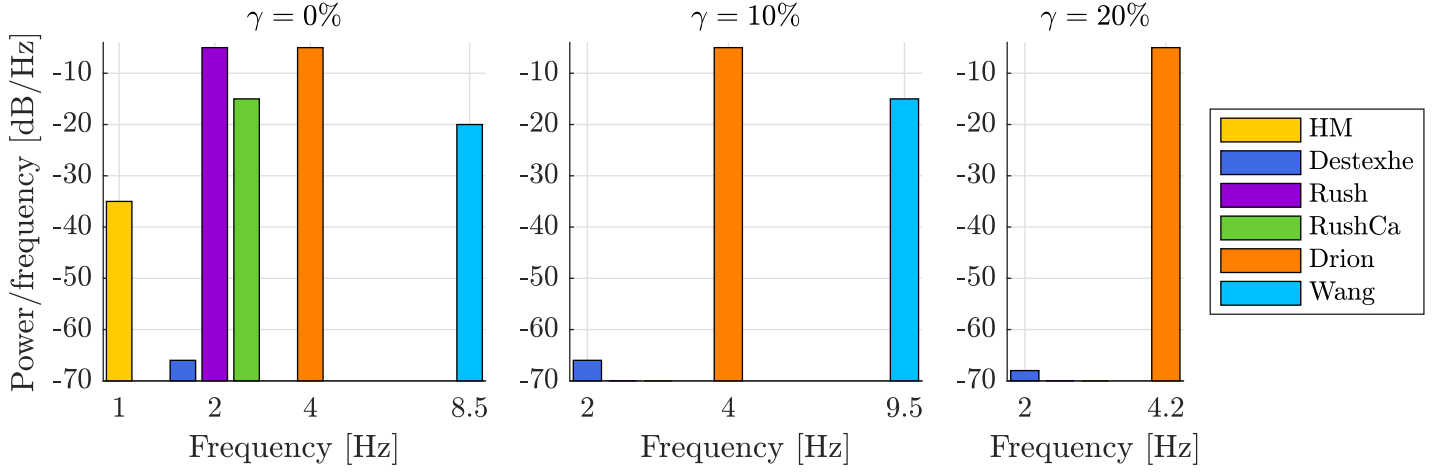


Figure 4.20 – Intensity of the spectral band power for each model and the associated population rhythm frequency for different values of the relative intrinsic variability. The intensity of the power spectral content is expressed in Power/Frequency, denoted P/f. - Destexhe and Drion maintain their rhythm followed by Wang for a lower variability.

4.6 Discussion

Slow negative conductance brings robustness at the network level in a thalamic neuron model

The role of the slow kinetics of the calcium channel activation has been proven crucial to obtain a robust switch for a single cell. Moving at the network level, the different computational experiments confirm that only the models integrating this slow time-scale feature have a robust rhythmic network activity, tunable properties and allow a population rhythm when they are subjected to intrinsic and extrinsic variability.

The switch from an asynchronous population rhythm to a synchronised rhythm is associated to two different information transmissions. When the population is not synchronised in tonic mode, the spikes carry the information to the cortex while in synchronised bursting, the information is blocked [59]. This switch is *robust* to synaptic plasticity and neuromodulation. Therefore, by mimicking variability in the extrinsic and intrinsic parameters, a model placed in network should continue to switch.

Drion model is robust as shown in [29]. The difference with the analysis performed in that paper comes from the broader ranges chosen for all the maximal conductances and the capacitance. The results are similar and confirm its robustness. In opposition, models that lack the slow activation of the calcium current cannot bear high variability. Their percentage of rhythmic networks rapidly drops. By consequent, as proposed in [25, 29], this slow positive feedback brought by the slow activation of the calcium current is necessary to have a robust model and makes the switching mechanism *independent on the network topology*. In contrast, existing thalamic network analysis focuses on the oscillation state rather than on the oscillation switch. So, they tune the synaptic connection in order to see a population rhythm but this is not compatible with the synaptic plasticity present in real networks [46, 50].

In addition to the robustness, the *tunability* of a model is important. According to the results exhibited in Figure 4.14, Destexhe model has a relatively good modulation, as well as Drion model. Their range of modulation corresponds to *physiological* values. Rush model is also modulated but the tonic frequency (≈ 350 [Hz]) and the intraburst frequency (≈ 450 [Hz]) are very high. Similarly, Wang exhibits a high intraburst frequency (≈ 500 [Hz]) with a large modulation while the tonic frequency is very small (≈ 10 [Hz]) with a small modulation.

Indeed, Rush model covers a broad range of tonic frequencies. But these frequencies are not physiological. The tonic frequency is around 50 [Hz] according to McCormick's recordings [50] and around 10 [Hz] in Contreras's recordings [15]. These ranges are much lower than the tonic frequencies exhibited by Rush model. Similarly, Wang model shows a very tiny modulation of the tonic frequency around 10 [Hz]. It is a rigid tonic spiking model while the bursting mode covers a large range around 500 [Hz] and even reaches 700 [Hz]. This huge difference between the two firing frequencies is not realistic. Therefore, Rush and Wang models are able to switch from tonic to bursting mode but the characteristics of their rhythms are far from those of thalamic neurons.

Then, the switch must be *robust across the scales*. If the size of the network increases, the model must be able to switch and displays a population rhythm. Figures 4.18 and 4.20 show that for a small intrinsic variability, Destexhe, Drion and Wang models sustain a population rhythm. Then, if the intrinsic variability reaches 20%, only Destexhe and Drion models reveal a rhythm.

Gathering all the computational experiments performed, at first at the cellular level and then at the network level, considering the robustness, the tunability and the population rhythm; Drion model displays the best results followed by Destexhe model. Wang model only maintains a rhythmic network activity for low variability. Regarding Rush model, its robustness at the cellular and network levels is poor and it presents a lack of physiological characteristics.

Therefore, these computational experiments that aim to discuss the assumption made on the activation of the T-type calcium channel confirm that models which lacks the slow activation are less robust through the different scales.

Complex conductance-based models

RushCa and HM models deserve a different discussion. The RushCa model exhibits bad firing properties (see Figure 4.14). However, as a reminder, the purpose of this modified model is to point out that the *robustness* is better when the activation of the calcium channel is no more instantaneous. This goal is achieved as shown either by the robustness at the cellular level in Figure 3.5 and by the increase of rhythmic networks in Figure 4.10. However, the model is created only by changing the calcium current activation. Deeper researches on the model could be performed to improve its tunability such as verifying the time scales of the different currents for example.

The HM model must be analysed apart from the others because its number of conductances is about twice as the others. This particularity interferes in the computational experiments. Indeed, performing a uniform distribution on a high number of parameters leads to unfair tests because the random values picked in the ranges are more likely situated on the extremes bounds of the range [5]. So, HM models more likely simulated with sets of maximal conductances that are far from his initial nominal values. This leads to worse results.

Three ideas could solve this disadvantage between this high-dimensional model and the other models:

- Change of the distribution: all the conductance-based models would undergo the same computational experiments but instead of applying a uniform distribution to choose the set of maximal conductances and the capacitance, a Gaussian distribution could be used. The issue of the bad repartition of the uniform distribution would not exist any more for HM model.
- High number of varying conductances in HM model: by comparing the ionic currents between the models, HM added some "extra"-currents such as I_A and I_{K2} (see Table A.1). Therefore, only the ionic currents that are similar to the other models undergo intrinsic variability⁴. The comparison between the HM model with 11 and with 7 varying conductances is illustrated in Figure 4.21. The result of this reduction is not noticeable: the two curves are really close to each other.
- Transform each conductance-based model on a model with same comparable features and then apply the perturbations on these features. This solution is discussed with the other issues concerning the feasibility of the computational experiments.

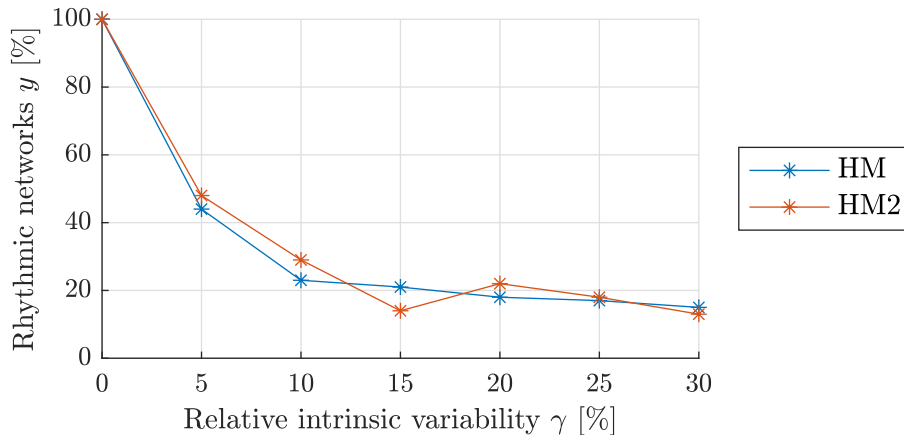


Figure 4.21 – Evolution of the percentage of rhythmic networks as a function of the relative intrinsic variability for the HM model in two situations. First, when all the conductances are perturbed (blue curve, HM) and then, when only similar conductances present in the other conductance-based model are perturbed (orange curve, HM2).

⁴The conductances: g_{Nap} , g_A , g_{A2} , g_{K2a} , g_{K2b} , g_L are not subjected to variability.

Drion model robustness

Through all the experiments, Drion model has revealed a very high robustness and modulation. The origin of these good results comes from the establishment of the model compared to the others. The typical way to create a model is based on experimental recordings, fitting curves and tuning parameters. By contrast, Drion model is rooted in a deep understanding of the dynamics of the different currents present in the thalamus. Studies in the phase plane are performed as well as the analysis of the weighted contribution of each current in the firing patterns [36].

Feasibility/Reliability of the Computational Experiments

These computational experiments have contributed to confirm that the slow activation of the calcium current is necessary to bring robustness and tunability in a model. Additional works could be done to contribute to these experiments and improve their reliability.

- Firstly, the same analysis could be performed with a larger number of networks. It increases the repartition in the uniform distribution. For the population analysis, more cells could be integrated. However, the time of simulations is very huge which is a very constraining and limiting factor in all these computational experiments.
- Secondly, the models extracted from the literature differ in terms of number of ionic currents and on their associated kinetics (as described in Section 3.1). To improve the quality of the experiments, each conductance-based model could be reduced to common features called *dynamic input conductances* following the protocol given in [30]. These quantities mimic the role of the ion channels impacting a firing pattern at one specific *time scale* [30]. Consequently, for the conductance-based models studied in this thesis, the reduction of their different ionic currents would be performed by analysing at which time scale each current has a role. All the models would be reduced according to their own kinetics but the comparison between these "reduced" models would be fairer. Indeed, the perturbations would be added on these comparable features *i.e.* their dynamic input conductances and so the test would be more general. For example, the discussion about the high numbers of conductances present in HM model would not exist.

Physiological Interpretability and Physiological Utility

Both cellular and synaptic properties, respectively modelled by intrinsic and extrinsic parameters, influence the rhythm of a network. However, the rhythmic network activity must survive in presence of heterogeneity which is translated by a high spectral power in a confined frequency band in the spectrogram [23, 29].

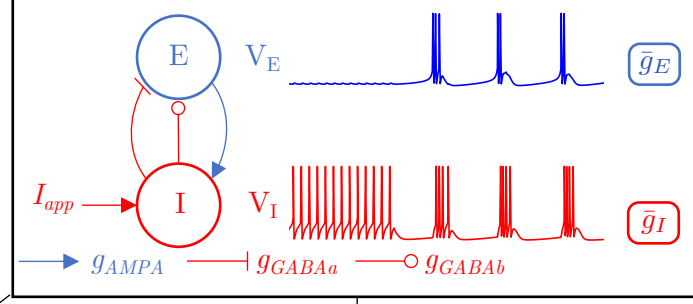
These experiments are representative of the switch between two modes that is independent from the regulatory mechanisms such as synaptic plasticity and neuromodulation. Indeed, synaptic connections are modified during learning. The modulation of these connections must not affect the switch and the synchronisation properties. In addition, the membrane characteristics evolve with neuromodulators but again, this alteration must not affect the rhythmic network activities.

These computational experiments unfold which models are robust to this variability and heterogeneity and so independent of the network topology. Therefore, such models are suited for deeper studies for example about the brain rhythmicity or the learning process during sleep.

4.7 Summary

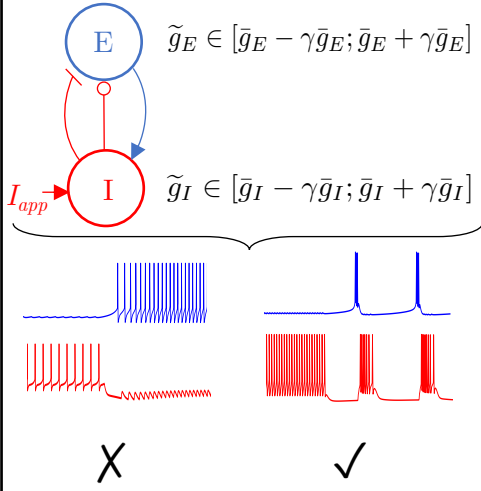
CONTRIBUTIONS

2-cells of a E-I circuit

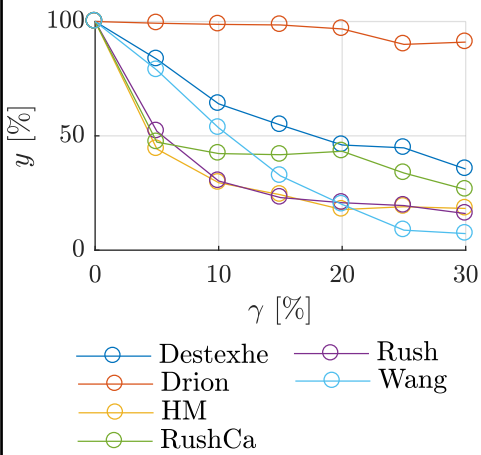


Robustness analysis

100 x 2-cells of in a E-I circuit

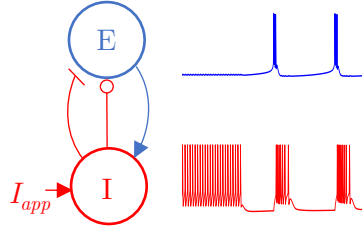


y : % of rhythmic networks
(switch + synchronous burst)

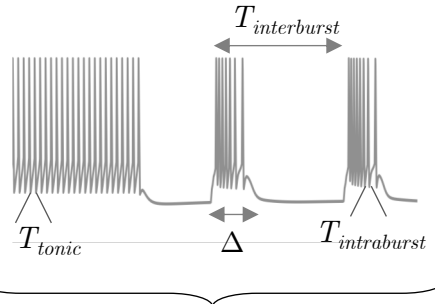


Tunability

100 x 2-cells of in a E-I circuit
for a given perturbation γ



Firing characteristics analysis



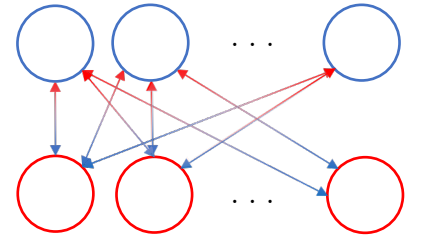
To verify in each model:

- ✓ $f_{tonic} < f_{intraburst}$
- ✓ physiological values
- ✓ range of modulation

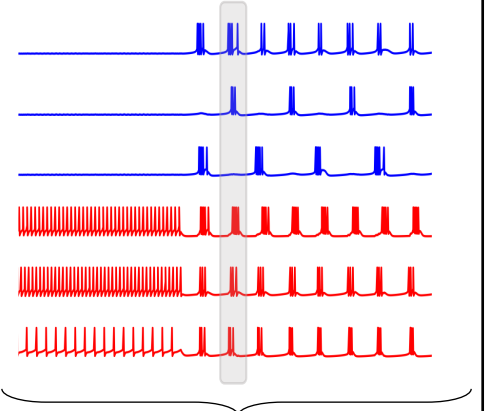
The rhythmic network activity
should be modifiable and not
display a rigid range for each
characteristics.

Population rhythm

100 cells **E** connected to 100 cells **I**



200-cells in a E-I circuit
for a given perturbation γ



spectrogram of the LFP
(sum of the post-synaptic currents)



synchronisation of the population

- Synaptic connections are perturbed to mimic **synaptic plasticity**
- Maximum conductances and C_m are perturbed to mimic the effect of the **neuromodulators**

Part III

Reduced Modeling

Chapter 5

From conductance-based models to hybrid models

5.1 Introduction

Conductance-based modeling is a powerful tool to simulate the electrical activity of a neuron. The procedure developed by Hodgkin and Huxley (HH) to reproduce the continuous-time flow of ionic currents is realistic and allows for a deep understanding of neuronal behavior. Conductance-based models have a real physiological interpretability. However, they are computed with high-dimensional non-linear equations, which lead to time-consuming simulations and so a limited use in population studies [31, 66].

In large networks, simpler models are necessary. In the early sixties, FitzHugh-Nagumo reduced the Hodgkin and Huxley model in a two-dimensional model and introduced useful tools specific to dynamical systems such as the phase portrait and the bifurcation analyses [34].

Meanwhile, the T-type calcium current has been proven essential to obtain new firing patterns. Taking into account this current changes the phase portrait of FitzHugh-Nagumo and considerably affects the reduced modeling [31].

This chapter explores the impact of the calcium on the reduced modeling. It starts with the state-of-the-art consisting in the reduction of the Hodgkin and Huxley model and the inclusion of the calcium current. Then, the impact of the calcium current in the phase portrait is described. The second part details two hybrid models based on the phase portrait analysis of the HH model with and without the integration of the calcium current.

5.2 Reduced models

5.2.1 HH model

The HH model reproduces accurately the behavior of a neuron where the sodium and potassium are the key players. As described in Section 2.2.3, it is a four-dimensional model. FitzHugh-Nagumo reduced this model by noticing that the sodium activation variable m_{Na} is faster than the other variables and the sodium inactivation variable h_{Na} varies on the same timescale as the potassium activation variable m_K [34]. Therefore, his reduced model respects two assumptions:

- instantaneous sodium activation: $m_{Na} = m_{Na,\infty}(V_m)$
- approximate linear relation h_{Na} and m_K : $h_{Na} = 0.89 - 1.1m_K$

The *reduced HH model* is described with the following equations:

$$C_m \dot{V}_m = -\bar{g}_{Na} m_{Na,\infty}^3 (0.89 - 1.1m_K)(V_m - V_{Na}) - \bar{g}_K m_K^4 (V_m - V_K) - g_L(V_m - V_L) + I_{app} \quad (5.1)$$

$$\dot{m}_K = \frac{m_{K,\infty}(V_m) - m_K}{\tau_{m_K}(V_m)} \quad (5.2)$$

It is a second-order dynamic system whose two variables are $V_m(t)$ and $m_K(V_m, t)$. The evolution of the membrane potential for a square-shaped excitatory current is illustrated in Figure 5.1 (a).

5.2.2 HH+Ca model

The HH model can only generate tonic firing. Therefore, a modified version of the HH model is necessary to obtain a burst firing and so it must take into account the calcium current with its slow activation property. Based on [31], the integration of this physiological feature is achieved by adding a non-inactivating voltage-gated calcium current I_{Ca} (only one activation gating variable and no inactivation gating variable) and a DC-current I_{pump} that accounts for hyperpolarising currents.

$$C_m \dot{V}_m = -\bar{g}_{Na} m_{Na}^3 h_{Na} (V_m - V_{Na}) - \bar{g}_K m_K^4 (V_m - V_K) - I_{Ca} - g_L (V_m - V_L) + I_{pump} + I_{app} \quad (5.3)$$

The previous parameters remain the same as in the HH model [38]. The additional calcium current follows the Ohm's law such as

$$I_{Ca} = \bar{g}_{Ca} m_{Ca} (V_m - V_{Ca}) \quad (5.4)$$

where \bar{g}_{Ca} is the maximum conductance, V_{Ca} is the calcium Nernst potential and m_{Ca} is the calcium activation gating variable. This gating variable is defined in the same way as the previous gating variable:

$$\dot{m}_{Ca} = \frac{m_{Ca,\infty}(V_m) - m_{Ca}}{\tau_{m_{Ca}}(V_m)} \quad (5.5)$$

where the equations of $m_{Ca,\infty}$ and $\tau_{m_{Ca}}$ are given in [31]. The inactivation of calcium channels (h_{Ca}) is very slow compared to the HH dynamics. Modeling this behavior by a slower adaptation of the calcium conductance does not affect the single spike generation [31].

This bursting mode is now feasible with the modified HH model, called *HHCa model*. The *three electrophysiological characteristics* of this mode are [31]:

- *spike latency*: the spike train starts after a certain amount of time after the injection of the applied current,
- *plateau oscillation*: the spike train occurs at a higher amplitude than the resting potential,
- *after-depolarisation potential (ADP)*: at the end of the bursting activity, a small depolarised potential is present. The potential does not directly reach the resting value.

The HHCa model is a five-dimensional system (with V_m , m_{Na} , h_{Na} , m_K and m_{Ca} as variables). The same reduction procedure of the HH model is followed. The excitability is governed by the membrane potential V_m and the gating variable m_K . The reduced model is based on the same assumptions as the HH model but a new one is necessary to take into account the calcium current. Its kinetics can be deduced from the potassium gating variable kinetics such as: $m_{Ca} = m_K^3$

The reduced HH+Ca model is described with the following equations:

$$\begin{aligned} C \dot{V}_m &= -\bar{g}_{Na} m_{Ca,\infty}^3 (0.89 - 1.1 m_K) (V_m - V_{Na}) - \bar{g}_K m_K^4 (V_m - V_K) \\ &\quad - \bar{g}_{Ca} m_K^3 (V_m - V_{Ca}) - g_L (V_m - V_L) + I_{pump} + I_{app} \\ \dot{m}_K &= \frac{m_{K,\infty}(V_m) - m_K}{\tau_{m_K}(V_m)} \end{aligned} \quad (5.6)$$

This reduced model is a second-order dynamic system whose variables are $V_m(t)$ and $m_K(V_m, t)$. The evolution of the membrane potential for a square-shaped excitatory current is illustrated in Figure 5.1(b).

5.2.3 Phase portrait

The major added value of the reduction is to display the two variables in the *phase plane*. By definition, each axis corresponds to one state variable.

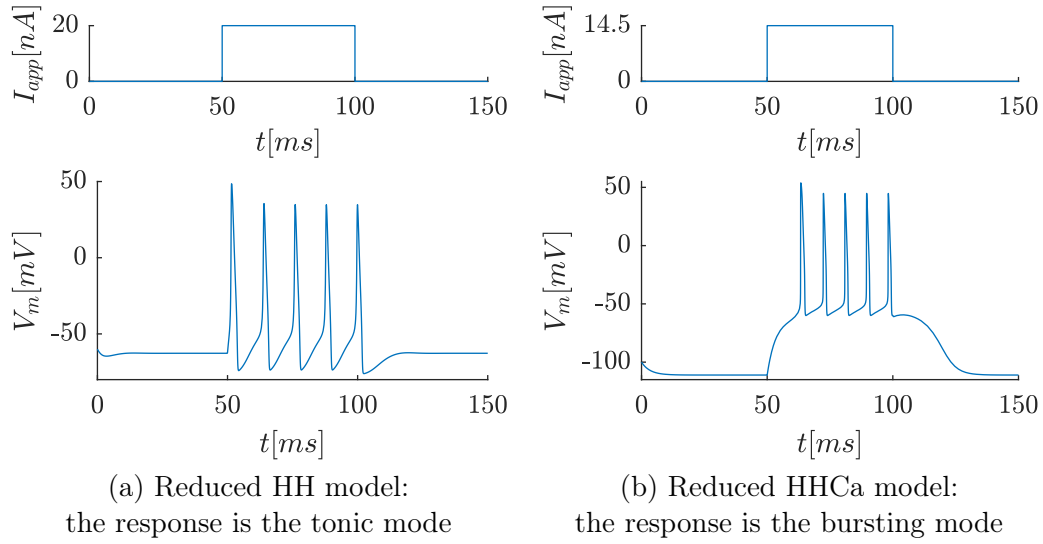


Figure 5.1 – Voltage-trace for square signal excitation of the reduced HH model with and without the integration of the calcium current (inspired from [31])

For a theoretical non-linear system with two variables x_1 and x_2 , it is interesting to draw the *nullclines* which are defined as the locus of points where one of the derivative is null:

$$\begin{cases} \dot{x}_1 = f_1(x_1, x_2) \rightarrow 0 = f_1(x_1, x_2) \\ \dot{x}_2 = f_2(x_1, x_2) \rightarrow 0 = f_2(x_1, x_2) \end{cases} \quad (5.7)$$

The intersections between the two nullclines where $\dot{x}_1 = 0$ and $\dot{x}_2 = 0$ defines the *fixed points*. The sign of the velocities and the nature of the fixed points helps to understand the trajectory in the phase portrait.

In the reduced HH model, the equations of the nullclines are:

$$\begin{cases} 0 &= -\bar{g}_{Na}m_{Na,\infty}^3(0.89 - 1.1m_K)(V_m - V_{Na}) - \bar{g}_K m_K^4(V_m - V_K) - g_L(V_m - V_L) + I_{app} \\ m_K &= m_{K,\infty}(V_m) \end{cases} \quad (5.8)$$

The first one is called the V_m -nullcline and represents all the (V_m, m_K) where $\dot{V}_m = 0$. Similarly, the second equation defines the m_K -nullcline and represents all the (V_m, m_K) where the $\dot{m}_K = 0$. This curve has a sigmoid shape. The nature of the fixed point is performed in Appendix D.1.1.

For the HHCa model, the nullclines become:

$$\begin{cases} 0 &= -\bar{g}_{Na}m_{Na,\infty}^3(0.89 - 1.1m_K)(V_m - V_{Na}) - \bar{g}_K m_K^4(V_m - V_K) \\ &\quad - \bar{g}_{Ca}m_K^3(V_m - V_{Ca}) - g_L(V_m - V_L) + I_{pump} + I_{app} \\ m_K &= m_{K,\infty}(V_m) \end{cases} \quad (5.9)$$

The m_K -nullcline remains the same as in the HH model but the V_m -nullcline is considerably affected by the presence of the calcium current. The nature of the fixed point is described in Appendix D.2.1.

After the derivation of the nullclines, the analysis of the phase portrait of each reduced model can be performed.

Reduced HH model

The phase portrait associated to the reduced HH model is shown in Figure 5.2 (left). When the stimulation is turned off, the potential remains at its resting value. It comes from the nature of the fixed point in the phase portrait, which is a stable fixed point. Acting as an attractor, wherever the initial conditions are chosen, the trajectory converges to this intersection (see Appendix D.1.1 for the derivation of the nature of the fixed point).

When the stimulation is turned on and if the current is large enough to remove the stability of the fixed point, the trajectory is driven by the velocity vectors (see Figure D.2 in Appendix D.1.2). This trajectory is attracted by a limit cycle (which is drawn as a circular flow in the vector field). When the trajectory follows the limit cycle, it corresponds to the spiking mode in the time evolution of the membrane potential.

When the depolarising current is removed, the fixed point retrieves its stability and the trajectory converges to this intersection associated to the resting potential value [31].

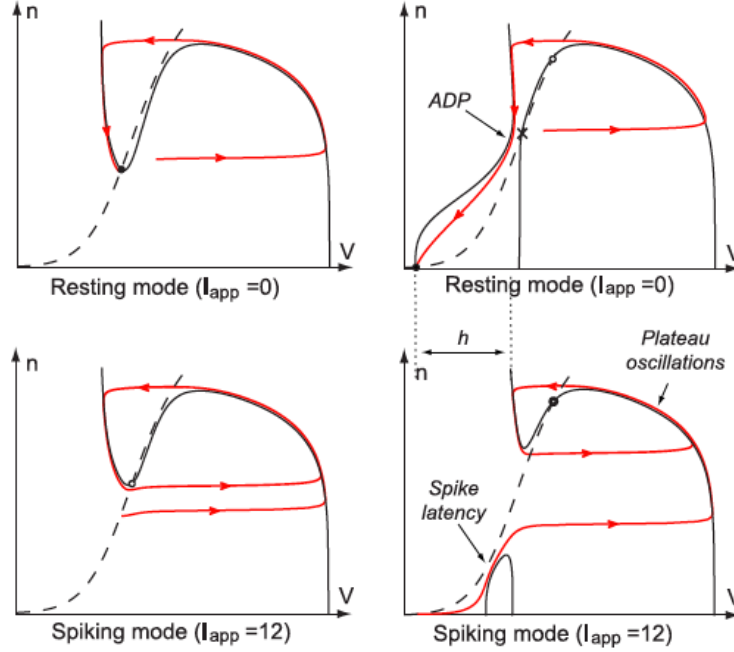


Figure 5.2 – Phase portraits of the reduced HH model without excitation (top) and in spiking mode (bottom). The V -nullcline (resp. n -nullcline) stands for the V_m (resp. m_K) -nullcline. It is drawn in full (resp. dashed) line. The trajectory is the red line. Black (resp. white) circle denotes a stable (resp. unstable) fixed point. The cross is a saddle point. The phase portrait is altered by the integration of the calcium current. Therefore, the trajectory and so the time-response of the neuron is different. The reduced HH model fires in tonic mode while the HHCa model fires in bursting mode [31].

Reduced HHCa model

The phase portrait associated to the HHCa model is shown in Figure 5.2 (right). At the beginning, no current is applied, the hourglass shape of the V_m -nullcline ensures a convergence to the fixed point on the left of the phase plane which means a hyperpolarised membrane potential. When the stimulation is turned on, the V_m -nullcline changes its shape and the intersection on the far left part of the plane is removed. The trajectory follows the path drawn by the velocity vectors. It must travel the region where the lower branch of the V_m -nullcline is closed to the m_K -nullcline. This region displays a vector field with a very small amplitude. The trajectory moves very slowly. The closer the curves, the slower the trajectory moves. This phenomenon is due to the ghost of the fold bifurcation. It highlights the first electrophysiological signature of the burst called the *slope latency*. The first spike is delayed compared to the onset simulation. Then, the trajectory reaches the spiking limit cycle.

The second electrophysiological signature comes from the relative position of the resting state (at -110 [mV]) and the spiking limit cycle. The spikes train of the burst approximately oscillates between -60 [mV] and 45 [mV]. By consequent, the amplitude of the *plateau* is equal to 50 [mV].

When the stimulation is turned off, the V_m -nullcline jumps back to its initial configuration, the hourglass shape. Therefore, the spiking limit cycle disappears and the fixed point recovers its attractiveness. The trajectory is driven by the vector field and must follow the V_m -nullcline. As the shape is a hourglass, the trajectory first moves to increasing values of V_m and then it goes back to the fixed point. This detour explains the third electrophysiological signature of the calcium current, which is

the *after depolarisation potential (ADP)* .

The three electrophysiological features of the burst pattern are entirely described with this new phase portrait (see Figure 5.3). It is not possible to retrieve them in the phase portrait of the HH model. The spike latency comes from the apparition of the lower branch of the V_m -nullcline. The plateau comes from the distance between the fixed point and the spiking limit cycle. And finally, the ADP exists due to the funnel of the hourglass [31].

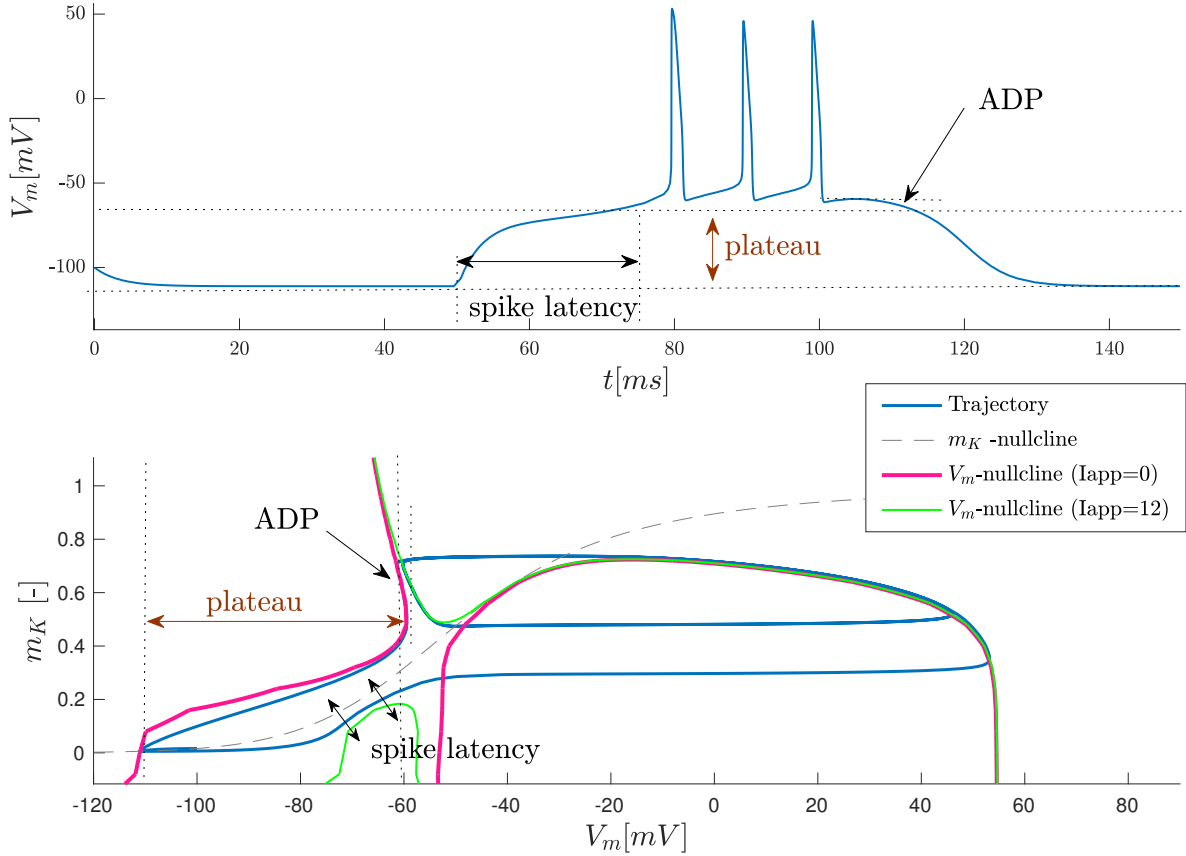


Figure 5.3 – Time evolution of the HH+Ca model (top) when a depolarising current is applied from $t = 50$ [ms] to $t = 100$ [ms] with its corresponding phase portrait (bottom). - The three electrophysiological signatures of a burst pattern are exhibited in both graphs. (inspired from [31])

5.3 Normal form and hybrid modeling

HH model

Instead of starting from the electrical analogy of the membrane and developing conductance-based models, the modeling procedure is based on the shape of the nullclines, the nature of the fixed points in the phase portrait and the bifurcation diagram. For the *HH model*, the cubic V_m -nullcline and the sigmoid m_K -nullcline have led to a fold bifurcation which has a key role in the excitability of the neuron. In a system of local coordinates centered at the bifurcation, the *fold normal form* is given by:

$$\dot{v} = v^2 - w + i + h.o.t. \quad (5.10)$$

where v is the membrane potential, w the dynamic variable, i is a re-scale input current and *h.o.t.* corresponds to higher order terms in v and w [31].

To simulate large-scale population of neurons, Izhikevich proposed to simplify the mathematical model [42]. He highlighted that the shape of the action potential is not very important because the trajectory comes back always at the same position as illustrated in Figure 5.4. He captures the sub-threshold dynamics of the neuron through differential equations and mimics the all-or-none nature of the spike with a hybrid reset mechanism. He reproduced the fast increase of the potential in the spike and its automatic return to the same low potential value called *reset* [31, 66]. Figure 5.5 reveals the concept of the reset mechanism in the phase portrait and the capture of the subthreshold mechanism.

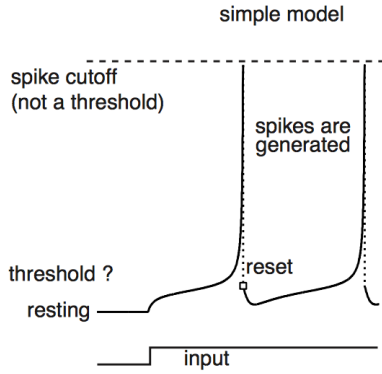


Figure 5.4 – Voltage reset in the mathematical model of Izhikevich [42]

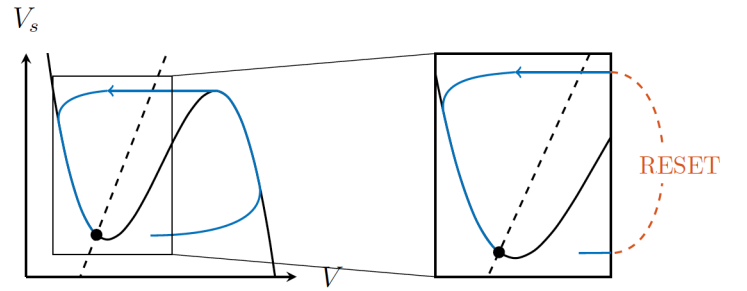


Figure 5.5 – Phase portrait of FZH model (left) and reset rule mechanism established by Izhikevich (right) - V -nullcline (resp. V_S nullcline) is in full (resp. dashed) line, the stable fixed point is the filled circle [66]

The *fold hybrid model* is defined as:

$$\begin{aligned} \dot{v} &= v^2 - w + I & \text{if } v \geq v_{th}, \text{ then} \\ \dot{w} &= \epsilon(av - w) & v \leftarrow c, w \leftarrow d \end{aligned} \quad (5.11)$$

with $v_{th} = 100$, $\epsilon = 1$, $a = 0.1$, $c = 0$ and $d = 50$.

This hybrid model reproduces very well the HH model with a monotonic return and no latency at the beginning since it is in tonic mode.

The v - and w -nullclines are respectively

$$\begin{aligned} 0 &= v^2 - w + I & \text{if } v \geq v_{th}, \text{ then} \\ 0 &= \epsilon(av - w) & v \leftarrow c, w \leftarrow d \end{aligned} \quad (5.12)$$

Notice that the v -nullcline is a parabola and the w -nullcline is a linear expression of v . Their shapes are well associated to the "zoom" of the nullclines around the fixed point on the phase portrait of the reduced HH model (see Figure 5.2 (b- left))

HHCa model

The presence of calcium current alters the shape of the nullclines of the HH model. By consequent, its previous normal form is too restrictive, it does not capture the complex phase portrait associated to HHCa model. The bifurcation is no more a fold bifurcation but a transcritical bifurcation. This can be seen in the evolution of the V_m -nullcline for an increasing value of the current. From Figure 5.6 (a) to 5.6 (b), the two vertical branches of the nullclines become closer. For one specific value of the current, the two vertical branches merge. Then, for higher current, the two branches split in one upper branch and one lower branch. Accordingly, the addition of the calcium current strongly alters the shapes of the nullclines.

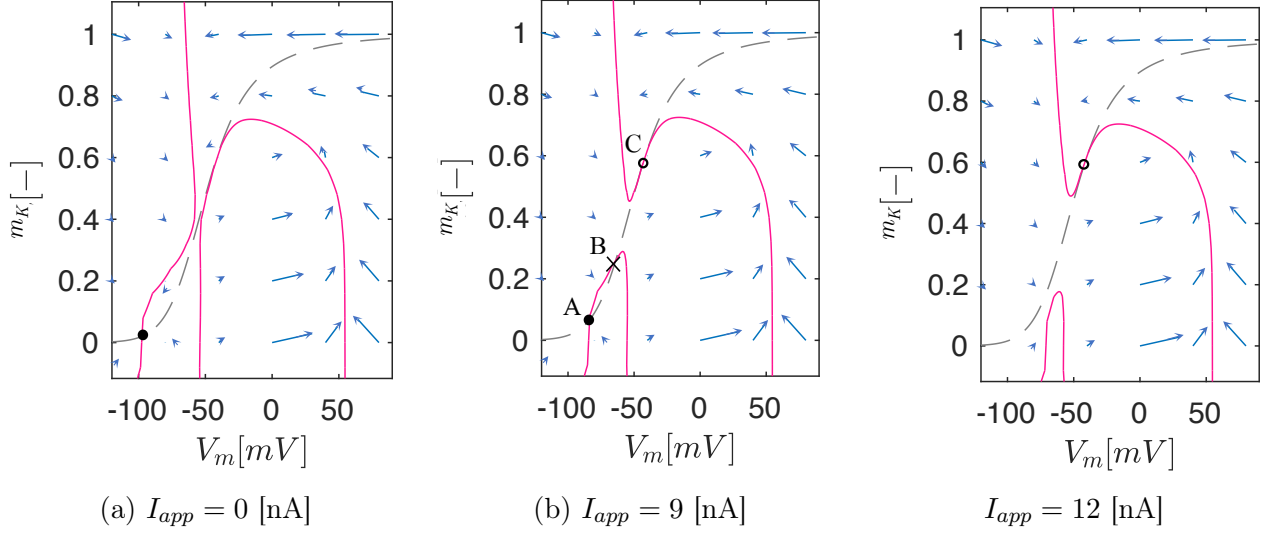


Figure 5.6 – Phase portraits of the reduced HHCa model for different values of the applied current. - The V_m - and the n -nullclines are respectively drawn in pink full line and grey dashed line and the velocity vectors are blue. The black circle (resp. white) corresponds to a stable (resp. unstable) fixed point and the cross is a saddle [31].

The normal form associated to this transcritical bifurcation is:

$$\dot{v} = v^2 - w^2 + i + h.o.t. \quad (5.13)$$

Following the Izhikevich approach, the transcritical normal form becomes the *transcritical hybrid model* which is described by:

$$\begin{aligned} \dot{v} &= v^2 - w^2 + I & \text{if } v \geq v_{th}, \text{ then} \\ \dot{w} &= \epsilon(aV - w + w_0) & v \leftarrow c, w \leftarrow d \end{aligned} \quad (5.14)$$

where w_0 stands for the calcium conductance.

If the parameter w_0 is positive, it corresponds to a low calcium conductance. The same behavior as the Izhikevich model is expected namely a train of regular spikes. By contrast with a negative w_0 , corresponding to a high calcium conductance, a bursting activity is expected.

Figure 5.7 gathers the different phase portraits for different values of I and w_0 .

- For a low calcium conductance ($w_0 > 0$), the w -nullcline intercepts the upper branch of the v -nullcline. The behavior is the same as the reduced HH model (see Figure 5.2 (left)).
- For a high calcium conductance ($w_0 < 0$), the w -nullcline intercepts the lower branch of the v -nullcline. Therefore, it is similar as the phase portrait of the reduced HHCa model (see Figure 5.2 (right))

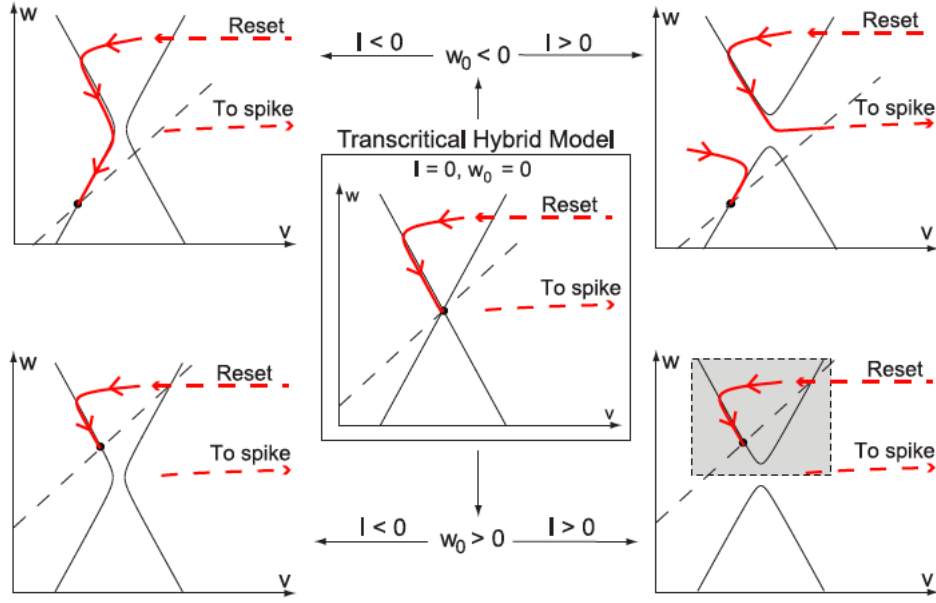
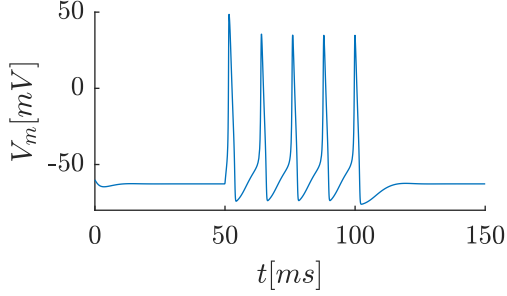


Figure 5.7 – Schematisation of the phase portraits of the transcritical hybrid model for positive and negative values of I and w_0 . The black full (resp. dashed) line corresponds to the v -nullcline (resp. w -nullcline). The trajectory is represented by a red line. The shaded area corresponds to the phase portrait of the fold hybrid model which is captured for $I > 0$ and $w_0 > 0$ [31].

5.4 Summary

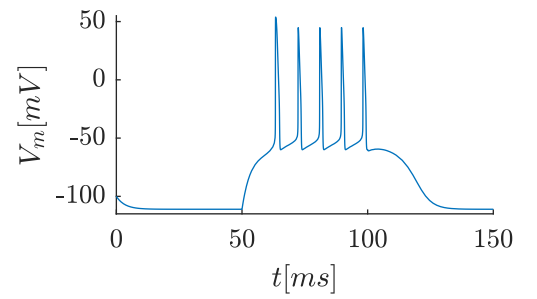
STATE-OF-ART

HH model



Add Calcium current

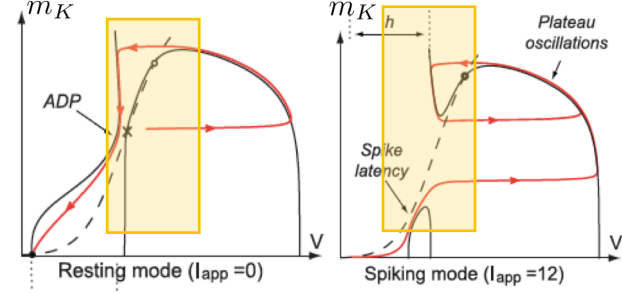
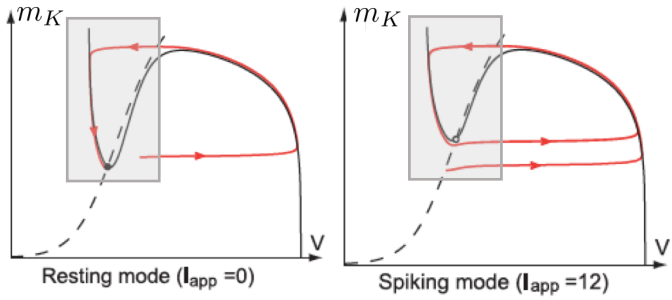
HHCa model



Cond.-based
Models reduction

Time-evolution
 V_m

Phase portrait



Fold normal form

v-nullcline : Parabola

m_K -nullcline: line

$$\dot{v} = v^2 - w + i + h.o.t.$$

Transcritical normal form

v-nullcline : two branches

m_K -nullcline: line

$$\dot{v} = v^2 - w^2 + i + h.o.t.$$

Normal form

Fold hybrid model

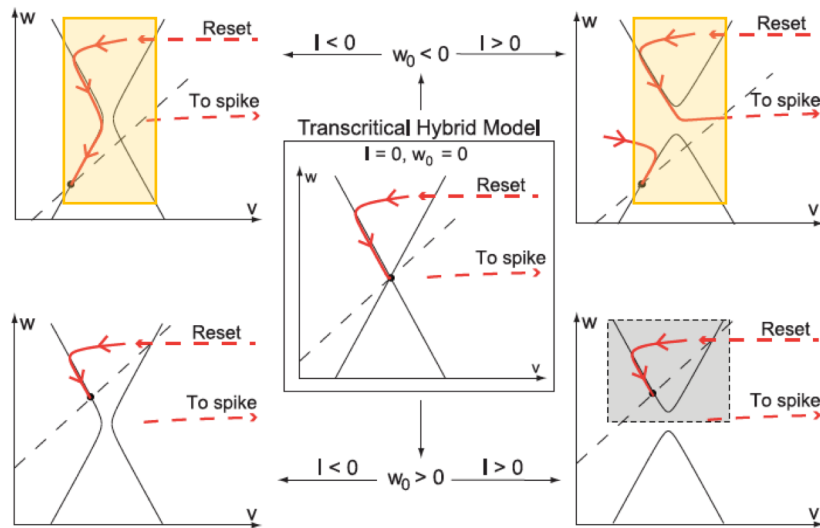
$$\begin{aligned} \dot{v} &= v^2 - w + I & \text{if } v \geq v_{th}, \text{ then} \\ \dot{w} &= \epsilon(av - w) & v \leftarrow c, w \leftarrow d \end{aligned}$$

Transcritical hybrid model

$$\begin{aligned} \dot{v} &= v^2 - w^2 + I & \text{if } v \geq v_{th}, \text{ then} \\ \dot{w} &= \epsilon(aV - w + w_0) & v \leftarrow c, w \leftarrow d \end{aligned}$$

Hybrid model
(add a reset rule)

density of calcium channels



High density

Burst firing

low density

Spiking

Chapter 6

Hybrid models of thalamic neuron

This thesis only investigates the modeling of thalamic neuron. As a reminder, a hybrid model consists of continuous-time differential equations reproducing the flow of ionic currents combined with a reset mechanism that accounts for the all-or-none principle of the spike [31, 66]. Then, a hybrid model of a thalamic neuron has to be able to *switch* from tonic mode to burst mode without mathematical manipulations [66]. In parallel, this switch has been proven robust in conductance-based models which integrates the slow dynamics of the calcium channel.

Accordingly, this section extends the transcritical hybrid model and integrates features specific to a thalamic neuron.

Then, in order to discuss the impact of the integration of the slow calcium channel dynamics, two hybrid models of the literature are discussed. The first model is the well-known Izhikevich model which captures the subthreshold dynamics of the reduced HH model. It is based on the fold hybrid form. The second model is the HYB model which takes into account the alteration of the phase portrait caused by the calcium current and is based on the transcritical hybrid model.

These two models are studied at the network level and they undergo the same computational experiments performed on the conductance-based models.

6.1 Transcritical hybrid modeling of thalamic neuron

A model describing a thalamic neuron must include the T-type calcium current, therefore the equation (5.14) of the transcritical hybrid model must be adapted. Indeed, if the parameter w_0 is positive, it corresponds to a low density of calcium current *i.e.* the T-type calcium channels are inactivated. By contrast, if w_0 is negative, it corresponds to a high density and so the T-type calcium channels are activated. In the thalamic neuron, the inactivation of the T-type calcium current is a ultra-slow mechanism (for driven by the calcium-dependent potassium current) (see Section 2.3.3). This feature is modeled by the addition of a variable z . Then, a cross-term " vw " is added to tune the slope of the v -nullcline [31]. The transcritical hybrid model of thalamic neuron is described with the following equations:

$$\begin{aligned} \dot{v} &= v^2 + bvw - w^2 + I - z & \text{if } v \geq v_{th}, \text{ then} \\ \dot{w} &= \epsilon(av - w + w_0) & v \leftarrow c, w \leftarrow d \\ \dot{z} &= -\epsilon_z z & z \leftarrow z + d_z \end{aligned} \tag{6.1}$$

where $a = 0.1$, $b = -3$, $c = 15$, $d = 15$, $\epsilon = 1$, $v_{th} = 80$, $\epsilon_z = 0.1$ and $d_z = 40$.

Low conductance mode

Figure 6.1 (left) displays the phase portrait for the small calcium conductance.

- When the stimulation is off, the resting state is positioned on the left branch of the v -nullcline Figure 6.1A (left).
- When a depolarising current is injected; the following sequence happens;

1. The v -nullcline splits in a upper branch and a lower branch and there is no more intersection between the v -nullcline and the w -nullcline. The trajectory is driven towards high potential values. It corresponds to the *spike generation*.
2. When the potential reaches the threshold value, the *reset* occurs setting v to c , w to d and z to a higher value ($z \leftarrow z + d_z$). The variable z acts as a hyperpolarising current. Indeed in the equation (6.1), z has the same impact as I with a negative sign. It brings closer the two branches. The w -nullcline intersects the v -nullcline and no more spike can be generated (see Figure 6.1B (left)).
3. Since the parameter z decreases following the equation (6.1), the cell slowly depolarises. It corresponds to the rise of the v -nullcline and so the interspike period. At one point, the v -nullcline is above the w -nullcline and so a new spike is generated.

This sequence is sustained until the stimulation is turned off.

High conductance mode

Figure 6.1 (right) displays the phase portrait for the high calcium conductance. The parameter w_0 is negative setting the w -nullcline lower in the phase portrait.

- When the stimulation is off, the fixed point is situated at the intersection between the left branch of the hourglass, representing the v -nullcline, and the w -nullcline (see Figure 6.1A (right)). This associated resting potential is lower than for a low-conductance model.
- When the stimulation is on, the following sequence happens;
 1. The depolarising current breaks the v -nullcline into an upper and a lower branch. There is no more intersection between the two curves, a *spike* can be generated (see Figure 6.1A (right)). However, the space between the lower branch and the w -nullcline is narrow (yellow trace). The trajectory progresses very slowly which corresponds to the spike latency characterising a burst.
 2. The potential reaches v_{th} and so the reset occurs. As previously, the variables change immediately and z increases. It brings the two curves spike closer (see Figure 6.1B (right)). The w -nullcline is lower due to a negative w_0 and it intersects the lower branch of the v -nullcline. The trajectory remains on the upper branch instead of relaxing back to the intersection. Driven by the velocity vectors, it can continue to move to increasing value of v and a new spike is immediately generated, and so on. The relative position between the resting hyperpolarised state and the limit cycle associated to the spike generation explains the second electrophysiological characteristic of the burst; the plateau.
 3. At each spike generation, z increases which is a synonym of the inactivation of the T-type calcium channels. Finally, the v -nullcline comes back to the hourglass shape. Therefore, the trajectory cannot move to high potential values and it has to follow the left branch of the v -nullcline and goes back to the hyperpolarised resting potential. The funnel forces the trajectory to firstly move towards increasing values of v and then reach the fixed point at a lower potential value. It corresponds to the third electrophysiological signature of the burst; the ADP. One sequence of *bursting* is over. There is no more a firing activity.
 4. The variable z is not reset any more, so it decreases following its equation ($\dot{z} = -e_z z$). By decreasing, the v -nullcline breaks into an upper and a lower branch. Then, these two branches move away.
 5. When the intersection between the lower branch and the w -nullcline is removed, the trajectory finds a path to reach high potential value corresponding to a spike.

The sequence is repeated as long as a current is applied. When the stimulation is turned off, the v -nullcline comes back to its hourglass shape and the trajectory is forced to relax back to its resting potential(see Figure 6.1A (right)).

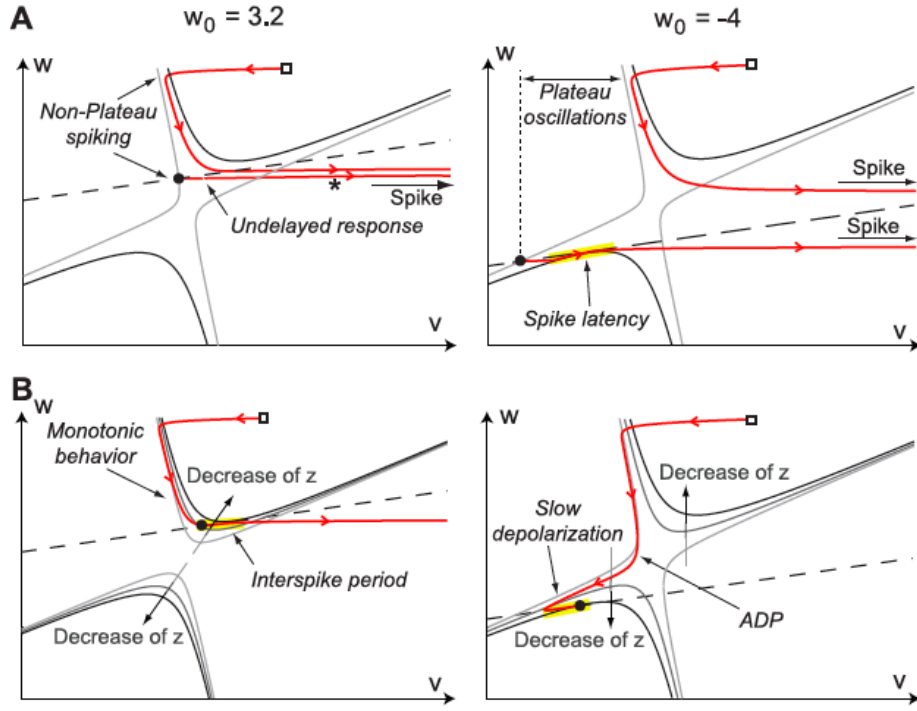


Figure 6.1 – Phase portrait of the transcritical hybrid model of a thalamic neuron for a low (resp. high) conductance mode on the left (resp. right). The red line is the trajectory. The square is the reset point. The dashed-line is the w -nullcline. When the simulation is on (resp. off), the v -nullcline is drawn in black (resp. gray). The different shades of gray are associated to value of z . The darker the curve, the smaller z . [31]

6.2 Hybrid models of thalamic neurons existing in the literature

Izhikevich

Izhikevich model is described by the following equations:

$$\begin{aligned} \dot{v} &= 0.04v^2 + 5v + 140 - v_s + I & \text{if } v \geq 30, \text{ then} \\ \dot{v}_s &= a(bv - v_s) & v \leftarrow c, v_s \leftarrow v_s + d \end{aligned} \quad (6.2)$$

where v stands for the membrane potential in [mV], u is the recovery variable. The parameters a , b , c and d are independent parameters which shape the firing pattern [42] and I is the excitatory current. It is an "improved" version of the fold hybrid model (see equation (5.11)). Indeed, the associated phase portrait consists in a parabola for the v -nullcline and a line for the v_s -nullcline.

Depending on the parameter values, Izhikevich affirms that his model can generate different firing patterns with different sets of parameters described in Figure 6.2.

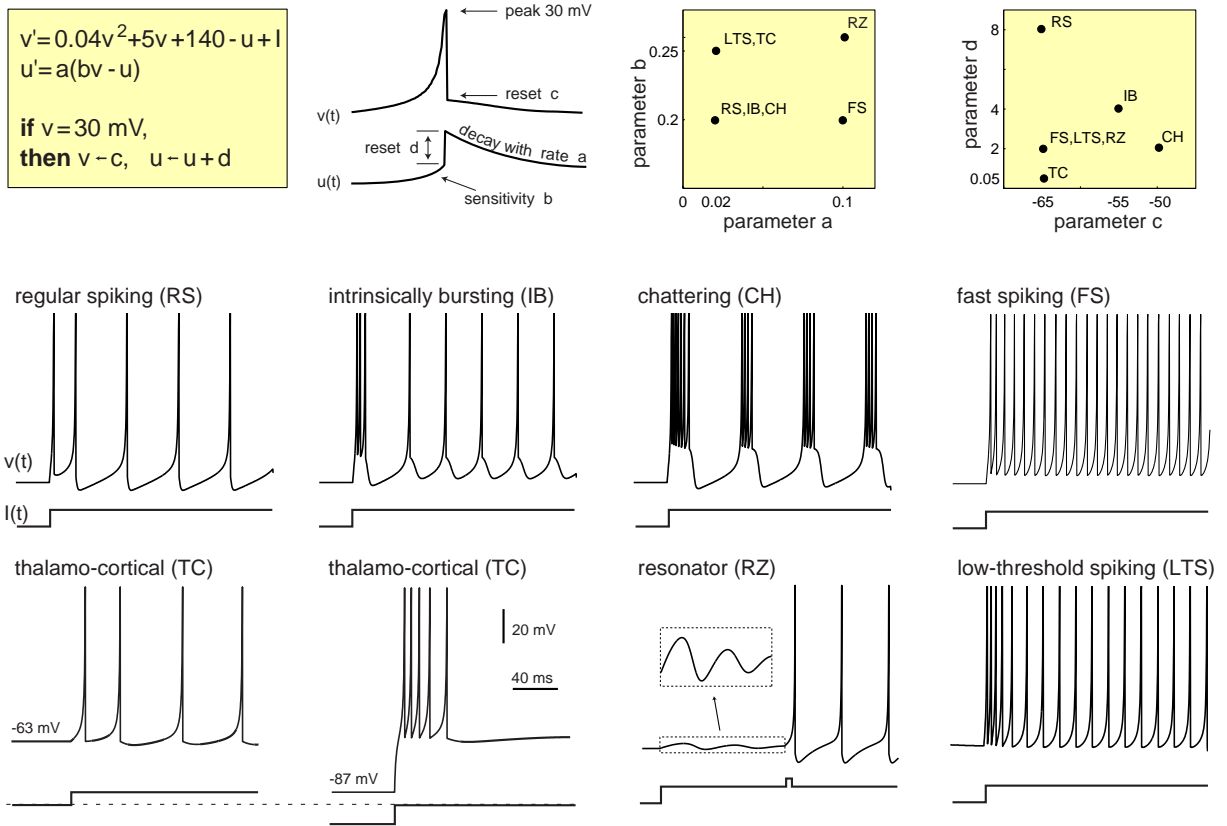


Figure 6.2 – "Simple model of spiking neurons" - *Electronic version of the figure and reproduction permissions are freely available at www.izhikevich.com [41, 42]*

HYB

This model is based on the transcritical hybrid model of the thalamic neuron (see Section 6.1 and [31]). It reproduces the shape of the nullclines in the reduced HHCa model, with the transcritical bifurcation and the ultra-slow inactivation of the T-type calcium current. Indeed, this model relies on a time-scale separation leading to three equations fast, slow and ultra-slow. The slow variable, previously noted w , is x_s and the ultra-slow, previously z , is x_{us} .

The improvement comes from the weighted sum in the first equation. The slow variable and the ultra-slow variable affect the membrane potential through gains noted g_s and g_{us} . It can be visualised as parallel feedback loops with their associated time scale and weight (see Figure 6.3). The density of calcium channels is determined by the sign of the slow feedback gain. If g_s is negative (resp. positive), the density is low (resp. high).

This model called HYB is described by the following equations:

$$\begin{aligned} \dot{v} &= (v - v_{shift})^2 - x_s^2 + b(v - v_{shift})x_s + g_s x_s - g_{us} x_{us} + I_{static} + I_{app} \\ \dot{x}_s &= \epsilon_s (a_s (v - v_{shift}) - x_s) \\ \dot{x}_{us} &= \epsilon_{us} (a_{us} (v - v_{shift}) - x_{us}) \end{aligned} \tag{6.3}$$

if $v - v_{shift} \geq v_{th}$
 $v \leftarrow c, x_s \leftarrow d_s, x_{us} \leftarrow x_{us} + d_{us}$

where v (resp. x_s and x_{us}) merges the membrane potential and fast variables (resp. all slow recovery variables and all ultra-slow adaptation variables), g_s (resp. g_{us}) represents the slow (resp. ultra-slow) equivalent gain, I_{static} is the static current determining the resting potential and I_{app} is the applied current. The other parameters are fixed throughout the analysis $b = -2$, $\epsilon_s = 1$, $\epsilon_{us} = 0.025$, $a_s = a_{us} = 0.1$, $v_{th} = 40$, $v_{shift} = -70$, $c = -45$, $d_s = 30$ and $d_{us} = 20$.

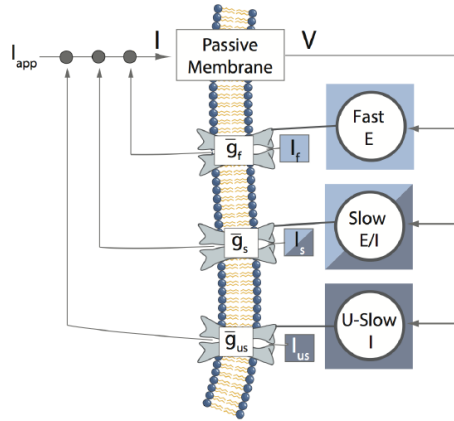


Figure 6.3 – Abstract reduced model with three gains contributing at different time scales. E (resp. I) means positive feedback (resp. negative) feedback and E/I is a mixed feedback [26].

6.3 Switch in Hybrid Models

Theses two hybrid models are not able to switch from tonic mode to burst mode following a hyperpolarising current. As a reminder, the hyperpolarised induced current aims to open calcium channels at lower value of the membrane potential (see Section 2.3.3). Therefore, in order to mimic a hyperpolarised induced bursting in a hybrid model, the switch from one mode to another is achieved by a switch in the parameters as illustrated in Figure 6.4.

Switch in Izhikevich model

According to Figure 6.2, this switch can be reproduced by changing the value of the parameter c from c_{tonic} equals to -65 to c_{burst} equals to -50 . The other parameters are fixed such as $a=0.02$ and $b=0.2$, $d=2$ and $I_{app}=15$ [42]. Figure 6.5 shows the two firing patterns and the mechanisms allowing the switch

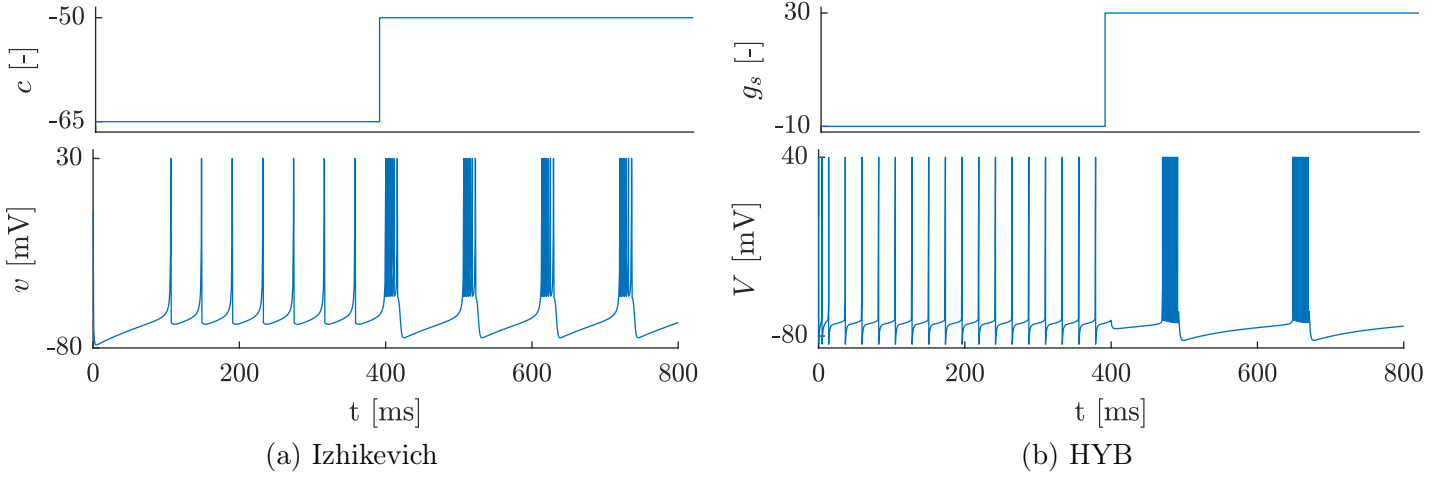


Figure 6.4 – Voltage trace (bottom) of a switch from tonic mode to bursting mode in Izhikevich model (left) and HYB model (right) thanks to a parameter value change (top)

between these two modes in the phase portrait.

- **Spiking mode** (see Figure 6.5, on the left): the trajectory starts from the reset value (blue square) at c_{tonic} which is above the v -nullcline. In this region, the trajectory is driven to the left which corresponds to the hyperpolarisation part. Then, it rapidly goes towards v_{th} , corresponding to the fast upstroke of the spike. When it reaches the threshold value, the reset mechanism occurs and the variables are positioned in the blue square. The same sequence can be reproduced and it perfectly draws the spike.

- **Bursting mode** (see Figure 6.5, on the right): when the first upstroke in the phase plane reaches v_{th} , the reset mechanism occurs and sets v to c_{burst} and v_s to $v_s + d$. By contrast to the spiking mode associated with c_{tonic} , c_{burst} is greater and so not included inside the parabola of the v -nullcline. This region drives the trajectory to the right which corresponds to the generation of the second spike. The reset mechanism occurs again and so on. After several spike generations, u has increased such as it lies inside the parabola where the trajectory is driven to the left. It corresponds to the end of the burst and the hyperpolarisation. Then, the reset takes place again and c_{burst} is still on the right of the v -nullcline, the whole process starts over again [66].

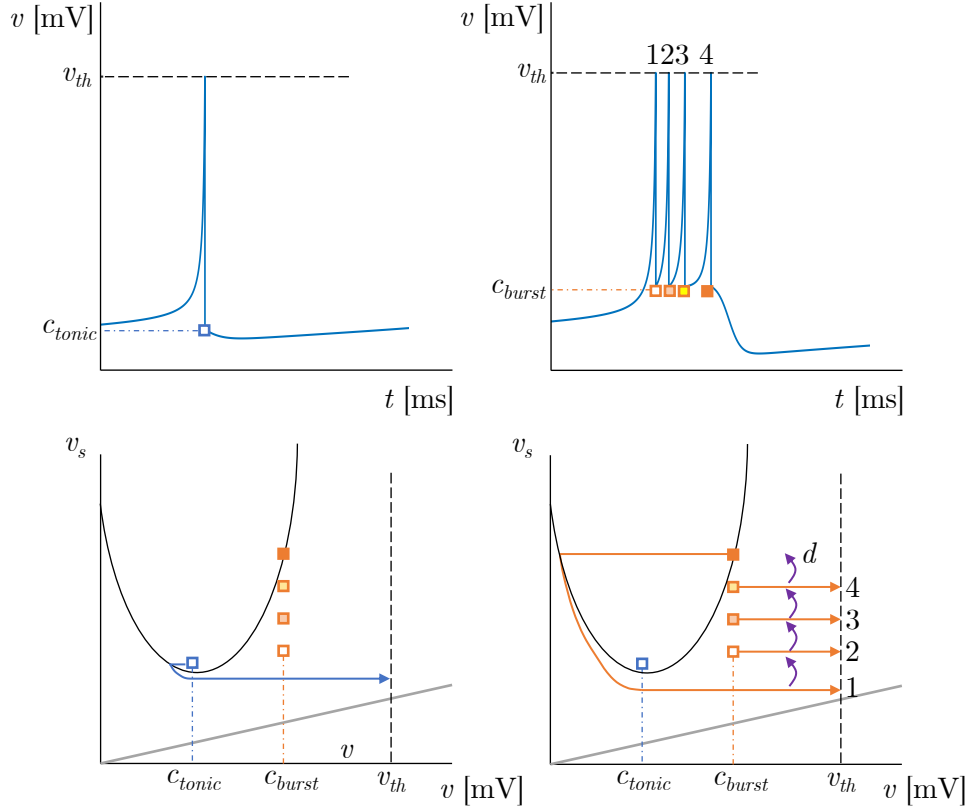


Figure 6.5 – Schematic description of the tonic mode (left) and bursting mode (right) in Izhikevich model with the voltage trace (top) and its associated phase portrait (bottom). The v -nullcline (resp. v_s -nullcline) is drawn in black (resp. gray) line. The reset point in tonic mode (resp. bursting mode) is the blue (resp. orange) square. (inspired from [66])

Switch in HYB model

By contrast to Izhikevich model, in the HYB model, the switch is not performed by changing the reset rule but by changing the value and the sign of g_s , which accounts for the slow equivalent gain (see Figure 6.4 (right)).

In a thalamic neuron, a hyperpolarisation-induced bursting is characterised by the de-inactivation of the T-type calcium channels (see Section 2.3.3). To reproduce this behavior, the density of calcium channels increases, which corresponds to a switch in the sign of the slow feedback gain from negative to positive [26].

The impact in the phase portrait can be explained with the phase portrait of the transcritical hybrid model shown in Figure 6.1.

The density of the calcium channel is fixed by the value w_0 in the transcritical hybrid model. In the phase portrait, a low (resp. high) density mode is visualised by moving the w -nullcline up to intercept the upper (resp. lower) branch of the v -nullcline. The position of this intersection governs the firing pattern (see Figure 6.1).

In the HYB model, w_0 is not in the slow time-scale equation. Therefore, the linear nullcline does not move. It is replaced by the action of the slow feedback gain in the first equation. If the density of the calcium channels is low, the slow feedback gain g_s is negative. In contrast, if the density of the calcium channels is high, the slow feedback gain g_s is positive [26]. In the phase portrait, it is no more the w -nullcline which moves but the v -nullcline. However, from a dynamic point of view, it is equivalent.

6.4 Network Analyses

This section studies these two hybrid models of thalamic neuron at the network level. Once more, the behavior of neuron populations in the thalamus relies on the excitatory-inhibitory circuit between the relay cells and the reticular nucleus cells. The switch at the cellular level induces a rhythmic synchronisation in the larger population.

The two hybrid models rely on two different normal forms; either a fold normal form like the HH model for the Izhikevich' or a transcritical normal form like the HHCa model for the HYB. Besides, the switch from tonic mode to bursting mode is based on a mathematical manipulation of the reset rule for Izhikevich while for the HYB model, the switch is a synonym of the de-inactivation of the T-type calcium channels.

The goal of the network analysis for these hybrid models is similar to the network analysis for the conductance based models. We want to show that models that lack the slow dynamics of the calcium current (such as Izhikevich model) are not able to handle variability that mimics the regulatory mechanisms present in the thalamic neurons population. Consequently, we will identify the hybrid model that is suitable for studies grounded on the synaptic plasticity or neuromodulation studies.

The same protocol as the network analysis of conductance-based model is followed. The robustness analysis is performed on a 2-cells E-I network, then the modulation properties are displayed, and finally, the population rhythm is computed through the derivation of the spectrogram of the LFP. The synaptic perturbations are exactly the same as those injected in conductance-based models (see Section 4.3.1). The main difference with the conductance-based models is the choice of the intrinsic perturbations. Previously, the maximum conductances and the capacitance were perturbed in order to reproduce the action of neuromodulators. Here for Izhikevich model, the parameters c et d are used to control the shape of the burst (see Section 6.3 and [42]). Similarly, for HYB, g_s and g_{us} dictate the firing mode and the number of spikes per burst [26].

6.4.1 ANALYSIS OF THE ROBUSTNESS

The robustness analysis is based on a 2-cells E-I network connected with two synaptic connections AMPA and GABA_A. Note that since it is not a real hyperpolarisation-induced bursting, GABA_A is sufficient to hyperpolarise the two populations of neurons.

On one side, in order to reproduce the synaptic plasticity, the connections are subjected to perturbations called *extrinsic perturbations* acting on the synaptic weight g_{syn} (see Section 4.3). On the other side, in order to reproduce the effect of neuromodulators, the parameters shaping the firing patterns are perturbed. These perturbations are called *intrinsic perturbations*.

Similarly, the parameters in the hybrid models are picked randomly following a uniform distribution in ranges subjected to the same *relative intrinsic variability* noted γ and expressed in %. The changes in parameter values correspond to the *intrinsic variability*.

Procedure

The robustness comparison between Izhikevich and HYB models is achieved by deriving the evolution of the percentage of networks that have *switched from tonic to bursting and generated a synchronous bursting* (noted y in %). It follows the same protocol as done for the conductance-based model (see Figure 4.5)

Results

Figure 6.6 illustrates the percentage of rhythmic networks as a function of γ . The first observation is the decrease of the rhythmic network activity with an increasing intrinsic variability. The second remarkable observation is the robustness of the HYB model against Izhikevich. Indeed after $\gamma = 5\%$, the percentage of rhythmic networks in Izhikevich model shrinks and then it always stays lower than HYB model.

Similarly to the conductance-based models, at $\gamma = 0\%$ when only the synaptic connections are perturbed, both models generate 100% of rhythmic networks. The extrinsic perturbation does not affect the robustness as much as the intrinsic perturbation.

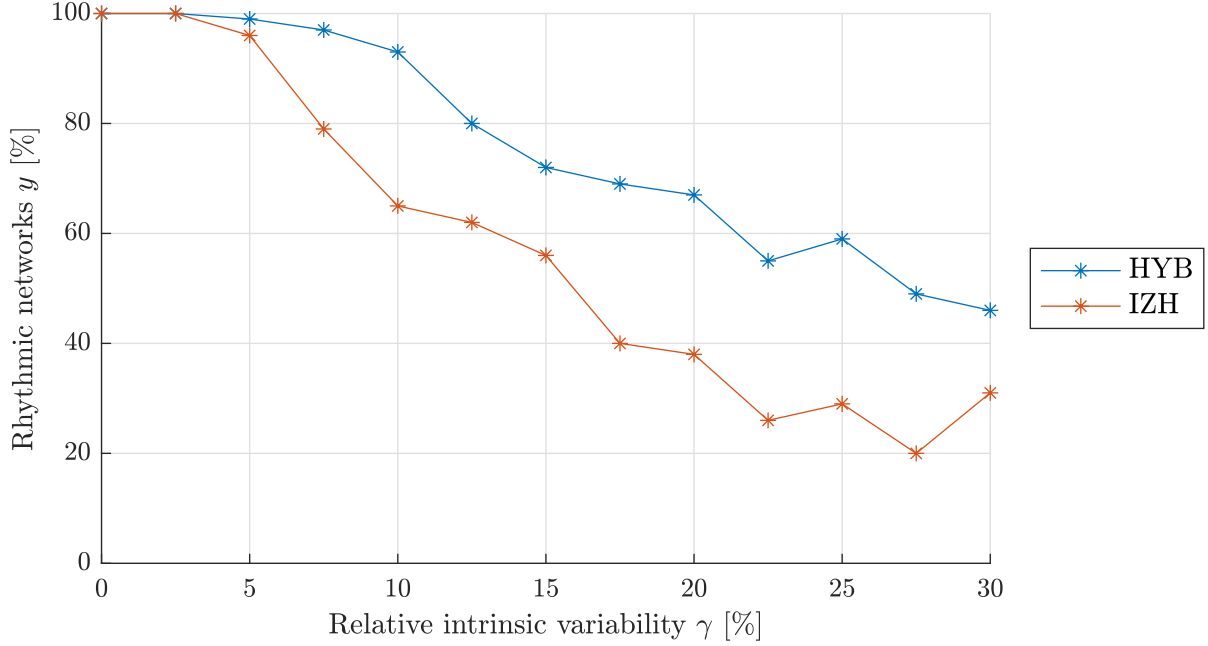


Figure 6.6 – Evolution of the percentage of rhythmic networks (y) as a function of the relative intrinsic variability (γ) for Izhikevich and HYB models computed with the nominal values of the intrinsic parameters.

The off-centering does not really impact the shape of the curves in both model (see Figure D.4 in Appendix D.3.2). As well as in the conductance-based modeling, some sets of parameters will provide better or worse results. In the sphere analogy (see Figure 4.7), it means good set of parameters are situated in the middle of the orange area.

6.4.2 ANALYSIS OF TUNABILITY

Procedure

An analysis similar to the one carried out for the conductance-based models is followed (see Section 4.4). The physiological property of the hyperpolarisation-induced bursting is interesting to exhibit (see equation (4.2)). Then, the different characteristics of the two firing patterns are displayed when the model is subjected to the maximum value of the relative intrinsic variability γ which gives at least 40% of rhythmic networks. The maximum value is called γ_* such as $y \geq 40\%$. For Izhikevich, γ_* is equal to 17.5% and for HYB is equal to 30%.

Results

• Physiological property

Figure 6.7 shows the evolution of the tonic and the intraburst frequencies of the rhythmic networks when the intrinsic relative variability (γ) increases.

The general observations are the same as the one done in Section 4.4 concerning the decrease of the percentage of rhythmic networks for an increasing value of γ , and the small impact of the synaptic plasticity on the modulation (at $\gamma = 0\%$).

The physiological property is verified in both models; they have a tonic frequency lower than the intraburst frequency.

• Tunability

Figure 6.8 shows the distribution of the four firing characteristics of the inhibitory cells. Similar results are shown for the excitatory cells (see Figure D.5 in Appendix D.3.3).

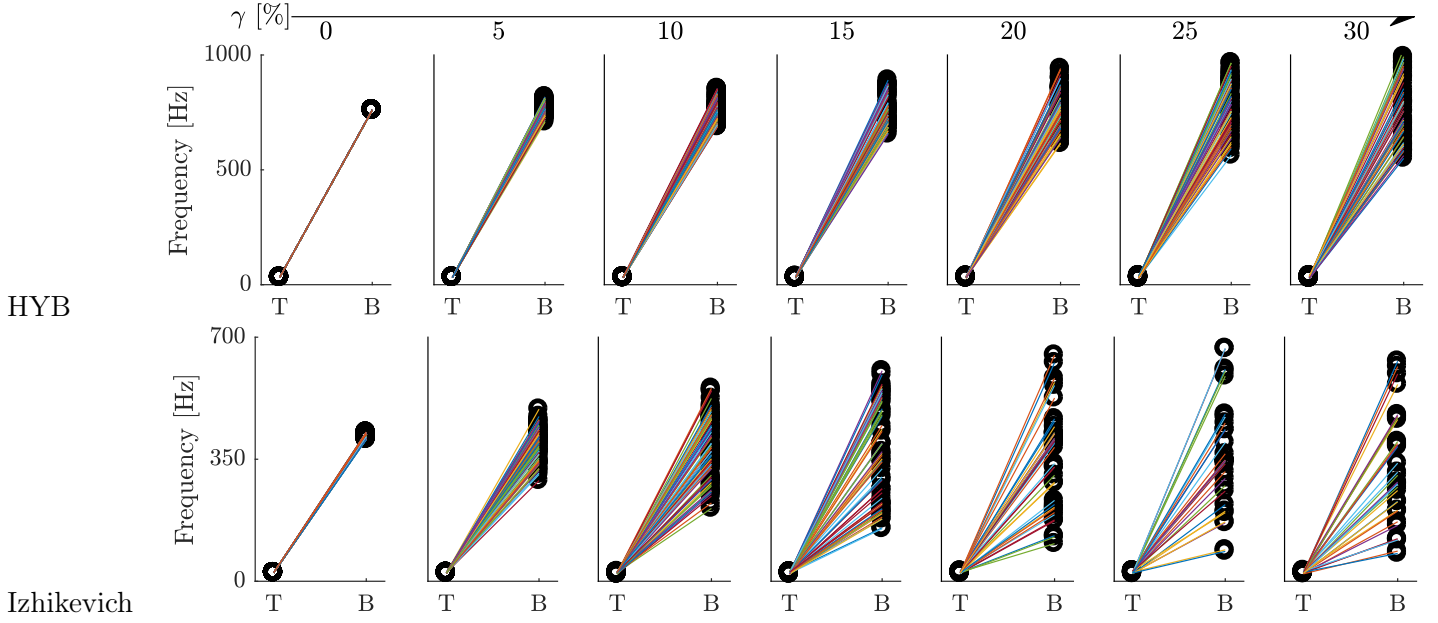


Figure 6.7 – Evolution of the relationship between the tonic frequency and the bursting frequency for each rhythmic network for an increasing relative intrinsic variability in Izhikevich and HYB models.

- Duty cycle: Izhikevich covers a wider range than HYB model.
- Interburst frequency: the mean of both models is physiological and they cover quite a wide range too.
- Tonic frequency: both means are physiological (according to [15, 50]) and the covered range is slightly bigger for the HYB model.
- Intraburst frequency: this characteristic is too high for the HYB model. For Izhikevich model, the mean is still quite high and the covered range is very large.

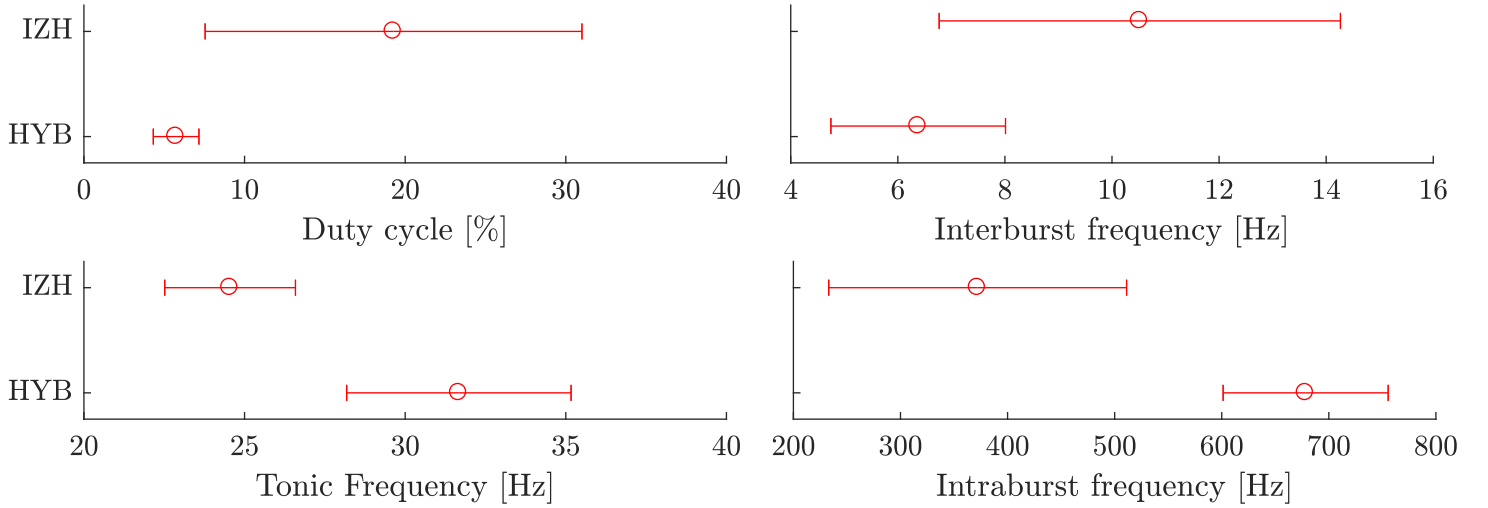


Figure 6.8 – Mean and standard deviation of the distribution of the four firing characteristics for the rhythmic networks in HYB and Izhikevich models computed for γ_*

6.4.3 ANALYSIS OF HETEROGENEITY

Procedure

The computational experiment done to evaluate the activity of the population is exactly the same as the one carried out for the conductance based model (see Section 4.5). A 200-cells E-I network is created. The synaptic connections are exposed to the same variability as described in Section 4.3. Then, each cell is computed from parameters randomly picked following a uniform distribution in ranges subjected to the relative intrinsic variability γ .

The key interest of this computational experiment is even if at the cellular level, the voltage-traces are heterogeneous, a population rhythm exists as displayed in Figure 4.16. The population rhythm of the inhibitory cells are compared in two situations; either when only the synaptic connections are subjected to perturbations or both synaptic connections and the parameters are subjected to perturbations (for an relative intrinsic variability equal to $\gamma = 10\%$).

Results

Figure 6.9 illustrates the spectrograms of the LFP recorded in a 200-cells E-I network where only the inhibitory cells are represented. The spectrograms associated to the excitatory cells are displayed in Figure D.6 in Appendix D.3.4. They show similar results.

At 20 [s], the change in parameters values is supposed to induce a switch in the firing mode in each cell. The population rhythm results in the synchronisation of each cell. When both models are only subjected to extrinsic perturbations, they display a population rhythm indicated with a larger spectral power in a confined frequency band around 10 [Hz] for Izhikevich and respectively 6 [Hz] for the HYB model. The intensity of this band is higher for the HYB model.

Then, the parameters are subjected to intrinsic variability, the synchronisation of the cells is less pronounced, resulting in a smaller intensity of the spectral power band and a wider range of frequency. For both values of γ , Izhikevich displays a smaller intensity than the HYB model.

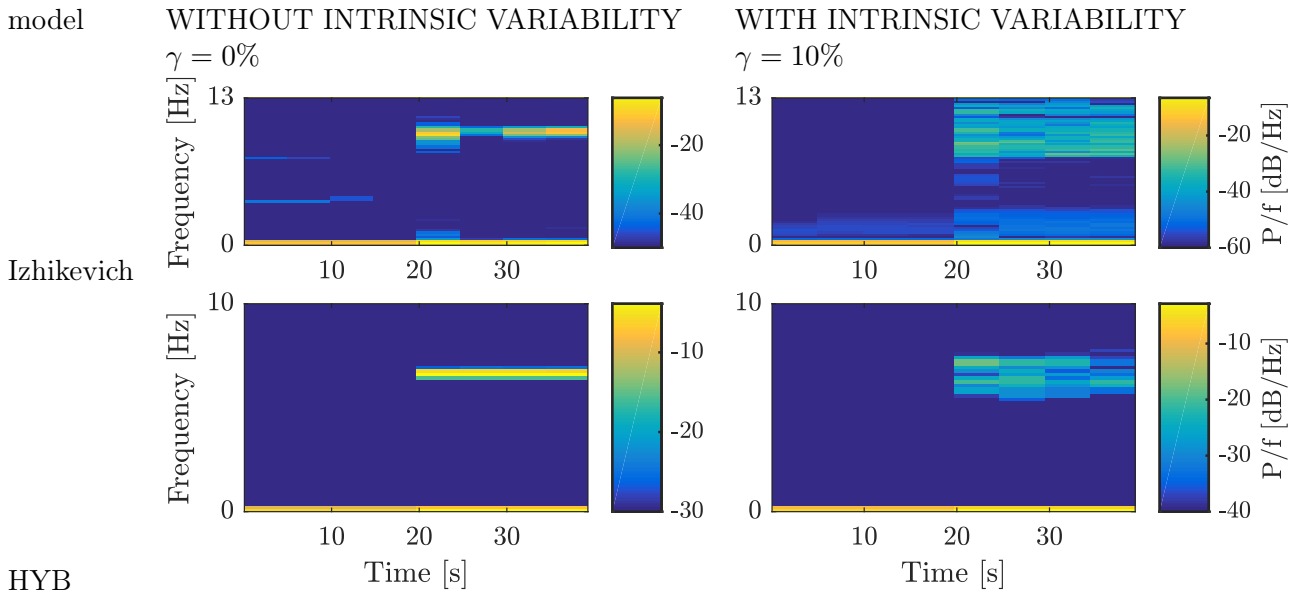


Figure 6.9 – Spectrogram of the LFP of the I-cells populations in a 200 network without intrinsic variability (on the left) and with a relative intrinsic variability of 10% (on the right) for Izhikevich model and HYB model. The intensity of the power spectral content is expressed in Power/Frequency, denoted P/f .

6.5 Discussion

This section aimed at studying two hybrids models of thalamic neuron at the network level. The thalamus is well-known for its state-dependent behavior. At the cellular level, the state change from awake to asleep is characterised by a switch from spiking to bursting. At the network level, this switch in the firing pattern is seen as a switch in the population rhythm; from an asynchronous behavior to a synchronisation of the population with the emergence of a slow frequency rhythm. Neuromodulation mechanisms and synaptic plasticity are two components interacting with this switch. In order to deeper study thalamic neuron at the network level, a model is expected to reproduce this switch property without being affected by these regulatory mechanisms [24, 25, 29, 31, 35, 50].

Therefore, this section compares two hybrid models relying on two distinct methods to reproduce the two firing patterns characterising the behavior of a thalamic neuron. On the one hand, Izhikevich model is based on the fold normal form. This phase portrait is derived from the reduction of the HH model. That model is known to mimic the sodium-potassium spike. At the cellular level, Izhikevich model is able to switch from tonic to burst mode thanks to a change of the reset rule. Indeed, this mathematical manipulation moves away from physiological interpretation. Besides, this reset alteration does not respect the interpretation of a hybrid model. The definition is founded to "the local approximation of the reduced conductance based model completed by a reset rule compatible with the global continuous-time dynamics" [66]. When Izhikevich modifies the rule, he destroys the translation to an equivalent continuous-time phase portrait [66].

On the other hand, the HYB model is based on the transcritical normal form which is a reduction of the HH model altered by the slow kinetics of the T-type calcium channels. The switch at the cellular level is achieved by changing the parameter reflecting the proportion of calcium channels which are not activated [26, 31]. The biological foundation of this model brings the robustness at the network level as proved by the different computational experiments. The model handles well regulatory mechanisms such as one network over two is still able to switch and burst synchronously when the parameters g_s (resp. g_{us}) are picked in the range $[70\%g_s; 130\%g_s]$ (resp. $[70\%g_{us}; 130\%g_{us}]$). The model is also very tunable. The high value of the tonic frequency can be decreased by reducing the excitatory current. Furthermore, the population rhythm when 200-cells are subjected only to synaptic variability is very distinguishable.

Accordingly, the Izhikevich model lacks physiological interpretation and so it cannot be used in neurocomputational studies. By contrast, HYB model is a good candidate for deeper network analysis.

However, the switch from one mode to another is achieved by changing the density of calcium channels. This alteration is achieved "manually" while in a real thalamic neuron, the de-inactivation of calcium channels occurs when the membrane potential is hyperpolarised. This mechanism can be integrated in the model by adding a new equation accounting for the voltage-dependent adaptation of the slow gain g_s in the ultraslow time scale [26]:

$$\tau_s \dot{g}_s = a_{g_s}(v - v_s) - g_s + g_{s,min} \quad (6.4)$$

Thanks to this fourth equation, the model can simulate a real hyperpolarisation-induced-bursting as shown in Figure 6.10.

This adapted model is now a very good candidate for more complex computational experiments. It reproduces the real hyperpolarisation-induced bursting at the cellular level and it is robust to synaptic variability and intrinsic variability [28]. Its advantage compared to Drion model is its hybrid nature which leads to less time-consuming simulations.

As a preliminary comparison, the computation-time of the HYB model and Drion model for four experiments is given in Table 6.1.

The first simulation is the generation a HIB. Only the resolution of the differential equations is achieved, in order to obtain the membrane potential evolution. The gain by using the HYB model is equal to 55 [ms]. Then, the second experiment is the generation of 100 circuits of 2-cells connected. Only the firing characteristics are memorised. Using the hybrid model saves 9 [min]. The third (resp.

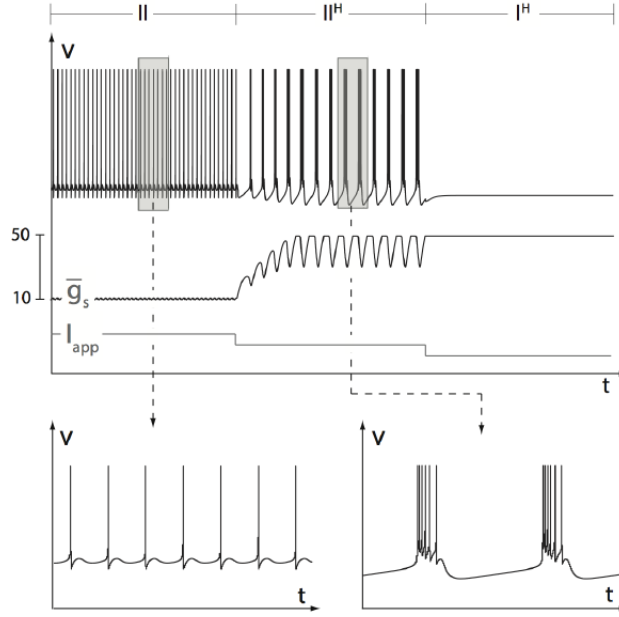


Figure 6.10 – The HYB model reproduces a hyperpolarisation-induced bursting - the step hyperpolarising current acts on the slow adaptation of the slow gain which in turn changes the firing pattern from tonic to bursting mode. (bottom) The tonic frequency is well lower than the interburst frequency [26]

fourth) experiment is the generation of a circuit of 200 (resp. 500) cells and to compute the LFP. Using the HYB model saves 6 [min] (resp. 23 [min]).

Experiment	Drion	HYB	Gain
HIB in 1cell [ms]	90	35	55
Characteristics of 100 networks of 2-cells[min]	16	7	9
LFP for 200 cells [min]	29	23	6
LFP for 500 cells	3h13	2h50	23 min

Table 6.1 – Computation-time comparison between Drion and HYB models for different experiments.

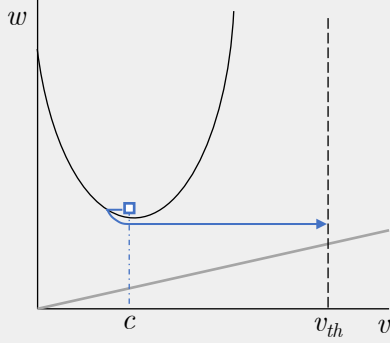
6.6 Summary

STATE-OF-ART

without the slow dynamics of the calcium current

Fold hybrid model

$$\begin{aligned}\dot{v} &= v^2 - w + I & \text{if } v \geq v_{th}, \text{ then} \\ \dot{w} &= \epsilon(av - w) & v \leftarrow c, w \leftarrow d\end{aligned}$$

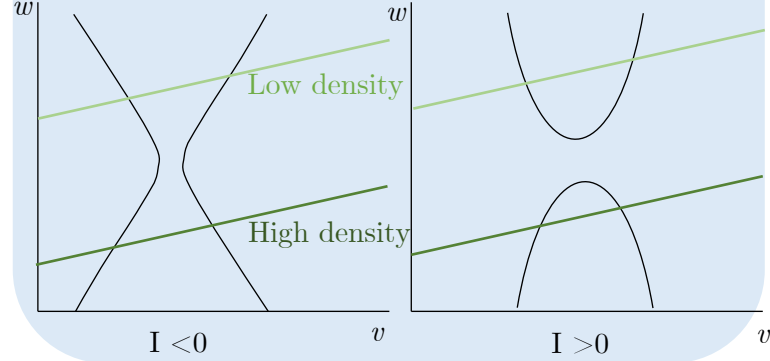


with the slow dynamics of the calcium current

Transcritical hybrid model

$$\begin{aligned}\dot{v} &= v^2 - w^2 + I & \text{if } v \geq v_{th}, \text{ then} \\ \dot{w} &= \epsilon(aV - w + w_0) & v \leftarrow c, w \leftarrow d\end{aligned}$$

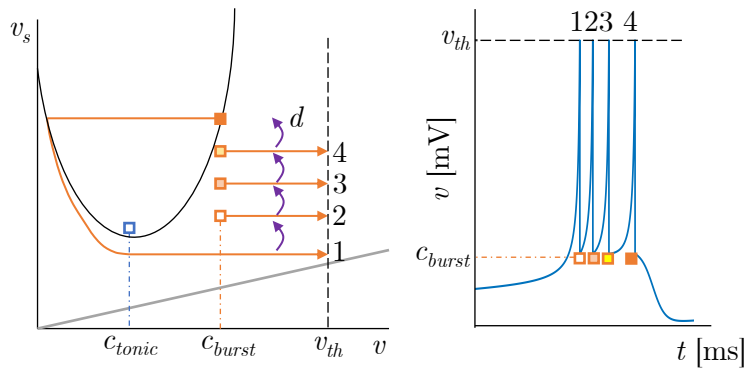
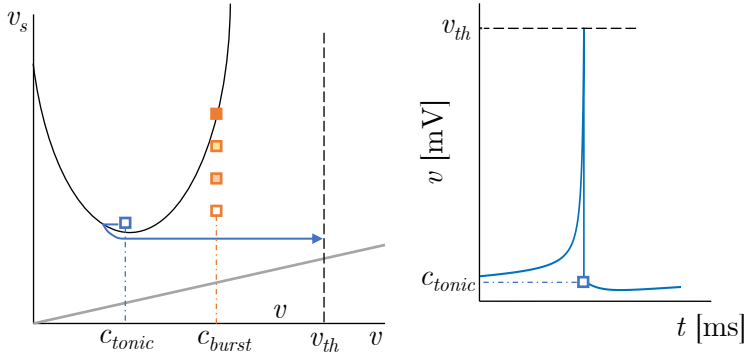
density of calcium channels



HYBRID MODELING OF THALAMIC NEURONS

Izhikevich model

$$\begin{aligned}\dot{v} &= 0.04v^2 + 5v + 140 - v_s + I & \text{if } v \geq 30, \text{ then} \\ \dot{v}_s &= a(bv - v_s) & v \leftarrow c, v_s \leftarrow v_s + d\end{aligned}$$



Switch from tonic to burst
= change the value of c
= alteration of the reset rule

HYB model

$$\begin{aligned}\dot{v} &= (v - v_{shift})^2 - x_s^2 + b(v - v_{shift})x_s + g_s x_s \\ &\quad - g_{us} x_{us} + I_{static} + I_{app} \\ \dot{x}_s &= \epsilon_s(a_s(v - v_{shift}) - x_s) \\ \dot{x}_{us} &= \epsilon_{us}(a_{us}(v - v_{shift}) - x_{us})\end{aligned}$$

if $v - v_{shift} \geq v_{th}$
 $v \leftarrow c, x_s \leftarrow d_s, x_{us} \leftarrow x_{us} + d_{us}$

Ultra-slow variable to mimic the de-inactivation of the T-type calcium current

Slow feedback gain
= density of the calcium channels

$g_s < 0$ = low density \rightarrow tonic mode
 $g_s > 0$ = high density \rightarrow bursting mode

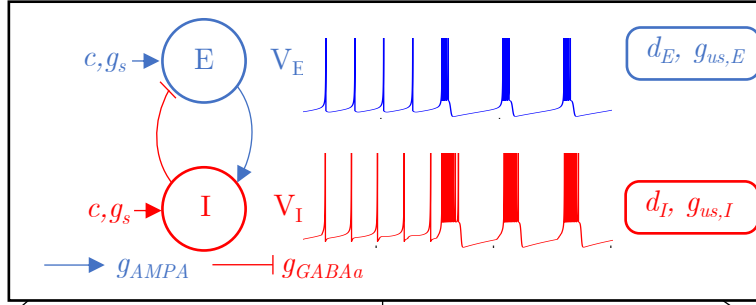
Switch from tonic to burst
= change the value of g_s
= change the density of calcium channels

CONTRIBUTIONS

2-cells of a E-I circuit

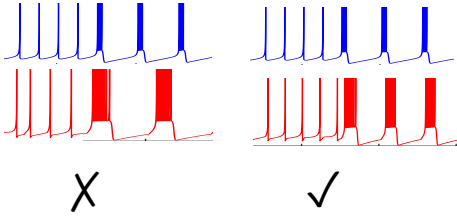
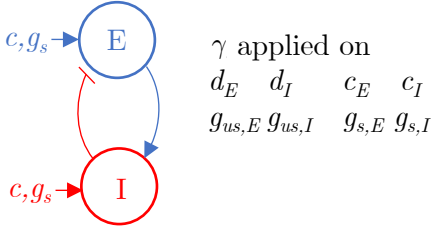
Izhikevich parameters:
 $c - d$

HYB parameters:
 $g_s - g_{us}$

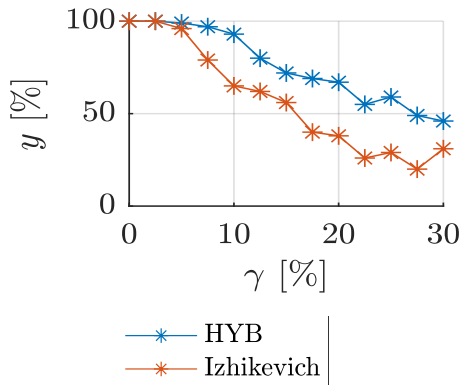


Robustness analysis

100 x 2-cells of in a E-I circuit

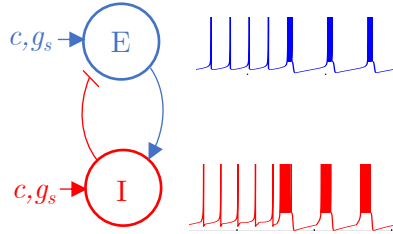


y : % of rhythmic networks
(switch + synchronous burst)

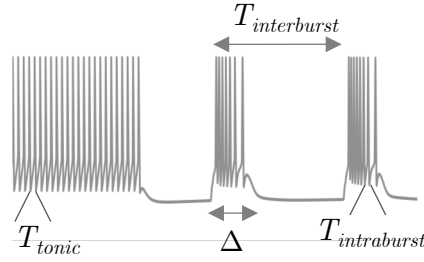


Tunability

100 x 2-cells of in a E-I circuit
for a given perturbation γ



Firing characteristics analysis



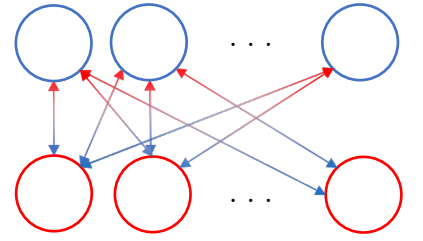
To verify in each model:

- ✓ $f_{tonic} < f_{intraburst}$
- ✓ physiological values
- ✓ range of modulation

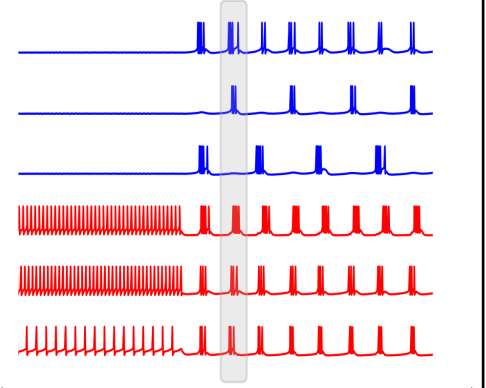
The rhythmic network activity should be modulable and not display a rigid range for each characteristics.

Population rhythm

100 cells E connected to 100 cells I



200-cells in a E-I circuit
for a given perturbation γ



spectrogram of the LFP
(sum of the post-synaptic currents)



synchronisation of the population

- Synaptic connections are perturbed to mimic **synaptic plasticity**
- Parameters implicated in the firing pattern are perturbed to mimic the effect of the **neuromodulators**

Part IV

Conclusion and Perspectives

Chapter 7

Conclusion and Perspectives

7.1 Summary

This thesis is devoted to the comparison of two classes of thalamic neurons models. One class integrates the slow activation of the T-type calcium current while the other class assumes that this activation is fast.

We show that the class integrating the slow kinetics provides better results in terms of robustness. This demonstration is performed at the cellular and network levels, for conductance-based models or reduced models. Therefore, the models of this class are suitable for studies concerning the neuromodulation or the synaptic plasticity. In opposition to the models of the other class, which assumes the fast activation of the calcium current, are fragile and rigid.

To reach this conclusion, the thesis is articulated into three main parts.

Part I sets the background which is necessary to enter the field of computational neuroscience. It reminds what a neuron is and its electrical analogy. Then, the first neuron model elaborated by Hodgkin and Huxley (HH) is derived. Besides, since this thesis only focuses on thalamic neurons, understanding the role and the behavior of the thalamus is fundamental. It exhibits two firing patterns depending on the state; during wakefulness, the neuron is in spike mode and during sleep, the neuron is in bursting mode. Considering a larger population, sleep is characterised by a neuronal synchronisation. This sleep-dependent activity is governed by the T-type calcium current.

Part II is dedicated to the conductance-based modeling of thalamic neuron. We compared five models; Destexhe (1998), Drion (2017), Huguenard and McCormick (1992) (HM), Rush and Rinzel (1994) (Rush), Wang (1994). These models differ in terms of parameter value, number of currents and their kinetics. Destexhe, Drion and HM models have considered the slow kinetics of the activation of the T-type calcium current while Rush and Wang models have set the activation at its steady-state value.

Then, this common reduction strategy is discussed at the cellular level in [35]. It is shown that if the activation of the calcium channels is fast, it merges with the activation of the sodium channel and the robustness of the bursting model is lost. Therefore, the first contribution is to compare the robustness of the five conductance-based models when the maximal conductances are uniformly scaled. Rush and Wang models are no more able to switch from tonic mode to bursting mode. They cannot mimic the state-dependent behavior of the thalamic neuron while the three other models switch.

We create a new version of the Rush model called RushCa which conserves the slow kinetics of the calcium channels activation. Contrarily to Rush model, this model can handle the perturbation and still switch.

Afterwards, moving to the network level, we were interested in thalamic neuron models which can reproduce the rhythmic activity without a change in the synaptic connections and can handle neuromodulation. Therefore, the same six conductance-based models were studied by perturbing the synaptic connections and the intrinsic parameters. For the robustness analysis, 100 E-I networks of

2-cells were generated for a growing intrinsic perturbation. Drion model leads in terms of robustness, followed by Destexhe and RushCa models. When the parameters are randomly picked in an interval of $\pm 30\%$ around their nominal values, HM, Rush and Wang models are only able to switch one out of five times. Their robustness is poor.

The tunability of rhythms at the cellular level of the 2-cells E-I networks in each model has been studied by displaying the characteristics of the firing patterns; the duty cycle, the tonic, the interburst and the intraburst frequencies. Only Destexhe, Drion and Wang models generate networks where the tonic frequency is lower than the intraburst frequency which is a property of the switch. However, Rush and Wang models present firing characteristics which are not representative of thalamic neurons. Then, HM and RushCa models do not display a nice tunability. This comes from the high-dimensional order of the HM model. For RushCa model, a deeper elaboration of the model might help. Indeed, only the activation of the calcium current has been changed without adapting the other kinetics.

Finally, the switch must be robust across the scales. An E-I circuit of 200 cells is created from each model with perturbations added on the synaptic connections and intrinsic parameters. Drion and Destexhe models are the only conductance-based models which present a population rhythm when their intrinsic parameters are subjected to 20%.

Part III investigated the reduced modeling. First, the reduction of HH model was performed and it leads to its description in the phase plane [34]. In parallel, including the calcium current in the HH model drastically affects the phase portrait [31]. Two hybrid models were developed based on these two distinct reduced models. One relies on the fold normal form while the other one relies on the transcritical normal form. Indeed, a hybrid model is an approximation of the phase portrait completed with a reset rule reproducing the all-or-none nature of the spike. Understanding the definition of a hybrid model and the alteration of the phase portrait caused by the presence of calcium is important to investigate the hybrid modeling of thalamic neuron.

After laying the foundation of the reduced modeling, we are interested in hybrid models that can fire in spiking mode and bursting mode in order to mimic thalamic neuron. We retrieve two models from the literature. On the one hand, Izhikevich model is an extended version of the hybrid model based on the fold normal form. It is able to switch from one mode to another by changing its reset rule [42]. On the other hand, HYB model leans on the transcritical normal form. This model switches by changing the parameter representing the density of calcium channels.

The same network analyses as those done on the conductance-based models were performed on these two hybrid models. Izhikevich model is less robust than the HYB model. On the one hand, this is explained by the origin of the switch that relies on a mathematical manipulation of the reset rule. This breaks the connection with the conductance-based modeling because it is impossible to retrieve an equivalent continuous phase portrait [66]. On the other hand, the HYB model is based on the new phase portrait founded from the reduced HH model with integrates the slow dynamics of the calcium current activation. Its parameters have a biological interpretability.

Through all these computational experiments performed at the cellular or the network levels, for conductance-based models, the slow kinetics of the calcium current activation has been shown to be primordial to ensure the robustness of the thalamic neuron model. Similarly, for hybrid models, the lack of the slow dynamics leads to fragile and rigid models which deviate from the biology.

In general, scientists elaborate their model following the HH model and add new currents. They fit the kinetics of each current with their experimental data. However, another way to establish a model starts with the deep understanding of the dynamics of the different currents present in the thalamus. Then, studies, in the phase plane, are performed as well as analysis of the weighted contribution of each current in the firing patterns as done in [29, 36]. This procedure drives the Drion model to be the most robust presented in this work.

In addition, as shown in this thesis, a robust thalamic neuron model does not necessarily require a complex biological description. The robustness key is the contribution of each current at the right time scale. The HYB model, which integrates this time-scale separation, is sufficient to reproduce a robust switch. The advantage of the HYB model, compared to a conductance-based model, is its lower computation-time. So, it is a good candidate for large neurons population.

7.2 Prospects

Implications in computational experiments

This thesis contributes to show the importance of the slow dynamics of the calcium current activation on thalamic neuron models through computational experiments performed both at the cellular and the network levels. It would be interesting to improve these experiments by increasing the number of cells and networks. It would require faster computers or longer periods. Moreover, a more general comparison procedure could be investigated. The conductance-based models have different currents and associated kinetics. They could be reduced to common features called *dynamic input conductances* following the protocol given in [27]. These quantities mimic the role of ion channels impacting a firing pattern at one specific time scale. All the models would be reduced to the same features according to their own kinetics and so the comparison would be more general.

Then, verifying the impact of the reduction strategy could be done for models of other brain parts that have the two firing patterns for example, the STG cell or the Purkinje cell.

Implications in applications of thalamic models

The interest on the thalamic neurons is not only a modeling challenge for the engineers but it also helps better understanding the pivotal role of the thalamus for neuroscientists. Indeed, the transition from wakefulness to sleep is correlated with a change in the processing of neuron signals [50, 59]. The synchronisation of neurons characterising the sleep state in the thalamus is associated with a filtering of the input information towards the cortex.

An extreme situation is the development of synchronised sleep oscillations into *absence epilepsy* during wakefulness. It is seen as a brain disconnection from the rest of the world [29, 62]. An absence seizure is characterised by a brief loss followed by a return of consciousness [17, 60]. The patient loses its ability to respond to sensory stimuli and he has no recall of the episode [45].

The hallmark of absences is a 3Hz synchronous network activity in the thalamic circuitry [39]. This typical feature is called spike-wave discharges (see Figure 7.1 (top)). This manifestation of absence epilepsy and sleep spindles (see Figure 7.1 (bottom)) have a common neuronal network mechanisms. It suggests a close relationship between them [61].

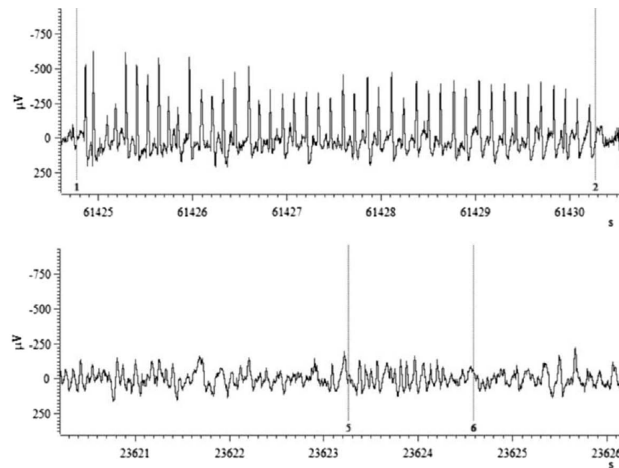


Figure 7.1 – EEG recording of spike-wave discharges (top) and spindle waves (bottom) in 8.6-month-old WAG/Rij rat - [61]

Voltage-activated T-type calcium channels play a major role in the generation of burst firing. It is thought that they have also a critical role in the mechanism of absence epilepsy. Besides, some experiments have detected changes in the gene encoding of these channels in some patients with epilepsies [10, 39]. The drug currently used in the anti-epileptic treatment is ethosuximide which is shown to block T-type calcium channels in thalamic relay neurons [60].

Therefore, this disease highlights the importance of a good thalamic neuron model that includes the biological behavior of the T-type calcium channels. Having a robust model is crucial to perform network simulations and therefore deeper studies on the impact of these channels.

Another interesting topic is to understand how the sleep contributes to memory; a property called sleep-dependent memory consolidation [49]. Some studies show a relationship between the rhythmic activity of the thalamus and the synaptic plasticity, and hence, in the process of memory consolidation [61]. The mechanisms underlying the relationship are still largely unknown. Robust models that reproduce the changes in thalamic rhythmic activity could help fitting this gap.

“ If you feel you are in a black hole, don't give up. There's a way out. ”

Stephen Hawking

Appendix A

Conductance-based models of thalamic neuron: detailed modeling

A.1 Hodgkin and Huxley model [38]

The HH model [38] follows these equations

$$C_m \dot{V}_m = -\bar{g}_{Na} m_{Na}^3 h_{Na} (V_m - V_{Na}) - \bar{g}_K m_K^4 (V_m - V_K) - g_L (V_m - V_L) + I_{app} \quad (A.1)$$

with $V_{Na} = 50$ [mV], $V_K = -77$ [mV], $C_m = 1$ [nF], $\bar{g}_{Na} = 120$ [mS], $\bar{g}_K = 36$. The applied current I_{app} is defined by

$$I_{app} = I_{cst} + I_{step}(t \geq T_{step,init} \& t \leq T_{step,end})$$

The dynamics of the gate variables are

$$\dot{m}_{Na} = \frac{m_{Na,\infty}(V_m) - m_{Na}}{\tau_{m_{Na}}(V_m)} \quad \dot{h}_{Na} = \frac{h_{Na,\infty}(V_m) - h_{Na}}{\tau_{h_{Na}}(V_m)} \quad \dot{m}_K = \frac{m_{K,\infty}(V_m) - m_K}{\tau_{m_K}(V_m)}$$

The time constant of a gate called X is defined as

$$\tau_X(V_m) = \frac{1}{\alpha_X(V_m) + \beta_X(V_m)} \quad X_\infty(V_m) = \frac{\alpha_X(V_m)}{\alpha_X(V_m) + \beta_X(V_m)}$$

The corresponding rate constants are

Sodium activation	Sodium inactivation	Potassium activation
$\alpha_{m_{Na}} = \frac{V_m + 35}{10 [1 - e^{-(V_m+35)/10}]}$	$\alpha_{h_{Na}} = 0.07 e^{-(V_m+60)/20}$	$\alpha_{m_K} = \frac{V_m + 50}{100 [1 - e^{-(V_m+50)/10}]}$
$\beta_{m_{Na}} = 4 e^{-(V_m+60)/18}$	$\beta_{h_{Na}} = \frac{1}{1 + e^{-(V_m+30)/10}}$	$\beta_{m_K} = 0.125 e^{-(V_m+60)/80}$

The steady-state variables and the time-constants are respectively shown in Figures A.1 and A.2.

Figure 2.8 is generated thanks to the following stimulation: $I_{cst} = 0$, $I_{step} = 50$ [nA], $T_{step,init} = 10$ [ms] and $T_{step,end} = 40$ [ms].

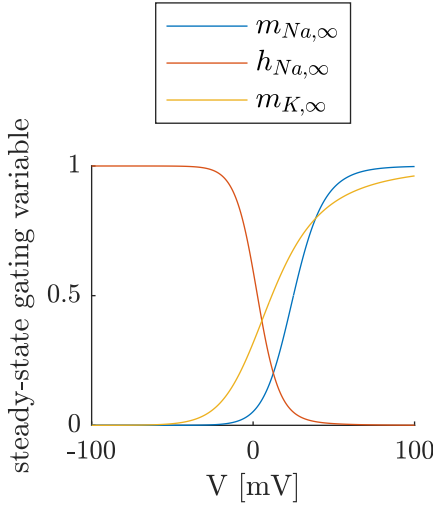


Figure A.1 – Steady-state gating variables [37]

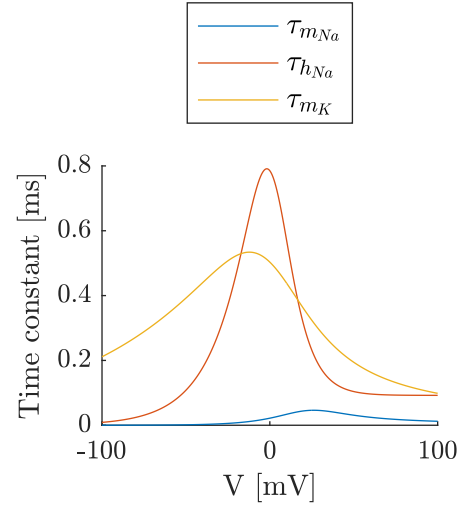


Figure A.2 – Time constants associated to the gating variables [37]

A.2 Huguenard and McCormick model [19]

Model equations

The principal equation governing the change in the membrane potential is

$$C_m \dot{V}_m = -(I_{Na} + I_{Nap} + I_L + I_T + I_{CaT} + I_A + I_{K2} + I_{Kleak} + I_{Naleak}) + I_{app} \quad (A.2)$$

In order to describe each ionic current with the associated gate, we used the follow notation; the current I_x has a activation gate m_x and an inactivation gate h_x . Table A.1 exhibits the Ohm's law of each current. I_{app} is composed of a constant applied current I_{cst} and I_{step} corresponds to a varying temporary step current.

I_x	Name of the current	Equation (Ohm's law)
I_{Na}	Transient Na^+	$I_{Na} = \bar{g}_{Na} m_{Na}^3 h_{Na} (V_m - V_{Na})$
I_{Nap}	Depolarisation-activated Na^+	$I_{Nap} = \bar{g}_{Nap} m_{Nap} (V_m - V_{Na})$
I_L	High-threshold Ca^{2+}	$I_L = \bar{g}_L m_L^2 (V_m - V_{Ca})$
I_{CaT}	Low-threshold Ca^{2+}	$I_{CaT} = \bar{g}_{CaT} m_{CaT}^2 h_{CaT} (V_m - V_{Ca})$
I_C	Ca^{2+} -activated K^+	$I_C = \bar{g}_C m_C (V_m - V_K)$
I_A	Transient and depolarisation-activated K^+	$I_A = \bar{g}_A m_A^4 h_A (V_m - V_K) + \bar{g}_{A2} m_{A2}^4 h_{A2} (V - V_K)$
I_{K2}	Slowly inactivating and depolarisation-activated K^+	$I_{K2} = \bar{g}_{K2a} m_{K2} h_{K2a} (V_m - V_K) + \bar{g}_{K2b} m_{K2} h_{K2b} (V_m - V_K)$
I_{Kleak}	K^+ leak	$I_{Kleak} = g_{Kleak} (V_m - V_K)$
I_{Naleak}	Na^+ leak	$I_{Naleak} = g_{Naleak} (V_m - V_{Na})$

Table A.1 – Ohm's equations of the different ionic currents described in the model of Huguenard and McCormick [19, 40].

Units

The potentials are expressed in [mV], the conductances in [μS], the current in [nA], the capacitance in [$\mu\text{F}/\text{cm}^2$] and the time in [ms].

Parameters

$V_{Na} = 45$, $V_{Ca} = 120$, $g_{Na} = 12$, $g_{Nap} = 7e - 3$, $g_{Naleak} = 2.65e - 3$, $V_K = -105$, $g_A = 20e - 3$, $g_{A2} = 15e - 3$, $g_{Kleak} = 7e - 3$, $g_{K2a} = 38e - 3$, $g_{K2b} = 26e - 3$, $g_c = 1$, $g_L = 0.8$, $C = 0.29$.

Description of the ionic current kinetics

Sodium activation I_{Na}	Sodium inactivation I_{Na}
$\alpha_{m_{Na}} = \frac{0.091(V + 38)}{1 - \exp(-(V + 38)/5)}$	$\alpha_{h_{Na}} = 0.016\exp((-55 - V)/15)$
$\beta_{m_{Na}} = \frac{-0.062 * (V + 38)}{1 - \exp((V + 38)/5)}$	$\beta_{h_{Na}} = 2.07/(\exp((17 - V)/21) + 1)$

NaP activation (I_{Nap})	high threshold Ca^{2+} activation	Ca^{2+} -activated K^+ activation (I_C) (I_L)
$\alpha_{m_{Nap}} = \frac{0.091 * (V + 38)}{1 - \exp(-(V + 38)/5)}$	$\alpha_{m_L} = \frac{1.6}{1 + \exp(-0.072 * (V - 5))}$	$\alpha_{m_C} = 2.5e5 * CaL * \exp(V/24)$
$\beta_{m_{Nap}} = \frac{-0.062 * (V + 38)}{(1 - \exp((V + 38)/5))}$	$\beta_{m_L} = \frac{0.02 * (V - 1.31)}{\exp((V - 1.31)/5.36) - 1}$	$\beta_{m_C} = 0.1 * \exp(-V/24)$

T-type activation (I_{CaT})	T-type inactivation (I_{CaT})
$m_{CaT,\infty} = 1/(1 + \exp(-(V + 57)/6.2))$	$h_{CaT,\infty} = 1/(1 + \exp((V + 81)/4.03))$
$\tau_{m_{CaT}} = 0.612 + \frac{1}{\exp(-(V + 131.6)/16.7) + \exp((V + 16.8)/18.2)}$	if $V < -80[mV]$ $\tau_{h_{CaT}} = \exp((V + 467)/66.6)$ else $\tau_{h_{CaT}} = \exp(-(V + 21.88)/10.2) + 28$

A activation (I_A)
$m_{A,\infty} = 1/(1 + \exp(-(V + 60)/8.5))$
if $V < -63$: $\tau_{m_A} = 0.37 + \frac{1}{(\exp((V + 35.82)/19.697) + \exp((V + 79.69)/-12.7))}$ else $\tau_{m_A} = 19$
A inactivation (I_A)
$h_{A,\infty} = 1/(1 + \exp((V + 78)/6))$
if $V < -63$ $\tau_{h_A} = \frac{1}{\exp((V + 46.05)/5) + \exp((V + 238.4)/-37.45)}$ else $\tau_{h_A} = 19$
A2 activation (I_A)
$m_{A2,\infty} = 1/(1 + \exp(-(V + 36)/20))$
if $V < -63$: $\tau_{m_{A2}} = 0.37 + \frac{1}{\exp((V + 35.82)/19.697) + \exp((V + 79.69)/-12.7)}$ else $\tau_{m_{A2}} = 19$
A2 inactivation (I_A)
$h_{A2,\infty} = 1/(1 + \exp((V + 78)/6))$
if $V < -73[mV]$ $\tau_{h_{A2}} = \frac{1}{\exp((V + 46.05)/5) + \exp((V + 238.4)/-37.45)}$ else $\tau_{h_{A2}} = 60$

K2 activation (I_{K2})
$m_{K2,\infty} = 1/(1 + \exp((V + 43)/-17))$
$\tau_{m_{K2}} = \frac{1}{\exp((V - 81)/25.6) + \exp((V + 132)/-18)} + 9.9$
K2 type A inactivation (I_{K2})
$h_{K2a,\infty} = 1/(1 + \exp((V + 58)/10.6))$
$\tau_{h_A} = \frac{1}{\exp((V - 1.329)/200) + \exp((V + 130)/-7.1)} + 120$
K2 type B inactivation (I_{K2})
$m_{K2b,\infty} = 1/(1 + \exp((V + 58)/10.6))$
if $V < -70$: $\tau_{m_{K2b}} = \frac{1}{\exp((V - 1.329)/200) + \exp((V + 130)/-7.1)} + 120$
else $\tau_{m_{K2b}} = 8.9$

Parameter values to obtain different firing patterns

Figure 3.2			
Parameters	Tonic	PIR	HIB
I_{cst}	0	0	1
I_{step}	2	-0.5	-0.9
$T_{step,init}$	100	1000	1000
$T_{step,end}$	500	2000	2000
g_{CaT}	0.3	0.3	1

Single-cell robustness analysis :

Figure 3.5, same excitation as HIB except that C_m is increased of 20% ($1.2C_m = 0.232$) or decreased of 20% ($0.8C_m = 0.348$).

Parameter values for the network simulations

Figure	4.8	4.9		
Conductance	set 0	set 1	set 2	set 3
C_m	0.29	0.2834	0.2724	0.2922
g_{Na}	12	11.81	11.78	11.92
g_{Nap}	7e-3	0.006686	0.006701	0.007117
g_{Naleak}	2.65e-3	0.00261	0.002838	0.002431
g_A	20e-3	0.02019	0.021867	0.01872
g_{A2}	15e-3	0.01513	0.01507	0.01616
g_{Kleak}	7e-3	0.006814	0.006832	0.007068
g_{K2a}	38e-3	0.03715	0.0399	0.0376
g_{K2b}	0.26e-3	0.02472	0.02734	0.02658
g_c	1	0.9502	1.03	0.9978
g_T	1	0.96035	0.9237	1.055
g_L	0.8	0.8060	0.7762	0.7562
I_{cst}	1.5			
I_{step}	-1.5			
$T_{step,init}$	6000			
$I_{step,end}$	110000			
$T_{transient}$	1000			
g_{AMPA}	0.1			
g_{GABA_a}	0.4			
g_{GABA_b}	2			

A.3 Destexhe model [22]

The membrane potential evolution is given by

$$C_m \dot{V}_m = -I_{Na} - I_K - I_{CaT} - I_{leak} + I_{app} \quad (A.3)$$

The detailed equation of the model describing with Ohm's law is

$$C_m \dot{V}_m = -\bar{g}_{Na} m_{Na}^3 h_{Na} (V_m - V_{Na}) - \bar{g}_K m_K^4 (V_m - V_K) - \bar{g}_{CaT} m_{CaT}^2 h_{CaT} (V_m - V_{Ca}) - g_{leak} (V_m - V_{leak}) + I_{app} \quad (A.4)$$

with $V_2(V) = V - V_{traub}$, $V_{traub} = -63$

Units

The potentials are expressed in [mV], the conductances in [mS/cm²], the current in [pA], the capacitance in [pF] and the time in [ms].

Parameters:

$V_{Na} = 50$, $g_{Na} = 0.1$, $V_K = -100$, $g_K = 0.08$, $V_{leak} = -82$, $g_{leak} = 5e - 5$, $V_{Ca} = 120$, $C = 1e - 3$

Description of the ionic current kinetics

Sodium activation (I_{Na})	Sodium inactivation (I_{Na})	Potassium activation (I_K)
$\alpha_{m_{Na}} = \frac{0.32 * (13 - V2(V))}{exp((13 - V2(V))/4) - 1}$	$\alpha_{h_{Na}} = 0.128 * exp((17 - V2(V))/18)$	$\alpha_{m_K} = \frac{0.032 * (15 - V2(V))}{exp((15 - V2(V))/5) - 1}$
$\beta_{m_{Na}} = \frac{.28 * (V2(V) - 40)}{exp((V2(V) - 40)/5) - 1}$	$\beta_{h_{Na}} = \frac{4}{1 + exp((40 - V2(V))/5)}$	$\beta_{m_K} = 0.5 * exp((10 - V2(V))/40)$

T-type activation (I_{CaT})	T-type inactivation (I_{CaT})
$m_{CaT,\infty} = 1/(1 + exp(-(V + 50)/7.4))$	$h_{CaT,\infty} = 1/(1 + exp((V + 80)/5))$
$\tau_{m_{CaT}} = 1 + \frac{0.33}{exp(-(V + 100)/15) + exp((V + 25)/10)}$	$\tau_{h_{CaT}} = 28.3 + \frac{0.33}{exp((V + 48)/4) + exp(-(V + 407)/50)}$

Parameter values to obtain different firing patterns

Figure 3.3			
Parameters	Tonic	PIR	HIB
I_{cst}	$0.3e^{-3}$	$0.1e^{-3}$	$0.3e^{-3}$
I_{step}	0	$-0.4e^{-3}$	$-0.2e^{-3}$
$T_{step,init}$	0	800	1000
$T_{step,end}$	0	1500	2000
g_{CaT}	0.008	0.003	0.008

Robustness analysis at the cellular level

Figure 3.5, same excitation as HIB except that C_m is increased of 20% ($1.2C_m = 1.2e - 3$) or decreased of 20% ($0.8C_m = 0.8e - 3$).

Parameter values for the network simulations

Figure	4.8	4.9		
Conductance	set 0	set 1	set 2	set 3
C_m	1e-3	0.001023	0.0009821	0.0009543
g_{Na}	0.1	0.1045	0.1047	0.1019
g_{leak}	5e-3	5.005e-3	4.8e-3	5111e-3
g_K	0.08	0.07681	0.07987	0.0778
g_{CaT}	0.06	0.006136	0.005739	0.005773
I_{cst}	0.3e-3			
I_{step}	-0.6e-3			
$T_{step,init}$	6000			
$T_{step,end}$	110000			
$T_{transient}$	1000			
g_{AMPA}	0.1e-3			
g_{GABA_a}	0.2e-3			
g_{GABA_b}	1e-3			

A.4 Drion model [29]

The evolution of the membrane potential is given by

$$C_m \dot{V}_m = -I_{Na} - I_K - I_{CaT} - I_{K,Ca} - I_H - I_{leak} + I_{app} \quad (A.5)$$

By integrating the Ohm's law equations of each ionic current, the model is described as

$$\begin{aligned} C_m \dot{V}_m = & -\bar{g}_{Na} m_{Na}^3 h_{Na} (V_m - V_{Na}) - \bar{g}_{K,D} m_{K,D}^4 (V_m - V_K) - \bar{g}_{Ca,T} m_{Ca,T}^3 h_{Ca,T} (V_m - V_{Ca}) \\ & - \bar{g}_{K,Ca} m_{K,Ca\infty}(Ca) (V_m - V_K) - \bar{g}_H m_H (V_m - V_H) - \bar{g}_{leak} (V_m - V_{leak}) + I_{app} \end{aligned} \quad (A.6)$$

Units

The potentials are expressed in [mV], the conductances in [mS/cm²], the current in [μ A/cm²], the capacitance in [μ F/cm²] and the time in [ms].

Parameters

$C = 1$, $V_{Na} = 50$, $V_K = -85$, $V_{Ca} = 120$, $V_l = -55$, $V_H = -20$, $g_l = 0.055$, $g_{Na} = 120$, $g_{Kd} = 30$, $Kd = 170$.

Description of the ionic current kinetics

The gating variables are defined thanks to two mathematical expressions:

$$m_{X,\infty} = \frac{1}{1 + \exp((V + A)/B)} \quad \tau_X = A - \frac{B}{1 + \exp((V + D)/E)}$$

Param.	A	B	Param.	A	B	D	E
$m_{Na,\infty}$	35.5	- 5.29	$\tau_{m_{Na}}$	1.32	1.26	120	-25
$h_{Na,\infty}$	48.9	5.18	$\tau_{h_{Na}}$	$(0.67/(1 + \exp((V + 62.9)/-10.0))) * (1.5 + 1/(1 + \exp((V + 34.9)/3.6)))$			
$m_{Kd,\infty}$	12.3	-11.8	$\tau_{m_{Kd}}$.2	6.4	28.3	-19.2
$m_{CaT,\infty}$	67.1	-7.2	$\tau_{m_{CaT}}$	21.7	21.3	68.1	-20.5
$h_{CaT,\infty}$	80.1	5.5	$\tau_{h_{CaT}}$	410	179.6	55.	-16.9
$m_{H,\infty}$	80.	6.	τ_{m_H}	272.	-1149.	42.2	-8.73

The steady-state value of the activation gating variable of the calcium activated current ($m_{K,Ca,\infty}(Ca)$) is defined separately:

$$m_{K,Ca,\infty}(Ca) = (Ca/(Ca + Kd))^2$$

with $\dot{Ca} = (-k_1 \bar{g}_{CaT} m_{CaT}^3 h_{CaT} (V_m - V_{Ca}) - k_2 Ca)$.

Parameter values to obtain different firing patterns

Figure 3.4			
Parameters	Tonic	PIR	HIB
I_{cst}	1.5	-1.5	0
I_{step}	0	-1.4	-1.5
$T_{step,init}$	0	1000	1000
$T_{step,end}$	0	3000	5000
g_{CaT}	0.2	0.1	0.6
g_H	0.02	0.02	0.01
g_{KCa}	4	0	4
k_1	1.e-1	1.e-1	0.2e-1
k_2	1.e-1	1.e-1	0.02e-1

Robustness analysis at the cellular level

Figure 3.5, same excitation as HIB except that C_m is increased of 20% ($1.2C_m = 1.2$) or decreased of 20% ($0.8C_m = 0.8$).

Parameter values for the network simulations

Figure	4.8	4.9		
Conductance	set 0	set 1	set 2	set 3
C_m	1	1.038	1.025	1.05
g_l	0.055	0.0569	0.05236	0.05347
g_{Na}	170	163.1	171.1	164.5
g_{Kd}	40	39.63	38.76	38.08
k_1	$e - 1$	0.09544	0.1033	0.1003
k_2	$0.1e - 1$	0.009753	0.009898	0.009782
g_H	0.01	0.01048	0.01034	0.009839
g_{Kca}	4	4.017	4.185	4.018
g_{CaT}	0.55	0.5750	0.5574	0.5681
I_{cst}	1			
I_{step}	-3.6			
$T_{step,init}$	6000			
$I_{step,end}$	110000			
$T_{transient}$	1000			
g_{AMPA}	0.1			
g_{GABA_a}	0.4			
g_{GABA_b}	2			

A.5 Rush and Rinzel model [56]

The membrane potential evolution is described by:

$$C_m \dot{V}_m = -I_{Na} - I_K - I_{CaT} - I_{Naleak} - I_{Kleak} + I_{app} \quad (A.7)$$

The simplified version of the Wang's model is based on the observation that the activation of the calcium current is fast. They assumed that this activation is instantaneous [56, 68]. So, the T-type calcium current is modelled as

$$I_{CaT} = \bar{g}_{CaT} m_{CaT,\infty}^3(V_m) h_{CaT}(V_m - V_{Ca}) \quad (A.8)$$

Finally, the evolution of the membrane potential defined in this model consists in five ionic currents *i.e.* characterised by five conductances including two leak conductances

$$\begin{aligned}
C_m \dot{V}_m = & -\bar{g}_{Na} m_{Na,\infty}^3 (V_m) (0.85 - m_K) (V_m - V_{Na}) - \bar{g}_{Kd} m_K^4 (V_m - V_K) \\
& -\bar{g}_{CaT} m_{CaT,\infty}^3 h_{CaT} (V_m - V_{Ca}) \\
& -\bar{g}_{Naleak} (V_m - V_{Na}) - \bar{g}_{Kleak} (V_m - V_K) + I_{app}
\end{aligned} \tag{A.9}$$

Units

The potentials are expressed in [mV], the conductances in [mS/cm²], the current in [μ A/cm²], the capacitance in [μ F/cm²] and the time in [ms].

Parameters

$V_{Na} = 55$, $V_K = -85$, $V_{Ca} = 120$, $g_{Na} = 120$, $g_{Kd} = 10$, $g_{Naleak} = 0.01429$, $g_{Kleak} = 0.08571$, $\theta_s = -63$ [mV], $k_s = -7.8$, $\theta_h = -72$ [mV], $k_h = 1.1$, $\sigma_m = 10.3$, $\sigma_n = 9.3$, $\theta = 1$, $C_m = 1$.

Description of the ionic current kinetics

Sodium activation (I_{Na})	Potassium activation (I_K)
$\alpha_{m_{Na}} = \frac{0.1(V + 35 - \theta_m)}{1 - \exp(-0.1(V + 35 - \sigma_m))}$	$\alpha_{m_K} = \frac{0.01(V + 50 - \sigma_n)}{1 - \exp(-0.1(V + 50 - \sigma_n))}$
$\beta_{m_{Na}} = 4\exp(-0.05(V + 60 - \sigma_m))$	$\beta_{m_K} = 0.125\exp(-0.0125(V + 60 - \sigma_n))$

To compute h_{Na} is defined by $(0.85 - m_K)$. Then, τ_{m_K} is equal to $\frac{0.05}{\alpha_{m_K} + \beta_{m_K}}$.

T-type calcium current (I_{CaT}) is defined by

$$m_{CaT,\infty} = 1/(1 + \exp((V - \theta_s)/k_s))$$

CaT ²⁺ inactivation
$\alpha_{h_{CaT}} = \frac{1}{0.5 + \sqrt{0.25 + \exp((V - \theta_h)/k_h)}}$
$\beta_{h_{CaT}} = \frac{\exp((V + 150)/18)}{1.5 + \sqrt{0.25 + \exp((V - 80)/4)}} + 30$

Parameter values to obtain different firing patterns

Figure 3.5			
Parameters	Tonic	PIR	HIB
I_{cst}	15	0	15
I_{step}	0	-1.5	-16
$T_{step,init}$	0	500	500
$T_{step,end}$	0	1000	2000
g_{CaT}	0.3	0.3	0.3

Robustness analysis at the cellular level

Figure 3.5, same excitation as HIB except that C_m is increased of 20% ($1.2C_m = 1.2$) or decreased of 20% ($0.8C_m = 0.8$).

Parameter values for the network simulations

Figure	4.8	4.9		
Conductance	set 0	set 1	set 2	set 3
C_m	1	0.9855	0.9559	0.9748
g_{Na}	120	114.5	122.5	119.4
g_{Kd}	10	9.531	10.10	9.9739
g_{Naleak}	0.01429	0.014	0.015	0.01418
g_{Kleak}	0.08571	0.08975	0.0872	0.08997
g_{CaT}	0.3	0.3128	0.2965	0.3122
I_{cst}	15			
I_{step}	-16.2			
$T_{step,init}$	6000			
$I_{step,end}$	110000			
$T_{transient}$	1000			
g_{AMPA}	0.1			
g_{GABA_a}	0.4			
g_{GABA_b}	2			

A.6 Modified Rush and Rinzel model called RushCa

This model was created with the help of Ilario Cirillo, University of Cambridge.

The membrane potential evolution is described by:

$$\begin{aligned}
 C_m \dot{V}_m = & -\bar{g}_{Na} m_{Na,\infty}^3(V_m)(0.85 - m_K)(V_m - V_{Na}) - \bar{g}_{Kd} m_K^4(V_m - V_K) \\
 & -\bar{g}_{CaT} m_{CaT}^3 h_{CaT}(V_m - V_{Ca}) \\
 & -\bar{g}_{Naleak}(V_m - V_{Na}) - \bar{g}_{Kleak}(V_m - V_K) + I_{app}
 \end{aligned} \tag{A.10}$$

Units: they are the same as in Rush model.

Parameters Only these two parameters have changed $\sigma_m = 8$, $\sigma_n = 9$.

Description of the ionic current kinetics

CaT ²⁺ activation
$m_{CaT,\infty} = 1/(1 + \exp((V - \theta_s)/k_s))$
$\tau_{m_{CaT}} = \frac{1.7 + \exp(-(V + 28.8)/13.5)}{1 + \exp(-(V + 63)/7.8)}$

Parameter values to obtain different firing patterns

Figure 3.7			
Parameters	Tonic	PIR	HIB
I_{cst}	15	0	15
I_{step}	0	-1.5	-16
$T_{step,init}$	0	500	500
$T_{step,end}$	0	1000	2000
g_{CaT}	0.35	0.35	0.35

Robustness analysis at the cellular level

Figure 3.5, same excitation as HIB except that C_m is increased of 20% ($1.2C_m = 1.2$) or decreased of 20% ($0.8C_m = 0.8$).

Parameter values for the network simulations

Figure	4.8	4.9		
Conductance	set 0	set 1	set 2	set 3
C_m	1	1.042	0.9802	1.0132
g_{Na}	120	122.4	124.3	119.8
g_{Kd}	10	9.83	10.23	10.35
g_{NaLeak}	0.01429	0.01492	0.014	0.0139
g_{KLeak}	0.08571	0.08787	0.08164	0.0843
g_{CaT}	0.35	0.3579	0.363	0.334
I_{cst}	15			
I_{step}	-16.2			
$T_{step,init}$	6000			
$I_{step,end}$	110000			
$T_{transient}$	1000			
g_{AMPA}	0.1			
g_{GABA_a}	0.4			
g_{GABA_b}	2			

A.7 Wang model [67]

The evolution of the membrane potential is described

$$C_m \dot{V}_m = -I_{CaT} - I_g - I_{Na} - I_K - I_{Nap} - I_{leak} + I_{app} \quad (A.11)$$

He used his model of the T-type calcium current in 1991 [68] and replaced the activation variable by its steady-state value. He justified his assumption by the fast activation of the calcium current (similarly as Rush and Rinzel who used this T-type model and reduced it). The T-type current is described as

$$I_T = g_{Ca} m_{Ca,\infty}^3(V_m) h_{Ca}(V_m - V_{Ca}) \quad (A.12)$$

The model describes with the Ohm's law is given by

$$\begin{aligned} C_m \dot{V}_m = & -g_{Ca,T} m_{CaT,\infty}^3(V_m) h_{Ca,T}(V_m - V_{Ca}) - g_h m_h^2(V_m - V_h) - g_K m_K^4(V_m - V_K) \\ & - g_{Na} m_{Na,\infty}^3(V_m, \sigma_{Na})(0.85 - m_K)(V_m - V_{Na}) - g_{NaP} m_{NaP,\infty}^3(V_m, \sigma_{NaP})(V_m - V_{Na}) \\ & - g_l(V_m - V_l) + I_{app} \end{aligned} \quad (A.13)$$

Units

The potentials are expressed in [mV], the conductances in [mS/cm²], the current in [μ A/cm²] and the capacitance in [μ F/cm²].

Parameters

$C_m = 1$, $V_{Ca} = 120$, $V_H = -40$, $V_K = -80$, $V_{Na} = 55$, $V_l = -70$, $\sigma_K = 10$, $\sigma_{Na} = 6$, $\sigma_{NaP} = -5$, $\theta_h = -79$, $kh = 5$, $g_H = 0.04$, $g_{Kd} = 30$, $g_{Na} = 42$, $g_{NaP} = 9$, $g_l = 0.12$.

Description of the kinetics of each ionic current

For the depolarisation-activated Na⁺ current (I_{Nap}), the activation is the same as the activation of the sodium current with σ_{NaP} instead of σ_{Na}

Sodium activation (I_{Na})	Potassium activation (I_K)
$\alpha_{m_{Na}} = \frac{-0.1(V + 29.7 - \sigma_{Na})}{\exp(-0.1(V + 29.7 - \sigma_{Na})) - 1}$	$\alpha_{m_K} = \frac{-0.01(V + 45.7 - \sigma_K)}{\exp(-0.1(V + 45.7 - \sigma_K)) - 1}$
$\beta_{m_{Na}} = 4\exp(-(V + 54.7 - \sigma_{Na})/18)$	$\beta_{m_K} = 0.125\exp(-(V + 55.7 - \sigma_K)/80)$

H activation
$m_{H,\infty} = 1/(1 + \exp((V + 69)/7.1))$
$\tau_{m_H} = \frac{1000}{\exp((V + 66.4)/9.3) + \exp(-(V + 81.6)/13)}$

CaT ²⁺ activation	CaT ²⁺ inactivation
$m_{CaT,\infty} = 1/(1 + \exp(-(V + 65)/7.8))$	$h_{CaT,\infty} = 1/(1 + \exp((V - \theta_h)/kh))$
	$\tau_{h_{CaT}} = \frac{1}{1 + \exp((V - \theta_h)/kh)} \exp((V + 162.3)/17.8) + 20.0$

Parameter values to obtain different firing patterns

Figure 3.6			
Parameters	Tonic	PIR	HIB
I_{cst}	5	-2.5	2.5
I_{step}	0	-2.5	-3.5
$T_{step,init}$	0	500	500
$T_{step,end}$	0	1000	2000
g_{CaT}	0.8	0.8	0.8

Robustness analysis at the cellular level

Figure 3.5, same excitation as HIB except that C_m is increased of 20% ($1.2C_m = 1.2$) or decreased of 20% ($0.8C_m = 0.8$).

Parameter values for the network simulations

Figure	4.8	4.9		
Conductance	set 0	set 1	set 2	set 3
C_m	1	0.9792	0.9667	1.018
g_{CaT}	1	1.017	1.015	1.010
g_H	0.04	0.04134	0.03973	0.0411
g_{Kd}	30	30.31	28.52	28.69
g_{Na}	42	42.69	43.43	40.48
g_{NaP}	9	8.692	8.653	9.417
g_l	0.12	0.1219	0.1178	0.114
I_{cst}	-0.5			
I_{step}	-0.8			
$T_{step,init}$	6000			
$I_{step,end}$	110000			
$T_{transient}$	1000			
g_{AMPA}	0.1			
g_{GABA_a}	0.4			
g_{GABA_b}	4			

Appendix B

Julia pseudo-code of a thalamic neuron conductance-based model

TC.jl

```
1 ##### GATING FUNCTIONS #####
2 # Na: activation
3 alpha_mNa(V::Float64)= ...
4 beta_mNa(V::Float64) = ...
5 mNa_inf(V::Float64) = alpha_mNa(V)/(alpha_mNa(V)+beta_mNa(V))
6 tau_mNa(V::Float64) = 1/(alpha_mNa(V)+beta_mNa(V))
7
8 # Na: inactivation : hNa
9 # K: activation : mK
10
11 # CaT: activation
12 m_CaTinf(V::Float64) = ....
13 # if the activation is considered as slow
14 tau_mCaT(V::Float64) = ...
15
16 # CaT: inactivation
17 hCaT_inf(V::Float64) = ...
18 tau_hCaT(V::Float64) = ...
19
20 # Others currents
21
22 ##### EVOLUTION Vm: Cm dVm/dt = - sum (g_ion mion^a hion^b (Vm - Vion) +
23 Iapp
24 function dV(Cm::Float64, V::Float64, mNa::Float64, hNa::Float64, mCaT::
25 Float64, hCaT::Float64, #... other ionic gating variables, Iapp::Float64)
26 (dt)*(1/Cm)*(-gCaT*mCaT^a*hCaT^b*(V-VCa) -gNa*mNa^a*hNa^b*(V-VN) -gKd*mK^a
27 *(V-VK) - gl*(V-Vl) + Iapp
28 end
29 # a and b: fitting parameters depending on the model
30 # for instantaneous activation of calcium channels: -gCaT*mCaT_inf(V)^a*hCaT
31 ^b(V-VCa)
32
33 ##### DYNAMICS of the gates #####
34 dmNa(V::Float64,mNa::Float64) = (dt)*((1/tau_mNa(V))*(mNa_inf(V) - mNa))
35 dhNa(V::Float64,hNa::Float64) = (dt)*((1/tau_hNa(V))*(hNa_inf(V) - hNa))
36 dmK(V::Float64,mK::Float64) = (dt)*((1/tau_mK(V))*(mK_inf(V) - mK))
37 dhCaT(V::Float64,hCaT::Float64) = (dt)*((1/tau_hCaT(V))*(hCaT_inf(V) - hCaT)
38 )
39 ## if the activation of the calcium channels is slow:
40 dmCaT(V::Float64,mCaT::Float64) = (dt)*((1/tau_mCaT(V))*(mCaT_inf(V) - mCaT)
41 )
42
```



```

37 ##### RESOLUTION #####
38 function simulateTC(Cm::Float64, Icst::Float64, Istep::Float64, Tstepinit::
    Int64, Tstepend::Int64)
39     # Initial conditions
40     V::Float64=-70.
41     Vprev::Float64=-70.
42     mNa::Float64=mNa_inf(V)
43     hNa::Float64=hNa_inf(V)
44     mCaT::Float64=mCaT_inf(V) # if the activation is slow
45     hCaT::Float64=hCaT_inf(V)
46     #other currents gating variables intialisation
47
48     VV = zeros(Tdt)
49
50     # Euler resolution
51     for z = 1:Tdt
52         if(convert(Int64, Tstepinit/dt) >= z & convert(Int64,Tstepend/dt)<z)
53             Iapp = Icst +Istep
54         else
55             Iapp = Icst
56         end
57
58         V += dV(C,Vprev,mNa,hNa,mK,mCaT,hCaT,...,Iapp)
59         mNa += dmNa(Vprev,mNa)
60         hNa += dhNa(Vprev,hNa)
61         mK += dn(Vprev,mK)
62         mCaT += dmCaT(Vprev,mCaT) # if the activation is slow
63         hCaT += dhCaT(Vprev,hCaT)
64
65         Vprev = copy(V)
66         VV[z] = copy(V)
67     end
68
69     return VV
70 end

```

Simu_TC.jl

```

1  # Defines output directory
2  cd("/Users/...")
3
4  # Loads packages
5  using PyPlot
6  PyPlot.hold(false)
7
8  # Include model
9  include("TC_model.jl")
10
11 # Simulation parameters
12 const T=200
13 const dt = 0.01
14 const Tdt = convert{Int64}(T/dt)
15 const t = linspace(dt,T,Tdt)
16 const Icst = 1.
17 const Istep = -2.
18 const Tstepinit = 50
19 const Tstepend = 150
20
21 # Model parameters
22 const Cm =1.
23 const VNa = ..., const VK = ..., const VCa = ..., #Nernst potential of the
    other currents
24 const Vl = ...
25 const gNa =..., const gK=..., const gCaT=..., #max conductance of the other
    currents
26 const gl = 0.12*z
27
28 @time y = simulateTC_wang(C,Iapp, Istep, Tstepinit, Tstepend)
29
30 # figure generation
31 Figure
32 plot(t,y)

```


Appendix C

Additional results of conductance-based models at the network level

C.1 Tunability cell E

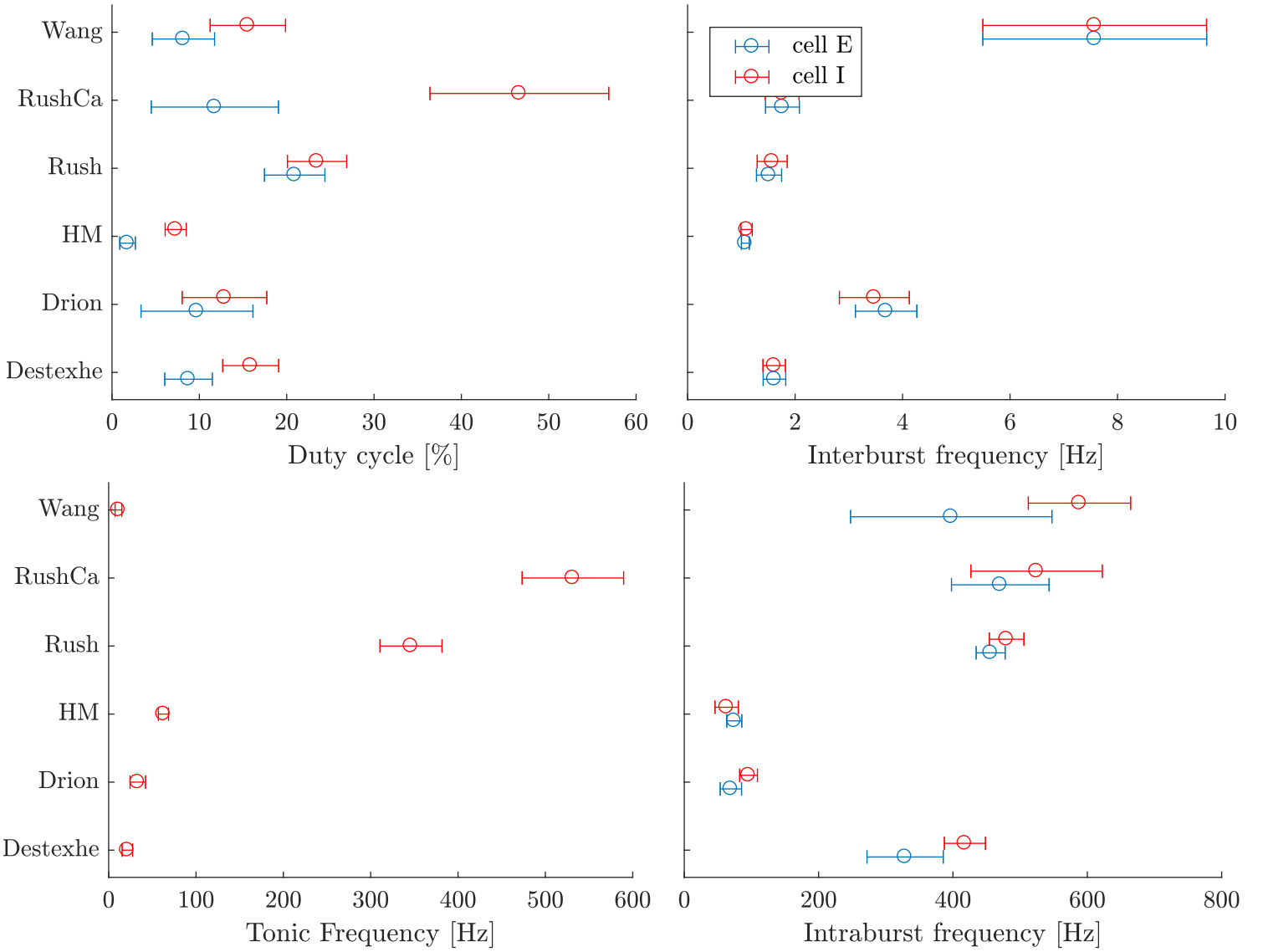


Figure C.1 – Mean and standard deviation of the distribution of the four firing characteristics for the rhythmic networks in each model computed for γ_*

C.2 Spectrograms of the LFP of the E-cells population

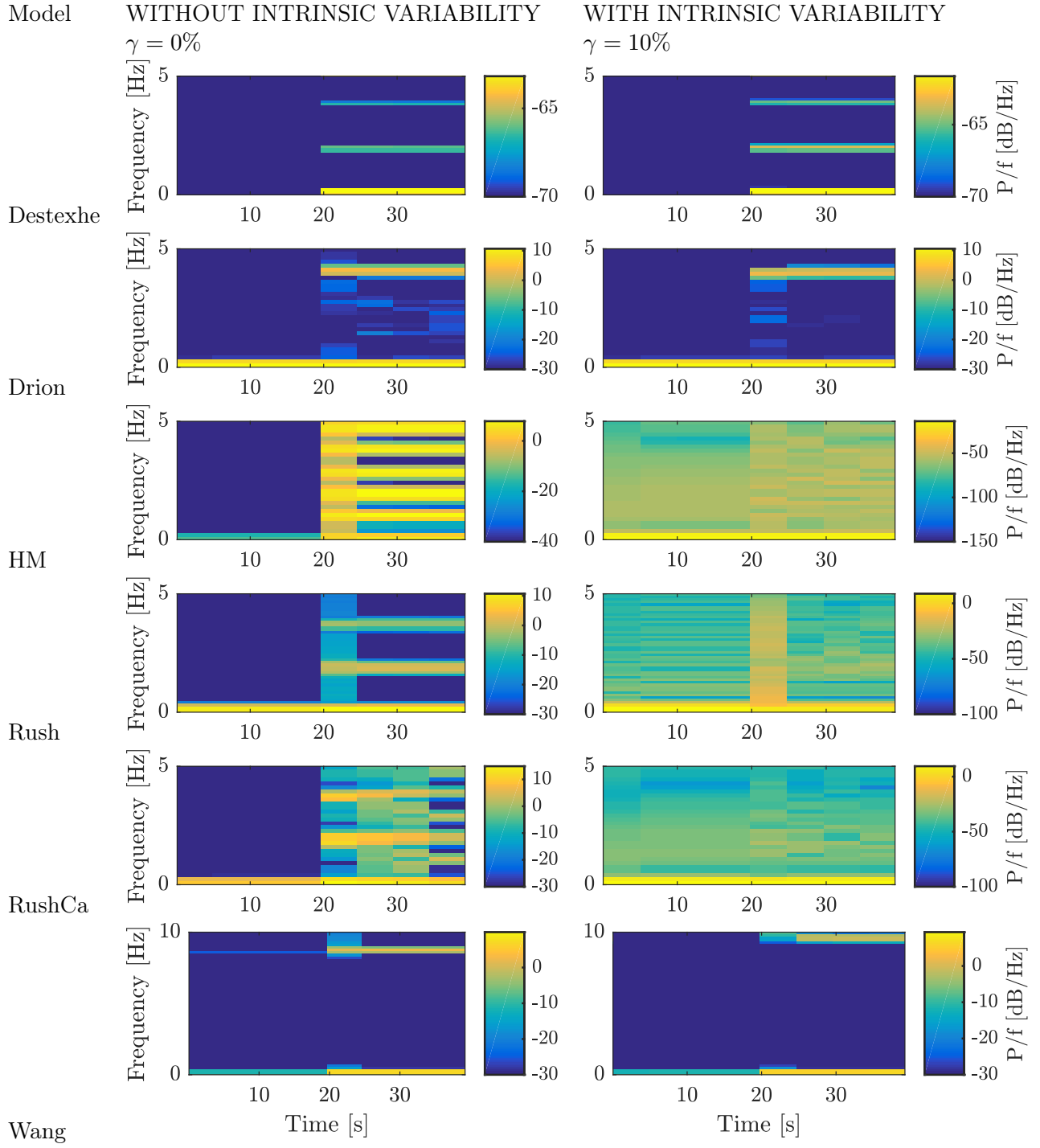


Figure C.2 – Spectrogram of the LFP of the E-cells populations in a 200 network without intrinsic variability (on the left) and with a relative intrinsic variability of 10% (on the right) for each model. The intensity of the power spectral content is expressed in Power/Frequency, denoted P/f .

Appendix D

Complement on hybrid modeling

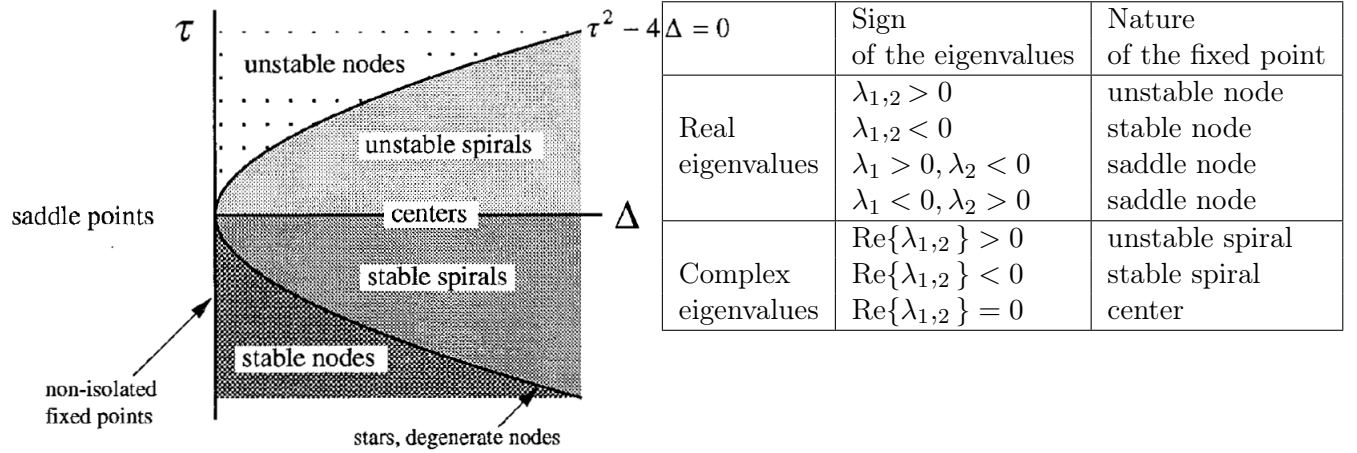
D.1 Reduced HH model

D.1.1 Nature of the fixed points

The nature of the fixed point (x^*, y^*) can be identified by considering the linearisation of the vector field at the fixed point. It means by computing the jacobian matrix A evaluated at (x^*, y^*) . The linearized system is given by:

$$\begin{pmatrix} \dot{V}_m \\ \dot{n} \end{pmatrix} = \begin{pmatrix} \frac{\partial f_1}{\partial V_m} & \frac{\partial f_1}{\partial n} \\ \frac{\partial f_2}{\partial V_m} & \frac{\partial f_2}{\partial n} \end{pmatrix}_{(x^*, y^*)} \begin{pmatrix} V_m \\ n \end{pmatrix} \quad (\text{D.1})$$

The sign of the real part of the eigenvalues of the jacobian matrix permit to determine the nature of the fixed point. As a reminder, the classification can be based on the trace and the determinant of the jacobian matrix (see Figure D.1a) or based on the sign of the eigenvalues (see Figure D.1b) .



(a) Diagram based on the trace τ and the determinant Δ of the jacobian matrix. [64]

(b) Table based on the sign for real eigenvalues and the sign of the real part for complex eigenvalues.

Figure D.1 – Classification of the type and the stability of all the fixed points. - The equivalence between the graph and the table comes from $\lambda_{1,2} = 0.5(\tau \pm \sqrt{\tau^2 + 4\Delta})$, $\Delta = \lambda_1 \lambda_2$ and $\tau = \lambda_1 + \lambda_2$

Depending on the applied current, the configuration on the phase plane is different and therefore the coordinates of the fixed point change.

Case 1: the applied current is not large enough, the fixed point is situated in the bottom left on the phase plane. For $I_{app} = 0$ [nA], the coordinates of the fixed points are $(-62.787, 0.276)$ and the

eigenvalues of the jacobian matrix evaluated at this point are:

$$\begin{aligned}\lambda_1 &= -0.2635 + 0.7844i \\ \lambda_2 &= -0.2635 - 0.7844i\end{aligned}\tag{D.2}$$

Since both eigenvalues have negative real parts, the fixed point is a stable spiral.

Case 2: the applied current is large enough, the intersection occurs at higher values of both variables. For $I_{app} = 12$ [nA], the coordinates of the fixed point are $(-53.248, 0.4245)$ and the eigenvalues of the jacobian matrix evaluated at this point are:

$$\begin{aligned}\lambda_1 &= 0.2857 + 0.7847i \\ \lambda_2 &= 0.2857 - 0.7847i\end{aligned}\tag{D.3}$$

Both eigenvalues have positive real parts, the fixed point is an unstable spiral.

The values themselves have not a significant role in the determination of the nature. Since it is a qualitative analysis, the numerical values are not discussed.

For one particular value of the applied current called I_{AH} , the fixed point corresponds to a center (the real part of the eigenvalues is zero). It defines a Hopf bifurcation.

D.1.2 Vector field

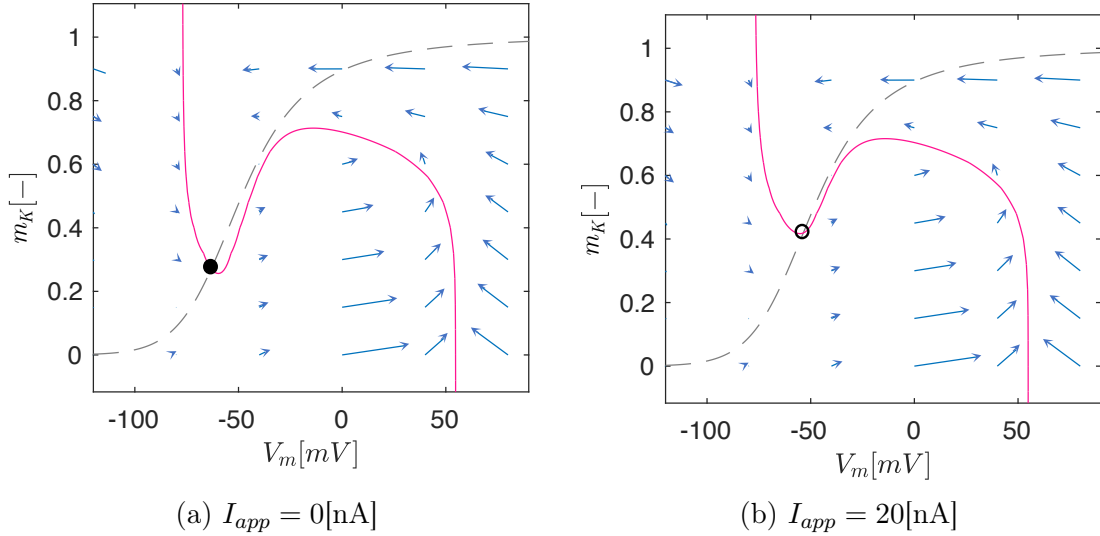


Figure D.2 – Phase portraits of the reduced Hodgkin-Huxley model without (left) and with an applied current (right). - The V_m - and the n -nullclines are respectively drawn in pink full line and grey dashed line and the velocities vectors are blue. The black (resp. white) circle corresponds to a stable (resp. unstable) intersection. [31]

D.2 Reduced HHCa model

D.2.1 Nature of the fixed points

Depending on the nullclines configuration the number and the position of the intersections vary.

For low current values (even negative values), the V_m -nullcline has a hourglass shape crossing in only one point the n -nullcline. This intersection is situated in the far left on the phase plane (see Figure 5.6). For example, if $I_{app} = 0$ [nA], the intersection occurs at $(V_m = -110.98$ [mV], $n = 5.7765 \times 10^{-3}$ [-]).

The eigenvalues of the jacobian matrix evaluated at this fixed point (see equation D.1) are

$$\begin{aligned}\lambda_1 &= -0.3005 \\ \lambda_2 &= -0.2372\end{aligned}\tag{D.4}$$

By referring to Figure D.1b, both eigenvalues are real and negative, the fixed point is a stable node.

With deeper analysis, two other intersections exist between the n-nullcline and the right branch of the V_m -nullcline. Due to numerical imperfections with the function `ezplot` on MATLAB, the curves do not intersect on the plot. In [31], there are identified as a saddle and a unstable point. It can be also deduced from the vector field.

If the current increases, there are three intersections (see Figure 5.6). The identification of their nature is sum up in the Figure D.3.

Points	Coordinates (V_m, n)	Value	Analyse	Nature
A	(-83.65, 0.0669)	$\lambda_{A,1} = -0.4468$	real, < 0	stable node
		$\lambda_{A,2} = -0.0348$	real, < 0	
B	(-63.99, 0.2587)	$\lambda_{B,1} = 0.6032$	real, > 0	saddle node
		$\lambda_{B,2} = -1.1845$	real, < 0	
C	(-48.20, 0.5032)	$\lambda_{C,1} = 3.4478$	real, > 0	unstable node
		$\lambda_{C,2} = 0.9242$	real, > 0	

Figure D.3 – Determination of the nature of the three fixed points for a intermediate value of the applied current in tabular form.

For higher current values, the two intersections between the lower branch of the V_m -nullcline and the n-nullcline merge. Then, only one intersection remains between the upper branch of the V_m -nullcline and the n-nullcline (see Figure 5.6). The eigenvalues of the jacobian matrix evaluated at this fixed point are

$$\begin{aligned}\lambda_1 &= 18.3975 \\ \lambda_2 &= 0.5967\end{aligned}\tag{D.5}$$

The fixed point is a unstable node. It could be deduced from the point C.

D.3 Additional Network Analyses of hybrid model of thalamic neuron

D.3.1 Parameters used for the simulations in Izhikevich and HYB models

Switch in hybrid models in Figure 6.4:

- Izhikevich

$$c_{tonic} = -65, c_{burst} = -50, d = 1$$

- HYB:

$$V_{th} = 40, a_s = 0.1 = a_{us}, b = -2, c = -45, d = 30, d_z = 20, V_{syn} = -75, \tau_s = 1, V_{ss} = -2., V_{shift} = -70, \epsilon_s = 1, \epsilon_{us} = 0.025, g_{s,tonic} = -10, g_{s,burst} = -30, g_{us} = 1, I_{app} = 15, T_{step} = 400$$

Rhythmic networks as a function of γ in Figure 6.6:

- Izhikevich: set 0: $d_E = 1.4, d_I = 1, c_{tonic} = -65, c_{burst} = -50, g_{AMPA} = 0.1 = g_{GABA_A}$

- HYB: set 0 :cell E: $g_{us,E} = 1.2$ and cell I $g_{us,I} = 0.8, g_{AMPA} = 1000, g_{GABA_A} = 100000$

Off-centering for Figure D.4 - Izhikevich:

same synaptic conductances

set 1: $d_E = 1.429, d_I = 0.9594, c_{E,tonic} = -66.76, c_{E,burst} = -49.07, c_{I,tonic} = -65.59, c_{I,burst} = -48.94$.

set 2: $d_E = 1.426, d_I = 0.9798, c_{E,tonic} = -62.57, c_{E,burst} = 50.42, c_{I,tonic} = -62.8, c_{I,burst} = -52.43$.

- HYB:

same synaptic conductances

set 1: $g_{us,E} = 1.214, g_{us,I} = 0.8295, g_{s,E,tonic} = -9.671, g_{s,E,burst} = 30.57, g_{s,I,tonic} = -10.43, g_{s,I,burst} = 29.54$.

set 2: $g_{us,E} = 1.240, g_{us,I} = 0.7924, g_{s,E,tonic} = -10.04, g_{s,E,burst} = 28.68, g_{s,I,tonic} = -10.48, g_{s,I,burst} = 29.92$.

Spectrograms in Figure D.6 and 6.9:

Same parameters as the one used for Figure 6.6.

D.3.2 Rhythmic network activity computed with the off-centered nominal values

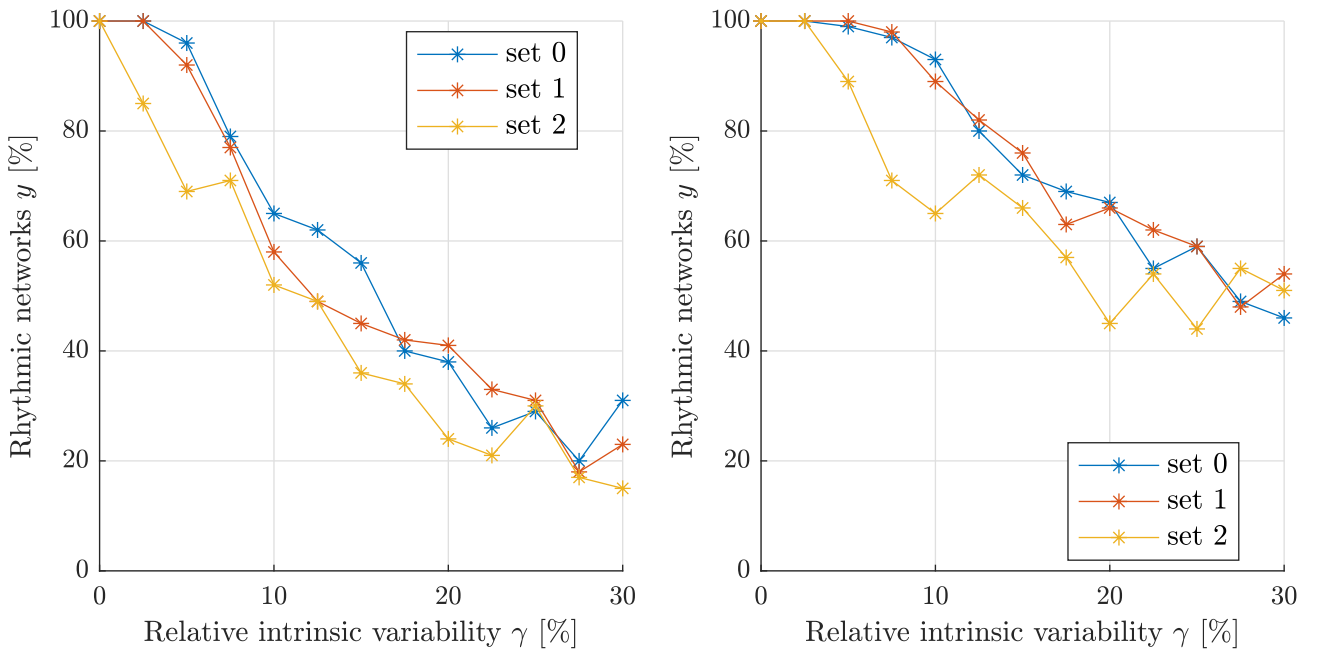


Figure D.4 – Evolution of the percentage of rhythmic networks as a function of the relative intrinsic variability for Izhikevich's model and HYB model computed with the nominal values of the intrinsic parameters and two off-centering set of parameters

D.3.3 Tunability analysis

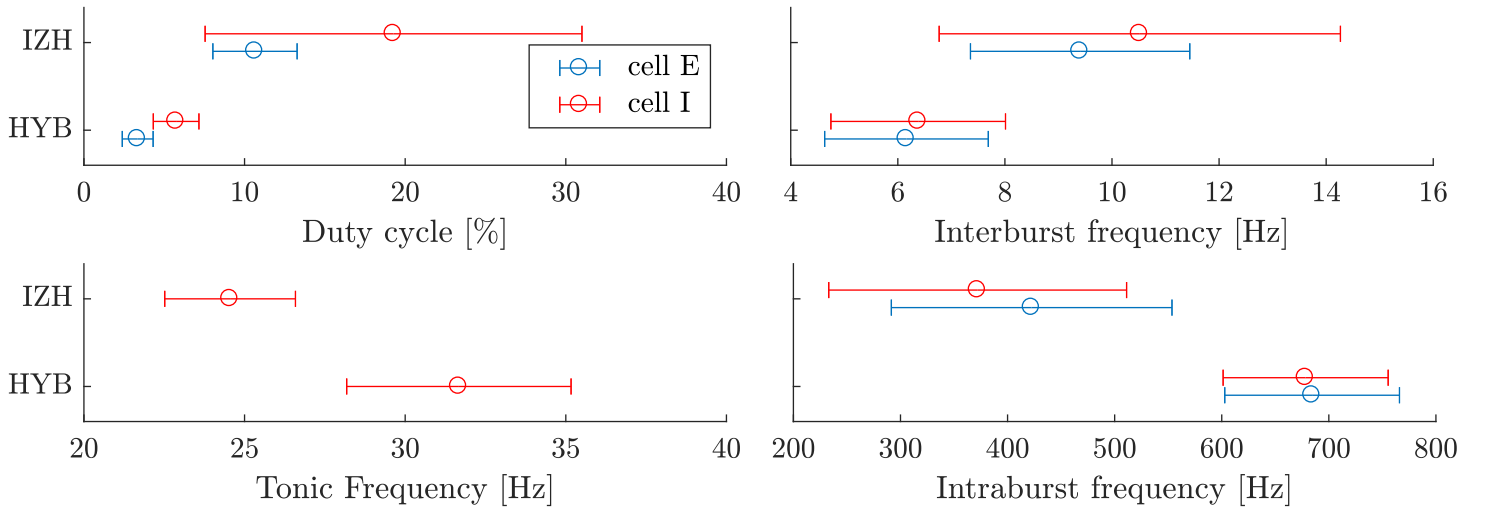


Figure D.5 – Mean and standard deviation of the distribution of the four firing characteristics for the rhythmic networks in HYB and Izhikevich model computed for γ_*

D.3.4 Population rhythm analysis

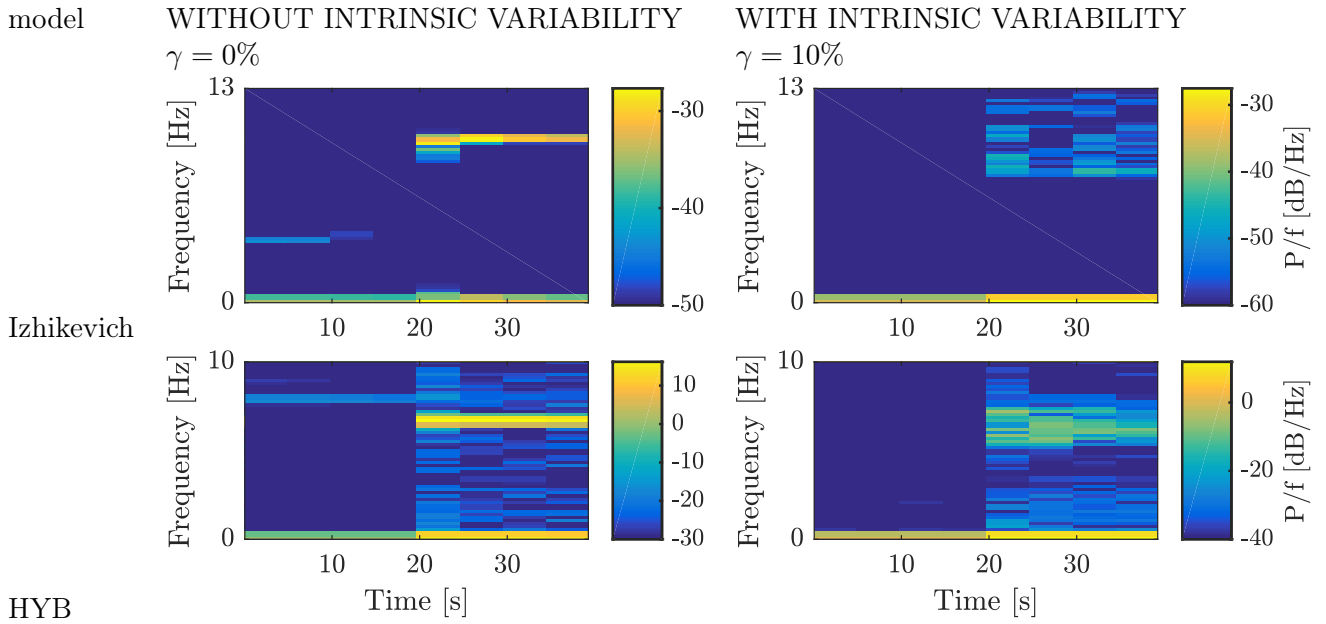


Figure D.6 – Spectrogram of the LFP of the E-cells populations in a 200 network without intrinsic variability (on the left) and with a relative intrinsic variability of 10% (on the right) for Izhikevich's model and HYB model. The intensity of the power spectral content is expressed in Power/Frequency, denoted P/f .

Bibliography

- [1] Excitability. <https://www.nature.com/subjects/excitability>. [Online; accessed: 2018-06-1].
- [2] Human brain project. <https://www.humanbrainproject.eu/en/>. [Online; accessed: 2018-04-20].
- [3] The thalamus. https://www.youtube.com/watch?v=fki7AmLma_I. [Online, accessed: 2018-02-22].
- [4] Vertical cut of an human brain. [https://www.news-medical.net/health/What-does-the-Thalamus-do-\(French\).aspx](https://www.news-medical.net/health/What-does-the-Thalamus-do-(French).aspx). [Online, accessed: 2018-02-21].
- [5] Volume of an n-ball. https://en.wikipedia.org/wiki/Volume_of_an_n-ball. [Online, accessed: 2018-03-17].
- [6] Yimy Amarillo, Germán Mato, and Marcela S Nadal. Analysis of the role of the low threshold currents $i(t)$ and $i(h)$ in intrinsic delta oscillations of thalamocortical neurons. *Frontiers in Computational Neuroscience*, 9:52, 2015.
- [7] Yimy Amarillo, Edward Zagha, German Mato, Bernardo Rudy, and Marcela S Nadal. The interplay of seven subthreshold conductances controls the resting membrane potential and the oscillatory behavior of thalamocortical neurons. *Journal of Neurophysiology*, 112(2):393–410, 07 2014.
- [8] Maxim Bazhenov, Igor Timofeev, Mircea Steriade, and Terrence J. Sejnowski. Model of thalamocortical slow-wave sleep oscillations and transitions to activated states. *Journal of Neuroscience*, 22(19):8691–8704, 2002.
- [9] Corinne Beurrier, Patrice Congar, Bernard Bioulac, and Constance Hammond. Subthalamic nucleus neurons switch from single-spike activity to burst-firing mode. *Journal of Neuroscience*, 19(2):599–609, 1999.
- [10] Stuart M. Cain, Michael E. Hildebrand, and Terrance P. Snutch. *T-Type Calcium Channels and Epilepsy*, pages 77–96. Springer Berlin Heidelberg, Berlin, Heidelberg, 2014.
- [11] E Carbone and H D Lux. Kinetics and selectivity of a low-voltage-activated calcium current in chick and rat sensory neurones. *The Journal of Physiology*, 386:547–570, 05 1987.
- [12] Richard Caton. Researches on electrical phenomena of cerebral grey matter. *9th Internal Medical Congress*, 3:246–249, 1887.
- [13] Neuroscientifically Challenged. 2-min neuroscience: Gaba. <https://www.youtube.com/watch?v=bQIU2KDtHTI>. [Online; accessed: 2018-03-11].
- [14] Neuroscientifically Challenged. 2-min neuroscience: The thalamus. https://www.youtube.com/watch?v=IF8_82e9RmQ&feature=youtu.be. [Online; accessed: 2018-02-27].
- [15] D. Contreras, R. Curro Dossi, and M. Steriade. Bursting and tonic discharges in two classes of reticular thalamic neurons. *Journal of Neurophysiology*, 68(3):973–977, 1992. PMID: 1432063.

- [16] Douglas A. Coulter, John R. Huguenard, and David A. Prince. Calcium currents in rat thalamo-cortical relay neurones: kinetic properties of the transient, low-threshold current. *The Journal of physiology*, 414:587–604, 1989.
- [17] Vincenzo Crunelli and Nathalie Leresche. Childhood absence epilepsy: Genes, channels, neurons and networks. *Nature Reviews Neuroscience*, 3:371 EP–, 05 2002.
- [18] Pollard CE Crunelli V, Lightowler S. Ca^{2+} current underlies low-threshold Ca^{2+} potentials in cells of the cat and rat lateral geniculate nucleus. *J Physiol* 413, pages 543–561, 1989.
- [19] John R. Huguenard David A. McCormick. A model of the electrophysiological properties of thalamocortical relay neurons. *Journal of Neurophysiology*, 68(4):1384–1400, 1992. PMID: 1331356.
- [20] A. Destexhe and C. Bedard. Local field potential. *Scholarpedia*, 8(8):10713, 2013. revision #135811.
- [21] Alain Destexhe, Thierry Bal, David A. McCormick, and Terrence J. Sejnowski. Ionic mechanisms underlying synchronized oscillations and propagating waves in a model of ferret thalamic slices. *J. Neurophysiol*, 76:2049–2070, 1996.
- [22] Alain Destexhe, Mike Neubig, Daniel Ulrich, and John Huguenard. Dendritic low-threshold calcium currents in thalamic relay cells. *Journal of Neuroscience*, 18(10):3574–3588, 1998.
- [23] Julie Dethier. The role of feedback in maintaining robustness and modulation across scales: Insights from cellular and network neurophysiology. 2015.
- [24] Julie Dethier, Guillaume Drion, Alessio Franci, and Rodolphe Sepulchre. Modulation of beta oscillations during movement initiation: modeling the ionic basis of a functional switch. 2013.
- [25] Julie Dethier, Guillaume Drion, Alessio Franci, and Rodolphe Sepulchre. A positive feedback at the cellular level promotes robustness and modulation at the circuit level. *Journal of Neurophysiology*, 114(4):2472–2484, 2015. PMID: 26311181.
- [26] G. Drion, A. Franci, V. Seutin, and R. Sepulchre. Modulation and robustness of endogenous neuronal spiking. *ArXiv e-prints*, nov 2013.
- [27] G. Drion, T. O’Leary, J. Dethier, A. Franci, and R. Sepulchre. Neuronal behaviors: A control perspective. In *2015 54th IEEE Conference on Decision and Control (CDC)*, pages 1923–1944, 2015.
- [28] Guillaume DRION. *Regulation of Excitability, Pacemaking, and Bursting: Insights from Dopamine Neuron Electrophysiology*. PhD thesis, University of Liege, 2013.
- [29] Guillaume Drion, Julie Dethier, Alessio Franci, and Rodolphe Sepulchre. Switchable slow cellular conductances determine robustness and tunability of network states. *PLOS Computational Biology*, 14(4):1–20, 04 2018.
- [30] Guillaume Drion, Alessio Franci, Julie Dethier, and Rodolphe Sepulchre. Dynamic input conductances shape neuronal spiking,. *eNeuro*, 2(1):ENEURO.0031–14.2015, Jan-Feb 2015.
- [31] Guillaume Drion, Alessio Franci, Vincent Seutin, and Rodolphe Sepulchre. A novel phase portrait for neuronal excitability. *PLOS ONE*, 7(8):1–14, 08 2012.
- [32] Daniel Elijah, Ines Samengo, and Marcelo Montemurro. Thalamic neuron models encode stimulus information by burst-size modulation. *Frontiers in Computational Neuroscience*, 9:113, 2015.
- [33] G.B. Ermentrout and D.H. Terman. *Mathematical Foundations of Neuroscience*. Interdisciplinary Applied Mathematics. Springer New York, 2010.

- [34] Richard FitzHugh. Impulses and physiological states in theoretical models of nerve membrane. *Biophysical Journal*, 1(6):445–466, 07 1961.
- [35] A. Franci, G. Drion, and R. Sepulchre. Robust and tunable bursting requires slow positive feedback. *ArXiv e-prints*, July 2017.
- [36] Alessio Franci, Guillaume Drion, Vincent Seutin, and Rodolphe Sepulchre. A balance equation determines a switch in neuronal excitability. *PLOS Computational Biology*, 9(5):1–16, 05 2013.
- [37] R. Heidelberger, M.N. Waxham, J.H. Byrne, and J.L. Roberts. *From Molecules to Networks: An Introduction to Cellular and Molecular Neuroscience*. Elsevier Science, 2003.
- [38] A. L. HODGKIN and A. F. HUXLEY. A quantitative description of membrane current and its application to conduction and excitation in nerve. *The Journal of physiology*, 117(4):500–544, August 1952.
- [39] John R. Huguenard. Neuronal circuitry of thalamocortical epilepsy and mechanisms of antiabsence drug action. *Adv. Neurol*, pages 991–999, 1999.
- [40] John R. Huguenard and D. A. McCormick. Simulation of the currents involved in rhythmic oscillations in thalamic relay neurons. *Journal of neurophysiology*, 68 4:1373–83, 1992.
- [41] Izhikevich. Simple model of spiking neurons. <https://www.izhikevich.org/publications/spikes.htm>. [Online; accessed: 2018-03-11].
- [42] E.M. Izhikevich. *Dynamical Systems in Neuroscience*. Computational neuroscience Dynamical systems in neuroscience. MIT Press, 2007.
- [43] H Jahnsen and R Llinás. Electrophysiological properties of guinea-pig thalamic neurones: an in vitro study. *The Journal of Physiology*, 349:205–226, 04 1984.
- [44] H Jahnsen and R Llinás. Ionic basis for the electro-responsiveness and oscillatory properties of guinea-pig thalamic neurones in vitro. *The Journal of Physiology*, 349:227–247, 04 1984.
- [45] George K Kostopoulos. Spike-and-wave discharges of absence seizures as a transformation of sleep spindles: the continuing development of a hypothesis. *Clinical Neurophysiology*, 111:S27–S38, 2018/06/03 2000.
- [46] Rodolfo R. Llinás and Mircea Steriade. Bursting of thalamic neurons and states of vigilance. *Journal of Neurophysiology*, 95(6):3297–3308, 2006. PMID: 16554502.
- [47] W.W. Lytton, A. Destexhe, and T.J. Sejnowski. Control of slow oscillations in the thalamocortical neuron: a computer model. *Neuroscience*, 70(3):673 – 684, 1996.
- [48] Steriade M. The corticothalamic system in sleep. *Frontiers in Bioscience*, 8:878–899, 2003.
- [49] Pierre Maquet. The role of sleep in learning and memory. *Science*, 294(5544):1048–1052, 2001.
- [50] David A. McCormick, , and Thierry Bal. Sleep and arousal: Thalamocortical mechanisms. *Annual Review of Neuroscience*, 20(1):185–215, 1997. PMID: 9056712.
- [51] David A McCormick, Matthew J McGinley, and David B Salkoff. Brain state dependent activity in the cortex and thalamus. *Current opinion in neurobiology*, 31:133–140, April 2015.
- [52] Patrick Meuth, Sven G Meuth, Daniel Jacobi, Tilman Broicher, Hans-Christian Pape, and Thomas Budde. Get the rhythm: Modeling neuronal activity. *Journal of Undergraduate Neuroscience Education*, 4(1):A1–A11, Fall 2005.
- [53] Thien Thanh Dang-Vu Oren M.Weiner. Spindle oscillations in sleep disorders: A systematic review. March 2016.

- [54] Martin Pospischil, Maria Toledo-Rodriguez, Cyril Monier, Zuzanna Piwkowska, Thierry Bal, Yves Frégnac, Henry Markram, and Alain Destexhe. Minimal hodgkin–huxley type models for different classes of cortical and thalamic neurons. *Biological Cybernetics*, 99(4):427–441, 2008.
- [55] Paula Rhodes and Rodolfo Llinás. A model of thalamocortical relay cells. *The Journal of Physiology*, 565(Pt 3):765–781, 06 2005.
- [56] Maureen E. Rush and John Rinzel. Analysis of bursting in a thalamic neuron model. *Biological Cybernetics*, 71(4):281–291, Aug 1994.
- [57] S. M. Sherman and R. W. Guillery. Functional organization of thalamocortical relays. *Journal of Neurophysiology*, 76(3):1367–1395, 1996. PMID: 8890259.
- [58] S. Murray Sherman and R. W. Guillery. The role of the thalamus in the flow of information to the cortex. *Philosophical Transactions of the Royal Society of London B: Biological Sciences*, 357(1428):1695–1708, 2002.
- [59] SM Sherman. Tonic and burst firing: dual modes of thalamocortical relay. *Trends in neurosciences*, 24(2):122–126, February 2001.
- [60] Hee-Sup Shin. T-type Ca^{2+} channels and absence epilepsy. *Cell calcium*, 40(2):191–196, August 2006.
- [61] Evgenia Sitnikova. Sleep spindles in rats with absence epilepsy. *Sleep Spindles & Cortical Up States*, 0(0):1–10, 0.
- [62] Evgenia Sitnikova. Thalamo-cortical mechanisms of sleep spindles and spike-wave discharges in rat model of absence epilepsy (a review). *Epilepsy Research*, 89(1):17 – 26, 2010. Special Issue on San Servolo Epilepsy Courses Alumni Meeting.
- [63] M Steriade, DA McCormick, and TJ Sejnowski. Thalamocortical oscillations in the sleeping and aroused brain. *Science*, 262(5134):679–685, 1993.
- [64] S.H. Strogatz. *Nonlinear Dynamics and Chaos: With Applications to Physics, Biology, Chemistry, and Engineering*. Studies in Nonlinearity. Avalon Publishing, 2014.
- [65] Roger D. Traub and Richard Miles. *Neuronal Networks of the Hippocampus*. Cambridge University Press, New York, NY, USA, 1991.
- [66] T. Van Pottelbergh, G. Drion, and R. Sepulchre. Robust modulation of integrate-and-fire models. *ArXiv e-prints*, September 2017.
- [67] X.-J. Wang. Multiple dynamical modes of thalamic relay neurons: Rhythmic bursting and intermittent phase-locking. *Neuroscience*, 59(1):21 – 31, 1994.
- [68] X. J. Wang, J. Rinzel, and M. A. Rogawski. A model of the t-type calcium current and the low-threshold spike in thalamic neurons. *Journal of Neurophysiology*, 66(3):839–850, 1991. PMID: 1661326.
- [69] Theodore G. Weyand, Michael Boudreaux, and William Guido. Burst and tonic response modes in thalamic neurons during sleep and wakefulness. *Journal of Neurophysiology*, 85(3):1107–1118, 2001. PMID: 11247981.
- [70] Wikipedia. The brain. <https://en.wikipedia.org/wiki/Brain>. [Online; accessed: 2018-06-1].
- [71] Qiang Zhou, Dwayne W. Godwin, Donald M. O’Malley, and Paul R. Adams. Visualization of calcium influx through channels that shape the burst and tonic firing modes of thalamic relay cells. *Journal of Neurophysiology*, 77(5):2816–2825, 1997. PMID: 9163395.